Université de Montréal

Spatially Guided Angiogenesis by Laser-Bioprinting

par Sayadeh Sara Hosseini Kolkooh

Département de pharmacologie et physiologie - Institut de génie biomédical - Faculté de médecine

Mémoire présenté
en vue de l'obtention du grade de Maîtrise ès sciences appliquées (M.Sc.A)
en génie biomédical

Mai, 2020

Université de Montréal
(Département de pharmacologie et physiologie/ institut de génie biomédical)

Ce mémoire intitulé

Spatially Guided Angiogenesis by Laser-Bioprinting

Présenté par

Sayadeh Sara Hosseini Kolkooh

A été évalué par un jury composé des personnes suivantes

Jonathan Ledoux
Président-rapporteur

Christos Boutopoulos
Directeur de recherche

Bruno Larrivée
Codirecteur

Houman Savoji
Membre du jury

Résumé

L'ingénierie tissulaire est reconnue comme une méthode potentielle pour réparer ou régénérer les tissus endommagés. Malgré de grandes avancées dans l'ingénierie tissulaire, la réussite de la construction de tissus complexes avec des réseaux vascularisés reste un défi. Dans les modèles d'angiogenèse actuels, les cellules endothéliales sont ensemencées au hasard, n'offrant pas de structure organisée. La technologie de bioimpression par laser offre une résolution d'impression précise. Par cette technique, les structures microvasculaires peuvent être construites pour la fabrication d'organes complexes, ou pour modéliser la progression de la maladie ou les modèles de réponse aux médicaments.

Dans cette étude, des techniques de bio-impression au laser ont été utilisées pour étudier le guidage de l'angiogenèse *in vitro*. Deux techniques basées sur le laser, le transfert direct induit par laser (LIFT) et le transfert latéral induit par laser (LIST) sont utilisées. Comparée à LIFT, la technologie LIST offrait des conditions idéales pour l'impression cellulaire telles que la concentration cellulaire requise pour la formation du tubes endothéliaux et l'uniformité du motif désiré. Nous avons réalisé le modelage de la formation de structures de type capillaire dans des motifs organisés via l'impression LIST. Les constructions de type capillaire formées présentent des motifs uniformes. Les structures formées ont été analysées par microscopie confocale et reconstruction d'images 3D. Bien que le développement de la lumière endothéliale soit incomplet, la technique développée possède le potentiel d'atteindre une stabilisation et un développement de la lumière si l'on recrute un deuxième type de cellule tel que les fibroblastes ou les péricytes.

Mots-clés : Bio-impression au laser, transfert direct induit par laser (LIFT), transfert latéral induit par laser (LIST), impression cellulaire, cellule endothéliale (EC), cellule endothéliale veine ombilicale humaine (HUVEC), micro modelage, microvaisseaux, structures capillaires.

Abstract

Tissue engineering has been well acknowledged as a potential method to repair or regenerate damaged tissues in the human body, fulfilling the limitations and shortage in autologous and organ transplantations. Despite great advances in engineering tissues with simple geometry and low requirement for oxygen and blood supply such as cartilage, skin and cornea, success in constructing 3D complex tissues with vascularized networks remains a major challenge. Angiogenesis plays an important role in vascular development in vivo. In current angiogenesis models, endothelial cells are seeded randomly not offering precise and desired patterning. Laser-based bioprinting technology offers precise and high cell printing resolution. By using laser-based bioprinting technology, microvascular structures can be constructed as a platform for complex organ fabrication, disease progression and drug response models.

In this study, laser-based bioprinting techniques are employed to study angiogenesis guidance *in vitro* by patterning endothelial cells. Two laser-based techniques, Laser-induced forward transfer (LIFT) and Laser-induced side transfer (LIST) are used as patterning tools. Compared to LIFT, LIST technology provided ideal conditions for cell printing such as required cell concentration for endothelial tube formation and pattern uniformity. In this study, we achieved the guidance of capillary-like structure formation in desired patterns via LIST printing. The formed capillary-like constructs featured precise patterns and uniformity. The structures were analyzed by confocal microscopy, 3D image reconstruction and frozen section procedure. Though lumen development was incomplete, it possesses the potential to attain further stabilization and lumen development if recruiting a second cell type such as fibroblast or pericyte.

Keywords : Laser based bioprinting, laser-induced forward transfer (LIFT), laser-induced side transfer (LIST), cell printing, endothelial cell (EC), human umbilical vein endothelial cell (HUVEC), micro patterning, microvessels, capillary structures.

Table of contents

List of tables

List of figures

List of acronyms

2D : Two dimensional

3D : Three dimensional

DBB : Droplet-based bioprinter

EBB : Extrusion-based bioprinter

ECM : Extra cellular matrix

HUVEC : Human umbilical vein endothelial cell

LBB : Laser-based bioprinter

LIFT : Laser-induced forward transfer

LIST : Laser-induced side transfer

PC : Pericyte

SMC : Smooth muscle cell

To my parents and my sister for their love, support and encouragement.

Acknowledgment

I wish to thank, first and foremost, Professor Christos Boutopoulos, for supervising me and for his valuable guidance. It was impossible to make through this study without his continuous effective support.

I would also wish to express my deepest gratitude to Professor Bruno Larrivée for his valuable suggestions and comments which extremely helped me in this study.

My research partner, Hamid Ebrahimi Orimi, was instrumental in completing the path of my research. For this, I am extremely grateful.

I would like to pay my special regards to Dr. Erika Hooker, for patiently assisting and supporting me in the lab through my research experiments.

This thesis would not be possible without the warm support of my family. I like to thank them deeply for their constant encouragement and their deep understanding through these years.

1. Introduction

Today, several medical treatments are performed to repair or replace tissue damage or organ failure caused via disease or trauma. Currently, the existing treatments consist of replacement with synthetic materials, organ replacement and autotransplantation. Although these treatments are lifesaving and allow recovery, major drawbacks restrict their applications and patients face difficulty post treatment. Organ transplantation is limited due to the shortage of organ donors compared to demand. Moreover, rejection risk by the patient's immune system exists and infection or disease transfer from the donor can be caused. On the other hand, allograft transplantation is restricted depending on the anatomy of the harvesting site and can lead to donor site complications, hematoma, infection and tissue lose (O'brien, 2011).

The developing field of tissue engineering aims to reconstruct or repair tissues by merging the principles of biology, bioengineering and medicine. Tissue engineering uses a combination of cells, growth factors and scaffolds to construct tissues that repair or regenerate their counterparts in the human body (Figure 1). This field has faced major advancement through the past decades, resulting in the construction of *in vitro* models for drug screening and understanding cell behaviour along with in vivo regeneration of damaged tissues. Today, tissue engineering has successfully developed *in vitro* engineered tissues like skin (L. Ma et al., 2003; Mei et al., 2012; Paquet et al., 2010), bladder (Atala, 2011), cartilage (Sanchez-Adams & Athanasiou, 2012), cornea, cardiac patch (Gaebel et al., 2011), intestine (Madden et al., 2018), urethra (K. Zhang et al., 2017), trachea (Park et al., 2019), and bone (Perry et al., 2003).

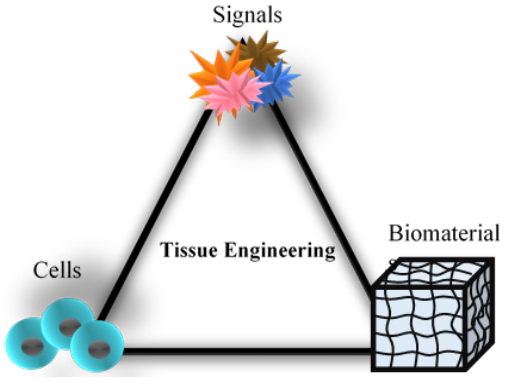

Figure 1. Tissue engineering triad.

However, current tissue engineering strategies have failed to construct complex tissues such as heart, kidney and liver. Despite success in developing the geometric complexity of tissue, the inability to generate a blood vessel system which can provide the essential nutrients and oxygen toward the tissue cells and extract metabolic waste still remains as a main limitation. *In vivo*, the vascular system branches into capillaries spaced at 200 µm which corresponds to oxygen diffusion limit (Figure 2). The success in constructing tissues such as skin, cartilage, bladder, bone and cornea is because these tissues have low oxygen consumption, require less blood vessels and possess a simple geometry or the engineered tissues are thin less than 200 µm thick. Most of the tissues depend on a vascular system with 200 µm optimal distance. Therefore, complex engineered tissue requires a vascular network with branching system 200 µm distance between the branches.

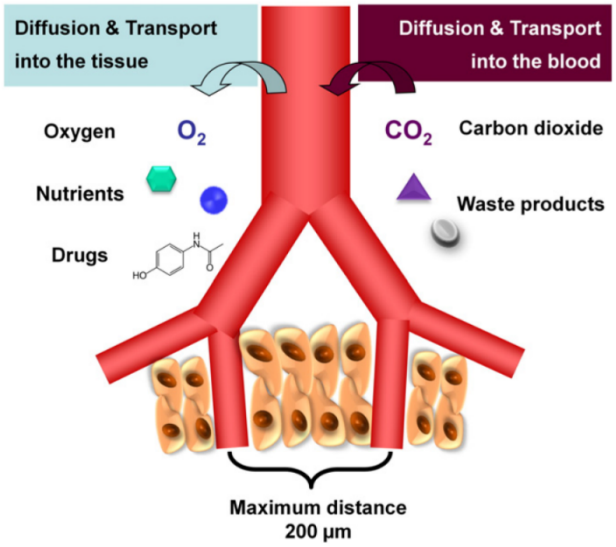

Figure 2. Schematic of transport and diffusion processes in vascularized tissues in vivo (Novosel, Kleinhans, & Kluger, 2011).

Several tissue engineering strategies have been developed to cope with the difficulty of designing and regenerating a complex and functional tissue. Modular tissue engineering designs building blocks that possess microstructural features such as specific tissue morphology and microvascular architecture. The designed modular tissues can be used to create larger biomimetic structures. The main advantage of this technique is creating microscopic structural features, the assembly techniques and the spatial resolution of the tissue modules can be further improved (Nichol & Khademhosseini, 2009). The scaffold-based technique provides a 3D

structure for the cells to attach and proliferate throughout the scaffold leading to the development of cell-laden grafts with similar features to the native tissue. These scaffolds can be constructed from naturally derived polymers such as hyaluronic acid, alginate, collagen and gelatin or synthetic polymers such as poly(lactic-co-glycolic acid) (PLGA), poly(glycolic acid) (PGA), poly(lactic acid) (PLA) and poly(e-caprolactone) (PCL). This strategy lacks the ability to induce the complex microstructure similar to tissues (Y. S. Zhang et al., 2017). Among different tissue engineering strategies, bioprinting emerges as a reproducible and scalable fabrication technique that enables the delivery of cells and biomaterials with precise control.

1.1 Anatomy of Vascular Tissue

Blood vessels play an important role in the circulatory system that delivers blood throughout the body. The vascular system is composed of arteries, arterioles, capillaries, venules and veins. The blood is transferred by the arteries from the heart into the circulatory system delivering it to the arterioles. Arterioles carry the blood to the capillaries, which exchange oxygen and nutrients. Venules then collect the blood containing carbon dioxide and metabolic waste and deliver it to the veins and subsequently to the heart (Mazurek et al., 2017).

Blood vessels are arranged in a multi-layer structure and the number of these layers depends on the physiological role they fulfill and the vessel location. The arteries and veins are constructed with 3 layers while the capillaries are formed by a single layer. The layers that construct the arteries and veins are the tunica interna, the tunica media and the tunica externa (Figure 3A).

The tunica interna is coated with a monolayer of endothelial cells (EC) called endothelium. ECs line the interior wall from the largest vessels to the smallest capillaries. Endothelium forms a cell barrier interface between the circulating blood in the vessel lumen and the vessel wall (De Angelis, Moss, & Pouton, 1996). Moreover, it allows blood flow without thrombogenicity and is infection resistant. Molecules are transferred by penetrating the endothelium to the nearby tissue or from the tissue to the vessel (Figure 3B) (Novosel et al., 2011).

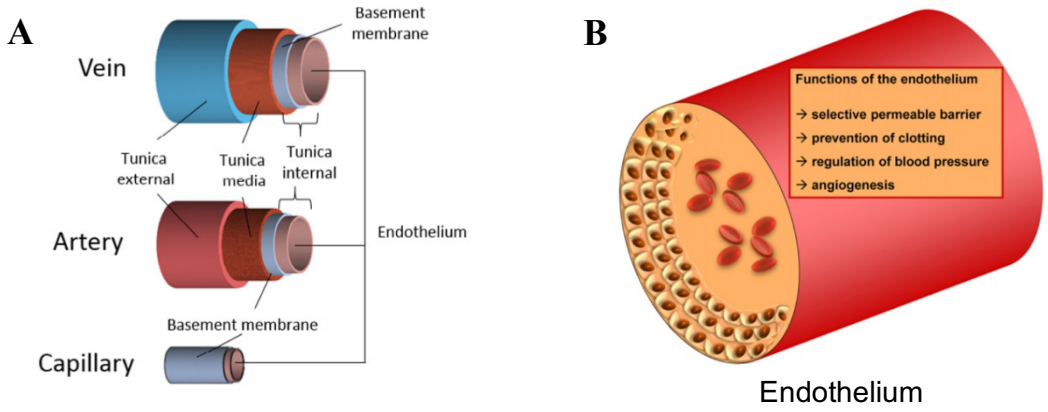

Figure 3. (A) The layer-by-layer structure of blood vessels. Adapted from (Datta, Ayan, & Ozbolat, 2017) (B) Functions of the endothelium (Novosel et al., 2011).

After the endothelium, the basement membrane is located which is composed of type IV collagen, laminin and fibronectin. The basement layer is circumvented by an elastin layer or the interna elastic lamina. The media is the next cellular layer after the tunica interna and is formed by smooth muscle cells (SMCs) and collagen type I and III (Berillis & Journal, 2013). The media layer is thicker in larger arteries and is encircled by elastic externa lamina. Arterioles compared to arteries have less SMCs and capillaries are coated by a discontinuous layer of pericytes (PCs) instead of SMCs (Figure 4A). SMCs along with collagen type I and III are arranged circularly around the vessel. In the media layer, SMCs are responsible for the contraction and dilation of the vessel. The tunica externa is the outer layer of a vessel surrounding the tunica media consisting of fibroblast cells implanted on a loose collagen matrix (ECM) and progenitor cells (Figure 4B).

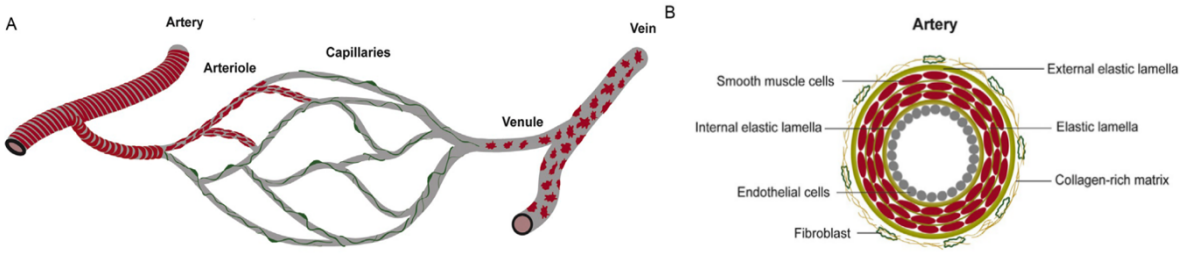

Figure 4. Vascular structure. (A) EC tubes of arteries, arterioles, venules and veins are coated by SMCs (red), while pericytes (PCs) (green) are the mural cells of capillaries (B) Transverse section of an artery showing major components of the vascular wall (Mazurek et al., 2017).

1.1.1 Vascular Cells

1.1.1.1 Endothelial Cells

A monolayer of EC lines the entire tunica interna in the vasculature structure. It is estimated that the endothelium in the human adult consists of 1 x 10^{13} cells approximately (Augustin, Kozian, & Johnson, 1994). EC tubes can lead to further vessel formation following the angiogenesis process. EC proliferation, invasion, migration, lumen formation and stabilization results in generating new vessels from the pre-existing vessels. The nascent vessels recruit mural cells to provide stabilization, perfusion regulation and to induce EC quiescence. Mural cells consist of SMCs and PCs. They are fundamental for vessel maturation, as uncoated nascent vessels undergo regression and pruning. SMCs coat arteries and veins while PCs form direct cell-cell contact with ECs in immature vessels and capillaries (Gaengel, Genové, Armulik, & Betsholtz, 2009). ECs and mural cells share a basement membrane constructed of extracellular proteins that creates a sheath around the endothelial tubes (Eble & Niland, 2009). The basement membrane sheath and the mural cells prevents ECs from leaving their position (Blasi & Carmeliet, 2002). EC plays a major role throughout the angiogenesis process and are also involved in diverse processes such as barrier function, coagulation, blood flow regulation, inflammation and in synthesis/degradation of ECM components (Cines et al., 1998).

1.1.1.2 Smooth Muscle Cells (SMCs)

The major component of the tunica media are the SMCs, which control the vascular contraction and relaxation state leading to blood flow regulation. Blood vessel contraction and relaxation is determined by a spectrum of contractile and cytoskeletal proteins. When recruited to an EC tube, they must form a functional tunica media layer and undergo differentiation, which is induced by transfer growth factor (TGF) (Greif et al., 2012).

1.1.1.3 Pericytes (PCs)

While SMCs are mural cells for vessels and arterioles, PCs are the mural cells of capillaries (Figure 5). PCs are embedded at the abluminal surface in the basement membrane. Their long cytoplasmic process allows them to interface with adjacent ECs through the basement membrane's gaps and, in some cases, outstretch to the neighboring capillaries (Mazurek et al.,

2017). These cells are produced by arterioles and possibly by bone marrow-derived progenitors (Lindblom et al., 2003). PCs are necessary for the stabilization of the new formed vessels, stopping further sprouting and providing support for adequate blood flow (Garner, 1994). EC tip cells recruit PCs to the new tubes by secreting platelet-growth factor subunit B (PDGF-B) which induces PC proliferation and migration. Due to the lack of specific PC markers, their functions and embryonic origins is not well-studied (Mazurek et al., 2017).

1.1.1.4 **Tunica Externa Cells**

The last vascular layer is the tunica externa which plays an important role in the health and disease of the vasculature. This layer is the least well studied layer compared to other layers. The tunica externa is formed by collagen-rich ECM which embeds nerves and lymphatics. It also consists of a microvascular network in larger arteries named vasa vasorum. Different cell types exist in this layer such as fibroblasts, lymphocytes, stem cells, mast cells, dendritic cells, resident macrophages and stem cell antigen (Sca)-1^+ progenitor cells (Wagenseil & Mecham, 2009). Fibroblasts construct the major portion of cells in the tunica (Mazurek et al., 2017).

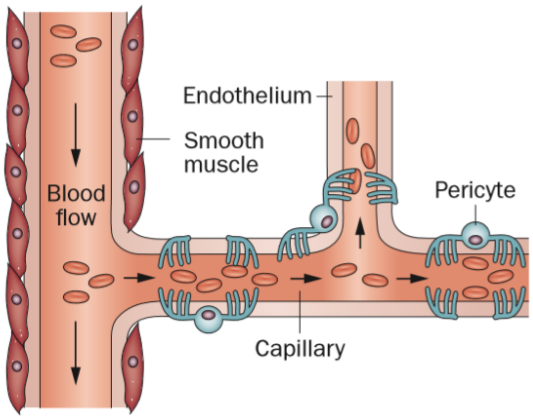

Figure 5. Arteriole coated with SMCs and capillary coated with PCs. Adapted from (O'farrell & Attwell, 2014).

1.1.2 **Vascular Extra Cellular Matrix (ECM)**

All existing tissues and organs in the human body consist of a noncellular component, ECM which provides the 3D network for the cells. ECM is constructed by two main groups of macromolecules: proteoglycans and fibrous proteins. It provides the underlying processes such as biomechanical and biochemical cues for tissue differentiation, morphogenesis and

homeostasis. Each tissue possesses a unique ECM composition which develops between the cellular elements (adipocyte, epithelial, endothelial and fibroblast cells) and protein microenvironment. The dynamic structure of ECM interacts with cells and produces signals to control cell events such as differentiation, proliferation, migration, adhesion, and survival. (Järveläinen, Sainio, Koulu, Wight, & Penttinen, 2009). The histologic structure of ECM includes the basement membrane and the intercellular matrix. The basement membrane is composed of a dense, thin fibrous layer that separates the connective tissue from a confluent layer of endothelial or epithelial cells lining the external interface of a tissue. The line of endothelial or epithelial cells plays as a barrier role against the external environment and in some tissues contributes in specific functions such as reabsorption, metabolism and filtration. These cells are attached to the basement membrane by matrix adhesion molecules and integrins. The intercellular matrix contains fibroblast and immune cells. It provides physical support for the surface cells and interacts with cells by secreting chemokines or soluble molecules (Bosman & Stamenkovic, 2003).

ECM is essential for the vascular wall features such as elasticity and tensile strength via elastic lamina and collagen fibers respectively (Figure 6) (Wagenseil & Mecham, 2009). Another vascular ECM feature is the ability to influence cellular behaviour and signaling. Vascular ECM is formed by elastin, collagen, fibronectin, glycoproteins, microfibrils and proteoglycans (Mazurek et al., 2017). In larger arteries, 50% of the vessels are constructed by collagen and elastin (Harkness, Harkness, & McDonald, 1957; O'Connell et al., 2008). Each vascular layer possesses a specialized ECM composition. In the tunica internal, the ECM is located on a thin basement membrane containing fibronectin, laminin, type IV collagen, perlecan, nidogen, heparin sulfate proteoglycans and other proteins. In microvessels, EC-PC interactions induce ECM and basement membrane construction (Stratman, Malotte, Mahan, Davis, & Davis, 2009). The basement membrane is fundamental for the regulation of EC proliferation, migration and tube formation (Davis & Senger, 2005). In the tunica media, SMC layers are separated by the elastic lamina and collagen bundles are located between the lamina. The collagen bundles possess no evident pattern in normal physiological pressure. However, with pressure increase, the bundles align circumferentially (Wagenseil & Mecham, 2009).

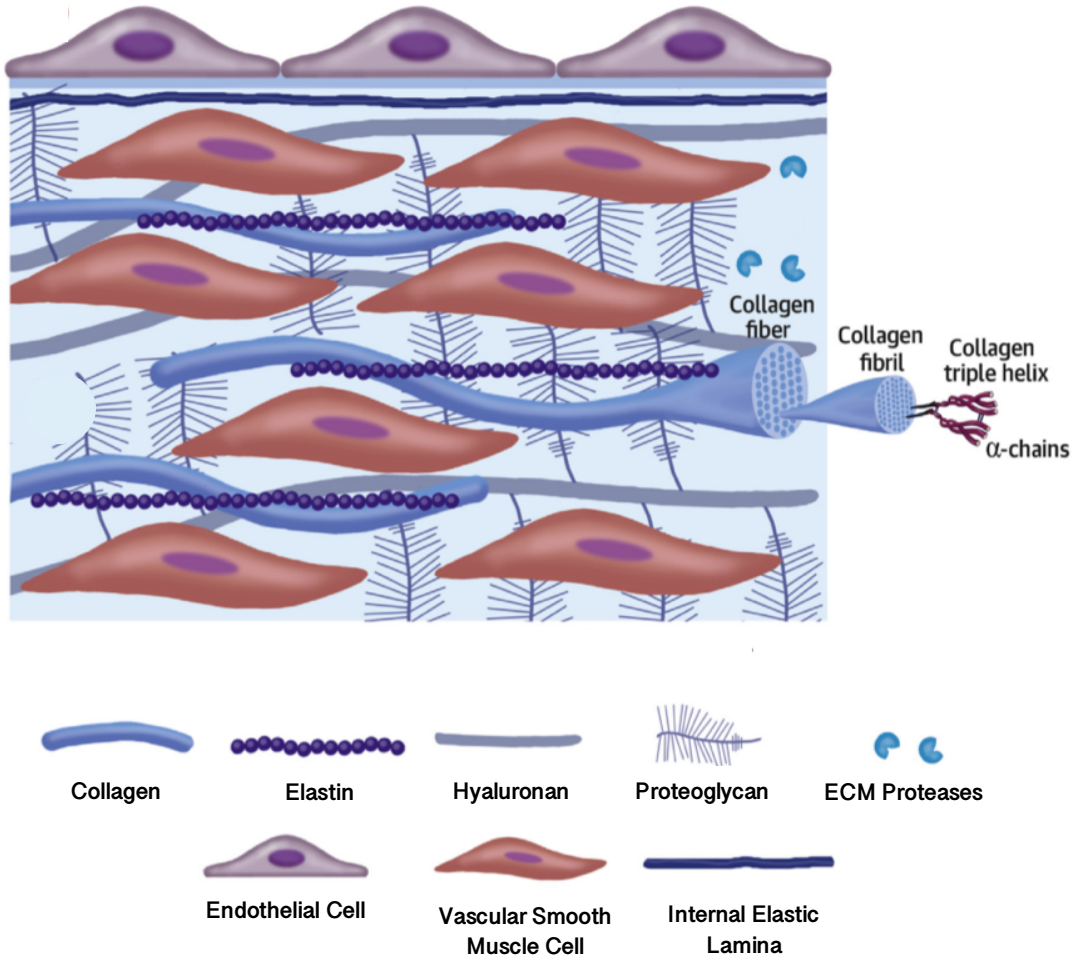

Figure 6. Key elements of vascular wall and ECM (Barallobre-Barreiro et al., 2020).

1.2 Angiogenesis

In vivo blood vessel formation is based on two processes: angiogenesis and vasculogenesis (Figure 7). In the embryo, vasculogenesis refers to primitive blood vessel formation via the assembly of newly formed angioblasts that differentiate into a primitive vascular network. The previous procedure is then followed by a complex remodeling process creating a functional vasculature (Swift & Weinstein, 2009). After primary vascular plexus generation, vessel sprouting occurs leading to network formation which then is remodelled into arteries and veins (angiogenesis) (Adams & Alitalo, 2007). Angiogenesis is the process of sprouting capillaries from the pre-existing blood vessels. The importance of angiogenesis is not only acknowledged in the physiological process but also in several diseases such as retinopathy,

cancer and rheumatoid arthritis (Risau, 1997). It is essential in tissue development and regeneration as well as in wound repair. Angiogenesis can be regulated based on previous mentioned conditions, it can be active for brief periods and then completely inhibited (Folkman, 1992).

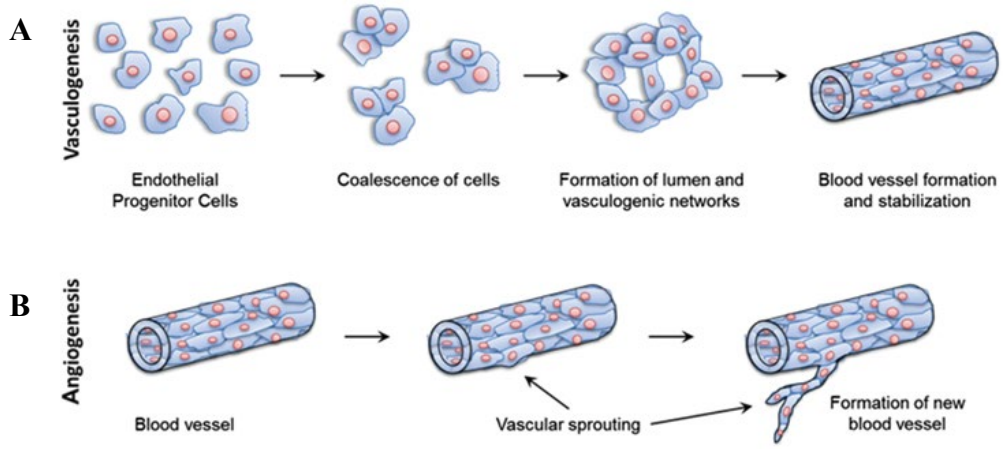

Figure 7. New blood vessel formation occurs via (A) Vasculogenesis and (B) Angiogenesis. Adapted from (Peak, Cross, Singh, & Gaharwar, 2016).

The dynamic process of angiogenesis requires the essential association of leading "tip" cells and "stalk" cells that follow the tip cells to form the lumen in vessel formation (Figure 8) (Gerhardt et al., 2003). The EC located at the end of the sprouts leading the new vessels is named "tip cell". Tip cells are ECs that change their quiescent state into a motile and invasive state and display filopodia extension when they receive proangiogenic signals. For the release of ECs prior to sprouting, proteolytic breakdown of basement membrane and mural cell detachment is required. The tip cell explores the surrounding for pro- and antiangiogenic guidance cues via their receptors. The existing matrix metalloproteases in the tip cells allow the degradation of the basement membrane (Blasi & Carmeliet, 2002). Endothelial stalk cells trail the tip cell to form a lumen and proliferate to help with the sprout elongation while maintaining their connectivity with the main vessel. Compared to tip cells, stalk cells demonstrate less filopodia and more proliferation. To construct vessel loops, tip cells anastomose with cells from nearby sprouts. The newly formed connections are stabilized by basement membrane creation, blood flow initiation and the involvement of mural cells. The sprouting procedure repeats until the proangiogenic signals subsides and the quiescent state is attained (Potente, Gerhardt, & Carmeliet, 2011).

Several angiogenic factors have been identified, including the members of the vascular endothelial growth factor (VEGF) family, transforming growth factors (TGF), platelet-derived growth factor (PDGF), angiopoietins, interleukins, tumor necrosis factor-α, and the members of the fibroblast growth factor (FGF) family (Otrock, Mahfouz, Makarem, & Shamseddine, 2007).

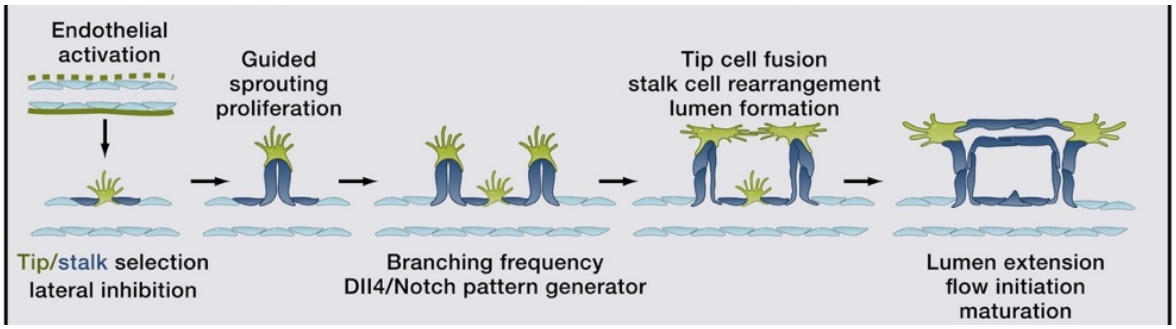

Figure 8. Tip cell and stalk cell association through the sprouting, guidance, branching, anastomoses and lumen formation processes of angiogenesis (Potente et al., 2011).

1.2.1 Angiogenic Factors

Vascular endothelial growth factor (VEGF) : The expression of VEGF-A (also referred to as VEGF) is related to significant steps in angiogenesis and vasculogenesis by binding to its related cell surface receptors (Otrock et al., 2007). It provokes proliferation, sprouting and tube formation of ECs (Ferrara, Gerber, & LeCouter, 2003). VEGF-A influences angiogenic processes involving ovulation, pregnancy, wound healing and blood pressure maintenance (Brown et al., 1992).

Angiopoietins and tie receptors: Angiopoietins and Tie receptors play a fundamental role throughout the angiogenesis process. The Tie2 receptor binds to angiopoietins (Ang1 and Ang2) and it is involved in vessel maintenance, stabilization and growth (Carmeliet, 2003).

Fibroblast Growth Factor (FGF) : FGF are heparin-binding protein mitogens which are involved in many EC related processes such as provoking EC proliferation and migration (Carmeliet, 2003).

Platelet-derived growth factor (PDGF) : PDGF exists in astrocytes, keratinocytes, epithelial cells, fibroblasts and other cell types (Bender, Cooney, Kandel, & Yamashiro, 2004). Studies on PDGF demonstrate their effect on angiogenesis *in vitro* and *in vivo* and also their ability to stimulate the proliferation of cultured SMCs and PCs (Edelberg et al., 1998).

1.3 Introduction to Bioprinting

Bioprinting is evolving as a promising method in the field of tissue engineering and can have revolutionary influence on biomedical sciences and pharmaceutics (Ozbolat, 2015). Bioprinting was first mentioned with cytoscribing collagen and fibronectin by Klebe in 1986, a technique of micropositioning cells and fabricating 2D synthetic tissues (Klebe, 1988). The recently developed bioprinting technique is used to fabricate live tissue and organs by depositing cells and other biologics layer-by-layer with the use of a computer-aided design. It allows very precise control on deposition of cells, DNA, growth factors, proteins and other bioactive substances to improve guidance of tissue formation. It possesses several advantages over the current tissue engineering strategies (Table 1).

Bioprinters require a set of equipment features and environmental factors in order to fabricate viable tissues (C. C. Chang, Boland, Williams, & Hoying, 2011).

1. Bioprinters require sterilization methods to prevent sample contamination while printing.
2. Bioprinter components should be compatible with ideal printing conditions such as humidity and temperature to simulate incubation environment for cell containing bioinks, maintain bioink humidity and to preserve tissue viability and fidelity.
3. The size of the nozzle and the printing surface plays an important role in the viability of the constructs. Therefore, they should be suitable with delivery methods related to the bioprinter modality.

Bioprinting allows patient specific tissue construction based on the image data from patients. In addition to controlled deposition of cells, it can also coculture multiple cells and extra cellular matrix (ECM) components locally.

Table 1. Comparison of tissue engineering methods (Mandrycky, Wang, Kim, & Kim, 2016).

	Assembly method		
	Bioprinting	**Molding**	**Porous scaffolds**
Materials	Natural and synthetic polymers High concentration cell solutions	Natural and synthetic polymers High concentration cell solutions Cell sheets	Natural and synthetic polymers Ceramics Metals
Resolution	10-1000 μm	> 500 nm	100 nm-1000 μm
Advantages	Control of tissue geometry across a wide range of scales; rapid production of scaffolds; precise cell and material patterning	Accurate control of small (< 100 μm) features; scaffold fabrication is rapid and often the molds are reusable; gentle on encapsulated cells	Controllable material properties (*e.g.* porosity, modulus); wide range of materials available for use
Disadvantages	Printing techniques may reduce cell viability or have unknown consequences; limited material selection due to crosslinking speed	Scaffolds are generally homogenous or require combination of multiple scaffolds to create patterns	Scaffold geometry is less controllable; technique may damage encapsulated cells or require seeding after assembly; less control of cell patterning
Techniques	Extrusion Laser-assisted Inkjet Stereolithography	Cell sheet stacking Lithography Injection molding	Electrospinning Phase separation Freeze drying Self-assembly

Figure 9A shows a comparison of a non-bioprinted versus bioprinted multilayer air-blood barrier model (Horváth et al., 2015). It is evident that bioprinting allows precise assembly of cells and ECM layers. Moreover, it provides an environment which supports cell-cell and cell-ECM interactions similar to the in vivo conditions. In a study (Figure 9B), bioprinted and 2D cultured HeLa cells were used as cervical tumor models. The results demonstrated that bioprinted HeLa cells formed tumor spheroids (Figure 9B1-B4) while 2D cultured cells only formed cell sheets (Figure 9(B5-B8)) (Zhao et al., 2014). Bioprinting also enables generation of

porous constructs along with controlled architecture and allows the integration of blood vessels into the constructs (Peng, Unutmaz, & Ozbolat, 2016).

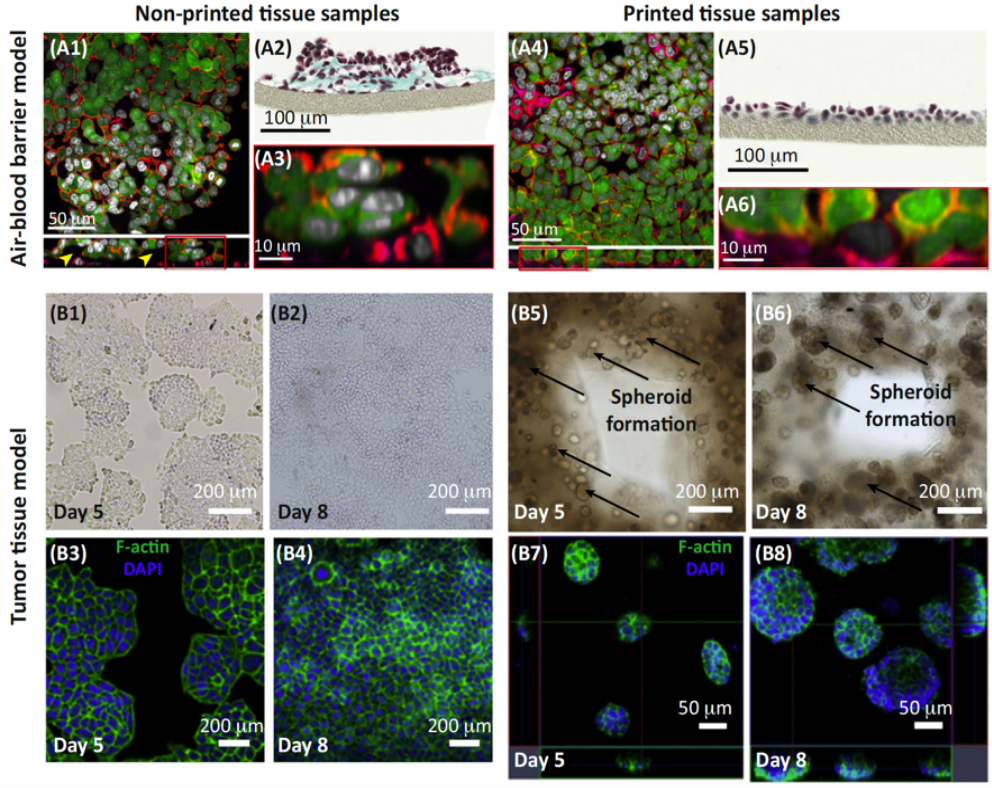

Figure 9. Comparison of non-bioprinted versus bioprinted tissue samples. An air-blood barrier model constructed of a Matrigel layer with seeded endothelial cells (ECs) on it followed by an Matrigel overlay with epithelial (A549) cells cultured on it (Horváth et al., 2015): (A1) The non-printed samples demonstrate a thick layer of Matrigel between the EC and the epithelial cells. (A2) Histological cross-sections display nonuniformity of the Matrigel layers and cells. (A3) Frontal cross-section demonstrates limited cell-cell interactions. (A4) The bioprinted air-blood barrier structure with uniform distribution and organization of the cells between the Matrigel layers. (A5) The histological cross-section shows a highly uniform thickness layer of the bioprinted tissue. (A6) Frontal cross-section shows a uniform layer of ECs at the bottom and a layer of epithelial cells at top. A cervical tumor model (Zhao et al., 2014): (B1-B2) phase-contrast microscopy images demonstrating HeLa cells in 2D culture at days 5 and 8. (B3-B4) Immunofluorescence microscopy images show HeLa cells possess elongated and flat morphology at days 5 and 8. (B5) Phase-contrast microscopy images demonstrates bioprinting deposited HeLa cells forming spheroids within gelatin/alginate/fibrinogen filament at day 5, (B6) on day 8 the spheroids grew larger by cell proliferation and aggregation. (B7-B8) Immunofluorescence images of the formed aggregates at days 5 and 8 (Peng, Unutmaz, & Ozbolat, 2016).

1.4 Bioprinting Technologies

Bioprinters are classified under three modalities, extrusion-based (EBB)-, droplet-based- (DBB) and laser-based bioprinters (LBB) (Figure 10, Table 2).

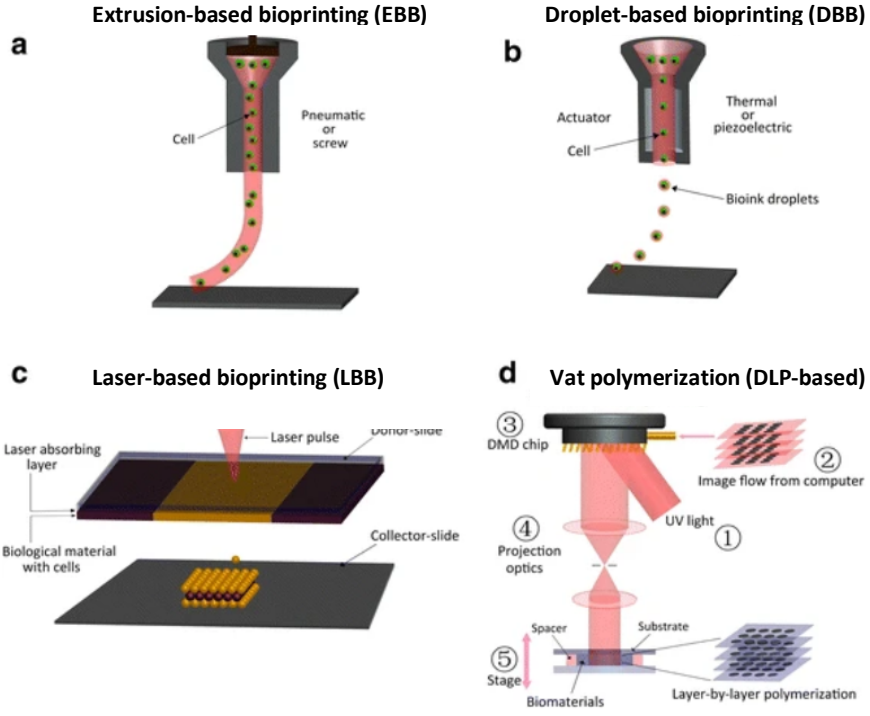

Figure 10. Schematic of bioprinting techniques (a) Extrusion-based (EBB) (b) Droplet-based (DBB) (c) Laser-based (LBB) (d) Vat polymerization bioprinters (P. He et al., 2018).

1.4.1 Extrusion-Based Bioprinters (EBB)

EBB is the most common modality used amongst bioprinters as an alternative to the scaffold-based strategy in recent years. Bioink is dispensed continuously through a micro-nozzle tip by a pneumatic or mechanical plunger to layout continuous cylindrical filaments (Figure 10a). Three main elements should be considered when using EBB: 1) adaptability of the viscosity, 2) the phase of the bioink before printing, and 3) selection of specific biomaterial (Y. He et al., 2016). Viscosity can be temperature or shear-thinning dependent and should be adjusted based on the printing methods used. The bioink used should be in a liquid state to prevent clogging in the nozzle. Also, the provided biomaterial should be compatible with different printing parameters (Derakhshanfar et al., 2018). This method offers predictability,

diversity and simplicity through utilization. The advantage of EBB compared to DBB is that it allows printing in high cell densities but possess low speed and resolution. Other advantages are a wide variety of biomaterial choices such as cell-encapsulated hydrogels and viscous polymers. This printing technology is considered less expensive than other bioprinter techniques. EBB enables the application of viscosity in a broad range of bioinks which consists of 30 mPa/s to above 6 x 107 mPa/s (Holzl et al.). Using higher viscosity biomaterials is more appropriate for mechanical stability of the structure while lower viscosity biomaterials are more suitable for cellular bioactivities (Bian et al., 2013; Little, Bawolin, & Chen, 2011). Printing larger filaments in diameter increases the mechanical support while inhibiting the nutrient and metabolic waste diffusion. The diameter decrease of the filaments resolves the exchange obstacle leading to the reduction of the mechanical properties. When printing cells, it is preferred to use bioinks with low viscosity to decrease the shear stress applied to the cells during extrusion. Crosslinking processes such as chemical- or physical- crosslinking mechanism is required for hydrogels to solidify post printing.

1.4.2 **Droplet-Based Bioprinters (DBB)**

In DBB bioprinters (also known as drop-on-demand or inkjet bioprinters), the bioink is delivered in the small form of droplets (1–100 picoliters; 10–50 μm diameter) to pattern desired structures layer-by-layer (Gudapati, Dey, & Ozbolat, 2016; Holzl et al.). Three models of DBB bioprinters that are used widely include thermal, piezoelectric and electrostatic DBB bioprinters (Figure 10b). In comparison to other bioprinter techniques, DBB offer fast printing with low cell density bioinks. The disadvantage of DBB is the limitation in the viscosity range of the bioinks that can be used. Furthermore, high viscosity and high cell density can result in the clogging of the printer head and nonuniform deposition (Datta et al., 2017). For DBB, the viscosity of the bioink is reported lower than 10 mPa s (Holzl et al.). The small nozzle may lead to high shear stress to the cells which can result in membrane damage causing cell death (Datta et al., 2017). Therefore, the bioink selection for DBB is limited Another disadvantage of DBB is named the “settling effect”. In the DBB setup, when the cartridge is supplied with the bioink, the bioink is well mixed at the beginning. However, through the printing process, the cells settle in the cartridge leading to cell aggregates. This increases the bioink viscosity which causes nozzle clogging (Pepper et al., 2011) (Mandrycky et al., 2016).

1.4.3 **Laser-Based Bioprinters (LBB)**

LBB is the only orifice-free printing method, it consists of two techniques of laser-induced forward transfer (LIFT) or vat photopolymerization. Vat photopolymerization is based on the light-induced reactions of the photopolymer substrate at the irradiated regions when exposed to ultraviolet leading to polymerization and hardening (Figure 10D). Vat photopolymerization includes stereolithography (SL), digital light processing (DLP), continuous liquid interface production (CLIP) and daylight polymer printing (DLP) by photocentric. LIFT technique was first introduced by Bohandy *et al*. more than 30 years ago for printing of inorganic materials (Bohandy, Kim, & Adrian, 1986) and widely adapted for printing biomaterials (Derakhshanfar et al., 2018). The main components that a LIFT bioprinter consists of is the laser beam source, a beam delivery system, a donor substrate and a receiver substrate. The donor or the receiver substrates are fixed onto a motorized holder connected to the computer program of the setup to provide required positioning with the laser beam (Figure 10C) (Koch et al., 2010). The top layer of the donor substrate is coated with an energy absorber layer such as gold or titanium, a thin layer of bioink is spread on top of the donor substrate. In the printing process, the laser beam is focused on an area between the energy absorbing layer and the bioink leading to the excitation of the absorbing layer to a higher vibrational energy state. The produced localized heat results in the vaporization of a bioink portion. The vaporization process creates a high-pressure bubble, bubble expansion produces a jet followed by bioink droplet ejection toward the receiver substrate (Bidanda & Bártolo, 2007; Devillard et al., 2014). The size of the ejected droplet depends on the laser pulse energy and the viscosity of the bioink. The receiver slide in this technique is pre-coated with gel materials such as fibrin, alginate and Matrigel, to reduce the impacting effect (Datta et al., 2017). Since LBB is orifice-free, nozzle clogging and shear stress applied to the cells is eliminated leading to high cell viability (95% and above) (Guillemot, Souquet, Catros, & Guillotin, 2010). Moreover, it enables the application of bioink materials with high viscosity among the range of 1 to 300 mPa/s. One of the main LBB advantages is higher printing resolution which depends on the laser energy, the pulse frequency, the distance between the donor and receiver substrates, bioink thickness, bioink viscosity along with wettability (Datta et al., 2017; Sasmal, Datta, Wu, & Ozbolat, 2018). Furthermore, other than cells, this technique allows printing of nucleic acids, growth factors and soil microparticles

(Antoshin et al., 2019). The required equipment for LBB is expensive compared to other bioprinter techniques and is time consuming to use. The receiver slide is coated with a metal film which can produce metal contamination (Datta et al., 2018). Despite these advantages, the preparation of each donor substrate required for each cell type is time consuming and difficulties are faced when co-printing multiple cell types and biomaterials. The challenge of preparing a thin and uniform bioink film is limiting for 3D printing. To print a structure with 1 cm^3 in dimension, preparation of a 1 m^2 bioink film is required (Orimi et al., 2020). The metallic residues in the printed construct resulting from the energy absorber layer can induce toxicity for cells. Table 2 provides a comparison between the EBB, DBB and LBB bioprinting techniques.

Table 2. Comparison of bioprinter technique. Adapted from (Murphy & Atala, 2014) and (Hölzl et al., 2016).

	EBB technique	**DBB technique**	**LBB technique**
Bioink viscosity	30-6 x 10^7 mPa s	<10 mPa s	1-300 mPa s
Gelation methods	Chemical, photo-crosslinking, sheer thinning, temperature	Chemical, photo-crosslinking	Chemical, photo-crosslinking
Preparation time	Low to medium	Low	Medium to high
Cell density	High, cell spheroids 200-1000 µm	Low <10^6 cells ml^{-1}	Medium (10^8 cells $ml^{-1)}$
Resolution	200-1000 µm	10-50 µm	10-110 µm
Single cell control	Medium	Low	Medium
Fabrication speed	Slow (700 mm s^{-1}-10 µm s^{-1})	Fast (10^5 droplets s^{-1})	Medium (200-1600 mm m*parison of* s^{-1})
Cell viability	80%-90%	>85%	>95%
Printer cost	Medium	Low	High

1.5 Cell Types for Printing

Cells are the key elements in the bioprinting of tissue structures. To form micro- or macro- scale tissues, the selected cells should be able to attach to the matrix and proliferate under the provided growth conditions. Cells are selected based on the following criteria: (1) cells should be able to simulate the physiological conditions of *in vivo* cells (2) the printed cells should preserve and develop their relevant physiological function in the matrix. To avoid the risk of immunogenic response, the cells should be obtained from the patients themselves rather than donors. The cell behaviour can be influenced by several factors related to the bioink composition and the biomaterial. The stiffness, the surface morphology and the functional groups of the biomaterial affect cell behaviour.

The selection of the cell incorporation method depends on several factors such as the aim of the study, the cell type and the printing technique. Two strategies are used for cellularization in 3D tissue printing: cell encapsulation throughout the printing procedure and seeding cells onto the already printed structure. The cell suspension method is suitable for sensitive and less proliferative cell types and cells that depend on interactions with the biomaterial. In this method, cells are mixed with the biomaterial before printing. Based on the applied printing technique, the cell containing biomaterial is then allowed to solidify through different methods. For the cell seeding approach, the cells can be seeded directly into the scaffold or they are mixed with a carrier material (X. Ma et al., 2018).

Three sources of cells are used for bioprinting applications: primary cells, stem cells and cell lines.

Primary cells: Primary cells are cells directly isolated from human or animal parent tissues and have the advantage of a similar karyotype and chromosome number to the tissue source (Lodish et al., 2003). If the cells are extracted at their healthy stage and through an appropriate procedure from the parent tissue, they are capable of recapitulating the tissue's specific behaviours and functions at a specific stage (Figure 11) (X. Ma et al., 2018). This allows the investigation of some basic *in vivo* cell behaviours using the primary cultured cells *in vitro* rather than invasive *in vivo* studies. For example, cardiomyocytes isolated from the heart tissue demonstrated spontaneously beating *in vitro* (Feinberg et al., 2007), osteoblasts harvested from

the bone deposit calcium phosphate and collagen (Bancroft et al., 2002) and ECs extracted from the umbilical vein form capillary-like structures when seeded onto an ECM matrix. Though harvesting primary cells for every tissue and organ was applicable, primary cells have low availability and, in some cases, can be very rare like cardiomyocytes. Moreover, they also have donor-to-donor or batch-to-batch variability and they are not patient specific making it less optimal for personalized applications. They also have limited lifetime in culture before reaching senescence. These difficulties have led to the development of cell lines (X. Ma et al., 2018).

Cell lines: Cell lines are cells that can be continuously subcultured *in vitro* and have been widely used to investigate both the basic cell and specific tissue functions. They are easy to use, inexpensive and simply obtainable. They also have a standard culture protocol and lack batch-to-batch variability. Several cell lines are used including epithelial, endothelial, connective tissue and cancer cells. Cancer cell lines are extensively used as models to investigate specific cancer behaviours *in vitro* (Kassem, Abdallah, Yu, Ditzel, & Burns, 2004).

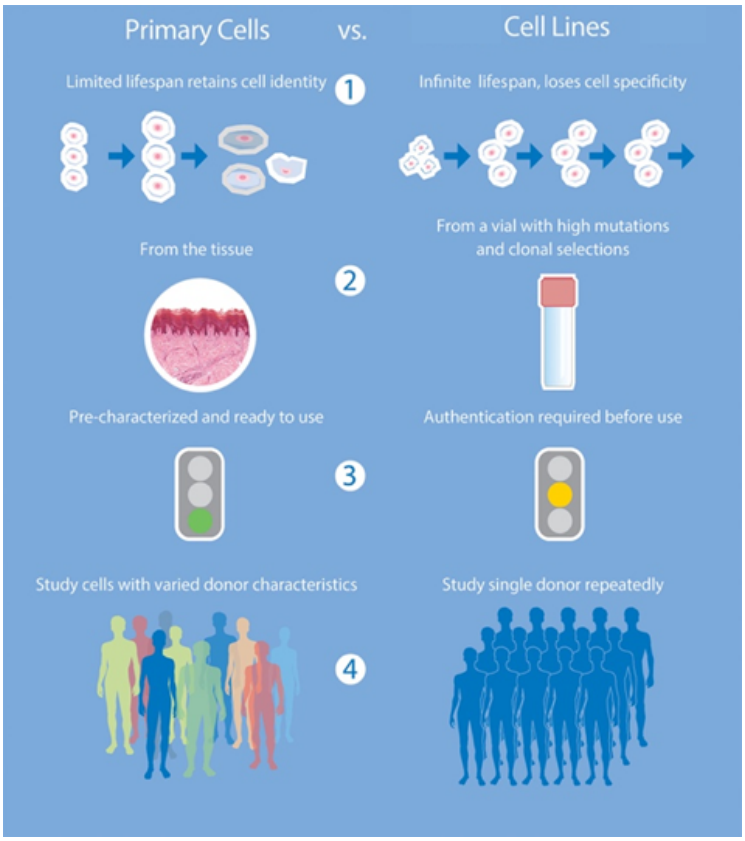

Figure 11. Primary cells vs cell lines. Advantages of primary cells over cell lines in biomedical research and drug discovery (Genetic Engineering and Biotechnology News, 2017).

However, cell lines should be modified genetically to induce immortality, making them different from the targeted cells. This should be taken into consideration when using tissue engineering applications (Kassem et al., 2004). Also, cell lines have unlimited differentiation which can result in the growth and formation of tumors *in vivo*. Similar to primary cells, cell lines are not patient specific (Kassem et al., 2004).

Stem cells: Stem cells are fundamental for human tissue development, maintenance and regeneration. Stem cells possess the ability to naturally differentiate extensively and at the same time directly differentiate into multiple cell lineages (Bianco & Robey, 2001). They are used for bioprinting applications when primary cells are less available and cell lines are not ideal (Figure 12). Generally, stem cells are in an undifferentiated state which allows them to self-renew and differentiate into multiple cell lineages. They are classified as mesenchymal stem cells (MSC), embryonic stem cells (ESC) and induced pluripotent stem cells (iPSC).

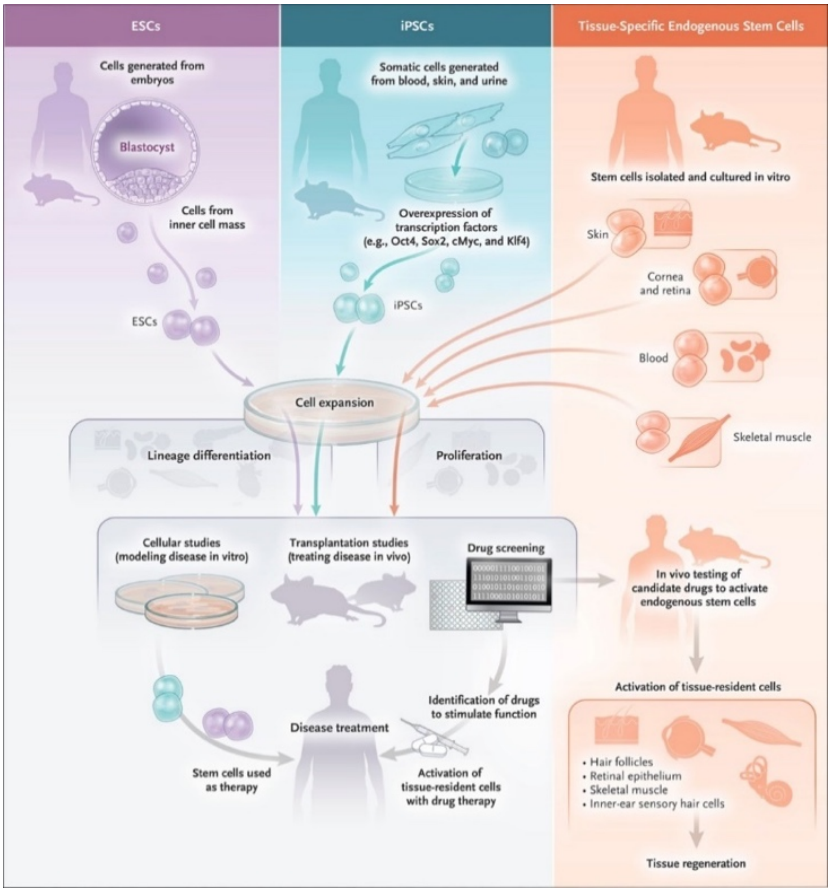

Figure 12. Types of stem cells and applications. Reproduced with permission from (Blau & Daley, 2019), Copyright Massachusetts Medical Society.

ESCs are harvested from a blastocyst (Thomson et al., 1998) and have the ability to differentiate into the endoderm, ectoderm and mesoderm layers (Smith, 2001). This allows ESCs to differentiate into over 200 cell types in the human body. The disadvantage of ESCs is that their unlimited growth factor feature can cause unlimited differentiation. Furthermore, ESCs are extracted from a discarded embryo which is limited in numbers and is controversial as a harvesting source (Thomson et al., 1998). The iPSCs are extracted from a mature fibroblast cell and similar to ESCs, iPCs also divide into the three germ layers with this difference that iPCs have the advantage to be obtained from the patient and be used for autologous implantation (Bellin, Marchetto, Gage, & Mummery, 2012). However, iPSCs vary batch-to-batch and most of the time, they are not functionally mature enough. They also have unlimited differentiation alike ESCs (Li, Zhu, & Young, 2017; Medvedev, Shevchenko, & Zakian, 2010).

1.6 ECM Biomaterials for Bioprinting

Biomaterial polymers play a crucial role in bioprinting. They should be selected with high consideration to meet the desired expectations of the bioprinted structure. Biomaterials used in regenerative medicine and biomedical applications include naturally derived or synthetic materials. Naturally derived biomaterials are often harvested from the human or animal tissue which consist of fibrin, alginate, collagen, Matrigel, gelatin, chitosan and hyaluronic acid. Some of the synthetic biomaterials that are currently used in bioprinting include poly(ε-caprolactone) (PCL), poly(ethylene glycol) (PEG), poly(l-lactic acid) (PLLA) and poly(lactide-co-glycolide) (PLGA) (Merceron & Murphy, 2015). Naturally derived and synthetic polymers each have their own advantages and disadvantages. The advantage of natural polymers is their ability to mimic the *in vivo* human ECM for the printed cells and their high biocompatibility. However, they have low mechanical stability limiting transplantation of the bioprinted structure. Synthetic polymers are of interest because their physical properties can be customized to suit specific applications. Their disadvantages include toxic degradation residue, low biocompatibility and poor mechanical properties due to degradation.

Based on the application of the tissue construct and considering the bioprinter technique employed, printing materials should possess ideal properties to facilitate both the printing and

the post printing process. These properties include viscosity, crosslinking-mechanisms, biocompatibility, mechanical properties, degradation and hydration (Figure 13).

Viscosity and cross-linking mechanisms define the printability of a biomaterial. Viscosity plays a crucial role when it comes to bioprinters with nozzle and can limit the biomaterial choice for bioprinters with low viscosity printing range such as DBB (Carrow, Kerativitayanan, Jaiswal, Lokhande, & Gaharwar, 2015).

To maintain cell viability when employing printing techniques that use localized heating such as thermal DBB and LIFT, the biomaterial should possess low heat conductivity to prevent cell death.

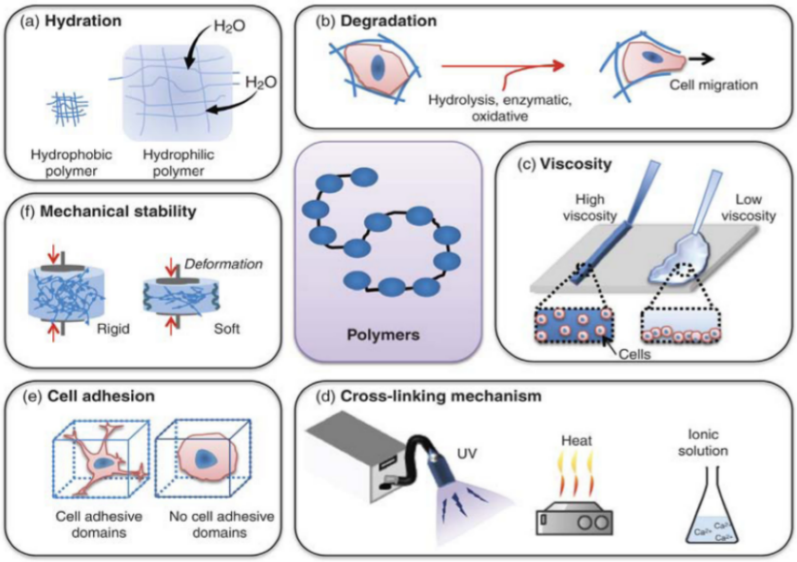

Figure 13. Polymer properties considered for bioprinting applications (Carrow et al., 2015).

Cross-linking of the biomaterial defines the final stability of the printed polymer network and also affects the viability of the cells embedded in the polymer. Cross-linking mechanisms include electrostatic-, pH-, photo-, ion- and temperature-based cross-linking mechanisms. EBB and DBB techniques enable printing of cells embedded in a biomaterial which forms a scaffold post printing. In the case of most of laser-bioprinting techniques such as LIFT, due to the inability in printing 3D structures, the ECM biomaterial is used as a receiver of the cell containing droplets and it is not deposited simultaneously via printing. Therefore, printability of biomaterial properties for LIFT is defined as “bioink printability”.

Biocompatibility of the polymer is essential for constructing viable tissues with the aim of not only preventing local or systemic host response, but also actively contributing to the biological goal and function of the construct. Biocompatibility consists of cell activity support, interaction with other internal tissues and promoting signaling systems (Murphy & Atala, 2014).

Cellular behaviour is determined by the physical properties of the biomaterial such as surface energy and hydrophilicity. Cell binding moieties are required for polymers to promote cell attachment and proliferation. The lack of cell binding surfaces leads to cell death in synthetic and some natural polymers such as gelatin which can be further improved by the addition of cell adhesive molecules.

The mechanical properties of a biomaterial should be carefully selected based on the structural requirements of the constructed tissue to mimic their native counterpart. Moreover, the maintenance of the mechanical properties is essential to provide support over a period of time until complete tissue development.

Biomaterial degradation rate should be tuned to be compatible with cell proliferation and the ability for the cells to produce their own ECM. For biomaterials that require degradation, produced residues should be non-toxic for *in vivo* applications. Toxicity can be the outcome of a physiological stimuli which includes small proteins and non-physiological stimuli such as pH temperature. Hydration properties are another property which should be considered when selecting a polymer. Hydration can greatly influence the viscosity and the porosity of the biomaterials which control viscoelasticity, mechanical strength and the pressure resulting from the nozzle during the printing process. Furthermore, hydration promotes oxygen and nutrient transfer to the embedded cells within the polymer mimicking *in vivo* conditions. However, due to the large pores existing in hydrophilic polymers, water uptake results in decreased mechanical strength (Carrow et al., 2015).

1.6.1 **Fibrin and Matrigel as Natural ECMs**

Both fibrin and Matrigel hydrogels can be used as the ECM scaffold for cell printing. Fibrin is a naturally occurring protein-based gel which has been long known as a scaffold for microvascular network formation *in vitro*. It is suitable as a naturally angiogenic scaffold due to its similarity to the physiological fibrin clot formed *in vivo* during coagulation process.

Moreover, fibrin produces cellular components of ECM proteins such as the basement membrane which is essential for forming a stable microvascular structure and type I collagen supplying it with the tensile strength required for tissue construction. Fibrin can be used to stimulate endothelial assembling in the long term by delivering contained growth factors during several days. It is composed of fibrinogen and thrombin (proteose enzyme) as fundamental components. Thrombin converts fibrinogen enzymatically into fibrin with a fibrillar 3D network (Figure 14).

The role of fibrin-based biomaterials has been studied as a biological ECM for tumor growth and wound healing process. Fibrin matrixes have high attachment to other biological surfaces along with biodegradable and biocompatible features. Furthermore, fibrin has cellular binding sites leading to superb cell seeding properties. Because of its specified interaction with vascular cells, fibrin has been considered as a potential scaffold for vascular tissue engineering. In addition, fibrin gels can be generated using the patient's own blood as an autologous scaffold to prevent immune response. This biodegradable matrix has been used in several tissue engineering applications including bladder, cornea, cartilage, nerve, bone, skin, liver, wound healing, urinary bladder, cardiac muscles and valves (Morin & Tranquillo, 2013; Shaikh et al., 2008).

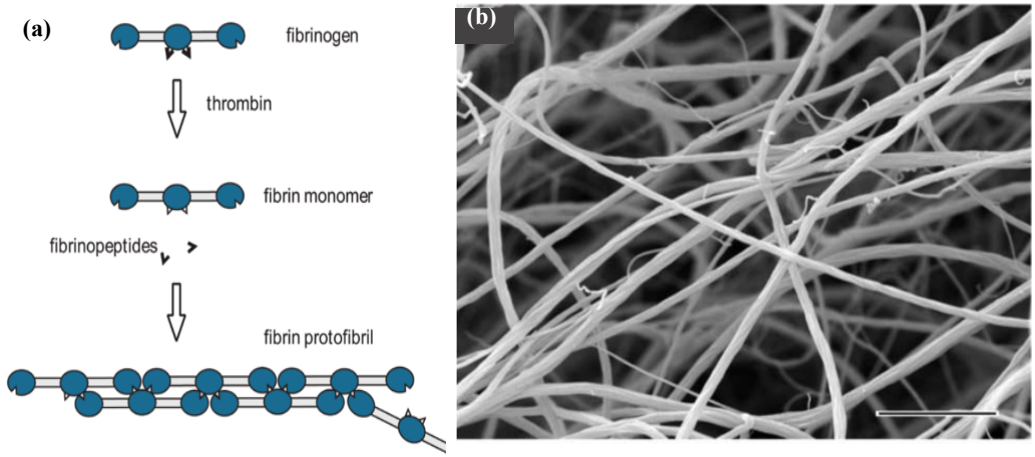

Figure 14. Fibrin formation. (a) Thrombin cleaves fibrinogen which detaches into fibrin monomer and fibrinopeptides. Fibrin monomers become unstable and form fibrin protofibrils that eventually create fibrin networks (Chernysh, Nagaswami, Purohit, & Weisel, 2012) (b) Scanning electron microscopy (SEM) of fibrin clot (Weisel, 2004).

Matrigel is the trademark name for a gelatinous protein mixture which is obtained from mouse tumors and is used as a basement membrane matrix (Figure 15). Studying the composition and function of the basement membrane has been difficult due to its thin structure. Matrigel has been found to contain basement membrane components such as collagen IV, enactin and laminin. This basement membrane ECM has been widely used to study cell differentiation, angiogenesis and tumor growth. Cell differentiation on Matrigel depends on the cell type and once differentiated, the Matrigel can be transplanted back into the animal tissue for repair or regeneration. Cells usually form 3D structures similar to the tissue source on or in this matrix. For example, ECs align one-hour post seeding and generate tube structures with lumens overnight.

Matrigel, is also used for *in vivo* applications to increase the growth of tumors, to study stimulators and inhibitors in angiogenesis, for improving graft survival and repairing tissue damage. Moreover, Matrigel is widely used for stem cells because it maintains the cells in an undifferentiated state (Hughes, Postovit, & Lajoie, 2010; Kleinman & Martin, 2005).

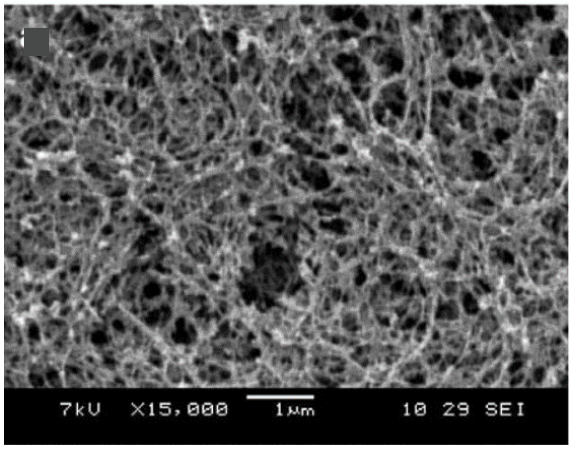

Figure 15. SEM image of Matrigel (Gelain, Bottai, Vescovi, & Zhang, 2006).

1.7 **Bioprinting Applications**

There is a high demand for engineered human tissues that are capable of mimicking specific function both *in vitro* and *in vivo*. Due to the bioprinting's great advantage in patterning multiple cells and biomaterials precisely, it has broad applications (Figure 16). Pre-clinical drug

screening and cancer research are considered as near-term applications while tissue and organ replacement in longer terms.

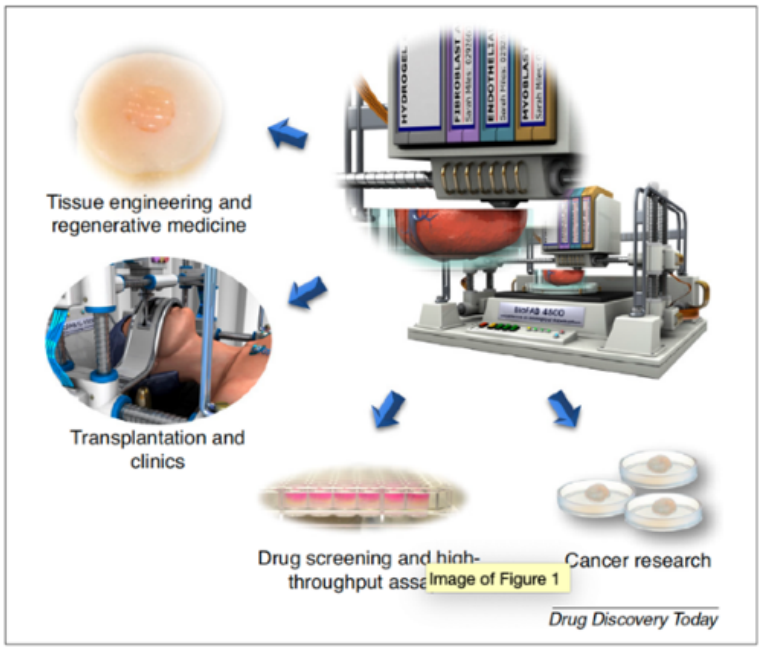

Figure 16. Bioprinting application areas (Ibrahim T. Ozbolat, 2016).

1.7.1 **Drug screening**

Today, only one out ten drugs enters the market after tested in clinical trials (DiMasi, Grabowski, & Hansen, 2015). A large number of drugs fail the clinical trial tests due to low efficacy, safety issues and adverse events (Waring et al., 2015). The path of drug discovery consists of three screening drug procedures starting with tests on 2D cell culture models, followed by testing on animal models and at the end being tested in clinical trials. 2D models lack the ability to simulate the complex 3D structure of the native tissue such as the cell-cell and cell-ECM interactions which makes them unpredictive and prevents them to be reliable as a model for *in vivo* responses. In addition, the drug screening models should enable high-throughput screening (HTS) prior to testing their toxicity in animal models. HTS is an automated drug discovery process that allows quick testing of a large sample of biological or chemical compounds for a specific biological target. To fasten the drug discovery process, unreliable and ineffective toxic compounds should be eliminated, and models should be developed to closely simulate the *in vivo* physiological conditions. Currently 3D *in vitro* models have promoted the

drug screening process by recapitulating the native tissue and their physiological response to drugs (Rimann & Graf-Hausner, 2012). Several techniques are applied to fabricate 3D models for drug screening such as microfluidics (Shin et al., 2012), micropatterned matrices (Sakar et al., 2012), a microwell (D. W. Lee et al., 2014), magnetic force- (Tasoglu et al., 2015) and acoustic force- (Xu et al., 2011) based techniques. Despite the advantages of 3D models, they also face several limitations such as batch-to-batch biological variation of ECM matrices and their requirement to large number of cells and cell types to construct a complex tissue-like structure. Furthermore, despite several improvements, 3D models still lack vascularization which plays a key role in tissue growth and drug delivery.

Bioprinting stands as a promising technique to generate 3D models such as organoids, organ-on-a-chip and tissue structures for drug screening, HTS and pharmaceutics. Bioprinting technique enables deposition of cells uniformly on the surface of the microdevices which is highly important for drug screening applications. Moreover, it allows co-deposition of multiple cell types precisely on the microdevice. Existing bioprinted drug screening platforms include those that are used for mimicking the liver organ. These platforms also show that bioprinting can be combined with microfluidic techniques for drug screening. Employing EBB, immortalized hepatocytes encapsulated in alginate were printed onto a platform. The liver platform by Chang *et al*, was used to demonstrate differential drug metabolism (Chang, Emami, Wu, & Sun, 2010). This system was further developed and used to evaluate the effect of radiation on tissue damage. This was obtained by printing microfluidic channels in co-cultures of liver (HepG2) and human epithelial cells (M10) both encapsulated in Matrigel (Snyder et al., 2011).

Another existing bioprinted drug platform are organ-a-chip systems that mimic specific functions of an organ and their interactions with the tested drug. Since organs are physiologically under the influence of other organs, to simulate *in vivo* environment for organ interactions, different organ specific cell types can be printed at different locations on a single platform. The organs are connected through a microfluidic circulatory system. This platform referred to as “human-on-a-chip, still faces several challenges and is under development by investigators (Huh, Hamilton, & Ingber, 2011).

EBB and DBB technologies have been already employed to generate drug screening platforms, but LBB modality has not been applied to pharmaceutical use yet (Ibrahim T. Ozbolat, 2016).

1.7.2 Tissue Regeneration

Several challenges such as tissue vascularization, limited mechanical and structural integrity and the necessity to incorporate multiple cell types exists in the creation of complex functional organs (Ozbolat & Yu, 2013). Therefore, bioprinting of these organs in clinically relevant dimensions remains elusive. The constructed tissues are mainly translated to transplantation in murine models which their physiological conditions differ from the human (Ozbolat, Peng, & Ozbolat, 2016), indicating the need to overcome the current limitations to reach the clinical transplantation stage of the bioprinted organs. Until now, only tissues with a simple, flat and hollow geometry have been fabricated by bioprinting. Tissues such as skin, cartilage and cornea have been already constructed and tested, and will soon be the first of the bioprinted tissues to reach clinical applications. Tissues such as blood vessels, urethras and tracheas are still under development and are likely to reach clinical application. Complex tissues such as kidney will require a longer time to overcome the existing challenges (Figure 17) (Murphy & Atala, 2014).

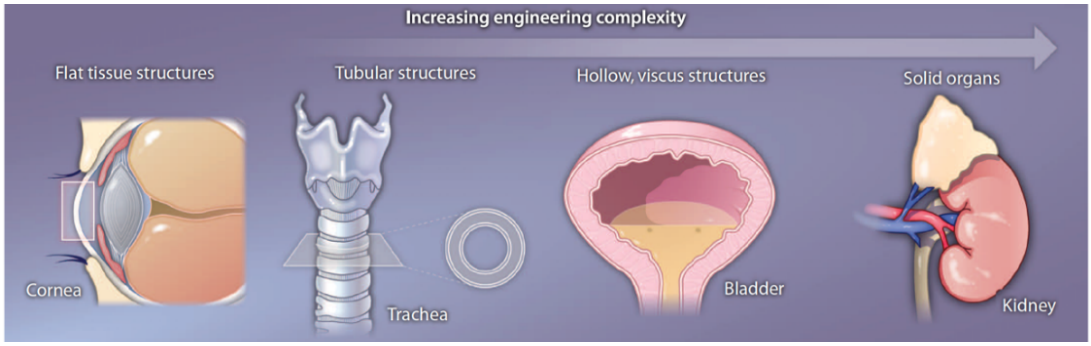

Figure 17. Four structural levels of complex tissues and organs. Tissues and organs are classified into four levels based on their structure complexity: Flat tissues structures such as the cornea , tubular structures such as the trachea and blood vessel, hollow structures such as the bladder, and the most complex organs are solid organs such as the kidney (Atala, Kasper, & Mikos, 2012) (Credit: C. Bickel/Science Translational Medicine).

1.8 Comparison of Different Bioprinting Technologies for Vascular Printing

Although, several bioprinting techniques can be used to fabricate vascular constructs and vascularized tissue, they differ extensively in fabricating constructs with viable, functional, anatomically precise, physiologically relevant and stable mechanical features. The appropriate bioink and bioprinter modality should be applied depending on the physiological function, target anatomy structure and target organ wherein vascularization is desired (Figure 18).

EBB techniques are used for creating vascular constructs with larger dimension and high aspect ratio compared to DBB and LBB techniques. EBB can be applied in direct and indirect printing approaches. The direct approach allows creating blood vessel models but lacks the ability to generate complex branched constructs. This is applicable with indirect printing which fabricates complex branched structures by printing sacrificial ink to produce lumen opening after sacrificial ink removal. The lumen openings are lined with cells for vessel formation.

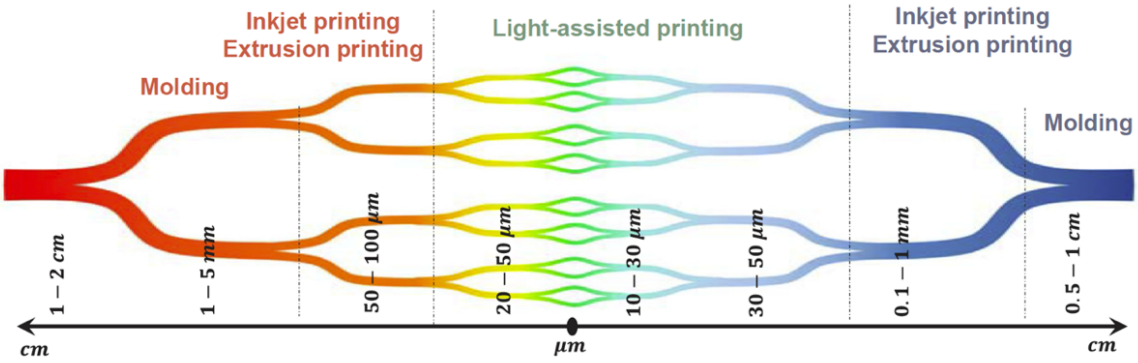

Figure 18. The summary of vasculature hierarchy (from arteries to veins) and the range of diameter at each level, along with current technologies used to generate biomimetic tissue construct (Miri et al., 2019).

Despite the great benefit of indirect printing in complex patterns, the layer thickness should be taken into consideration to avoid stair stepping effects resulted from blockages during sacrificial ink removal (W. Wu, DeConinck, & Lewis, 2011). EBB is easy to generate hollow channels for vessel formation but lining these structures with ECs for lumen development is still a challenge. Further improvement of EBB technology is required to fabricate precise and complex structures in the microscale. Due to this reason, in the literature, less studies have

considered EBB for micro-structures and limited number of micro-capillaries are formed by EBB compared to DBB and LBB.

The greatest advantage of the DBB technique is the ability to generate extremely small droplet sizes making it a high resolution bioprinter suitable for constructing micro-capillaries. It also allows fabrication of high-resolution structures and co-culture of multiple cell types in pre-defined patterns. Despite all the advantages, DBB is not capable of constructing large scale vessel structures. Bioink selection is a challenge when printing hydrogels. To avoid nozzle clogging, the bioink viscosity should be within a range that is compatible DBB nozzle. In addition, nozzle shear stress induces cell death, undesirable cell aggregation and bioink settling leading to nozzle clogging.

LBB technology offers the highest printing resolution for microvessel fabrication compared to EBB and DBB. It possesses the lowest cell damage with cell viability up to 95%. SL technique based on LBB, allows high precision patterning of branched microvascular structures mimicking *in vivo* vascular network. However, options of photocurable hydrogels and photo initiators are limited when using stereolithography (SL). Moreover, the possibility of toxicity exists when using these agents and the light. Due to inability of LBB in printing 3D structures and low mechanical properties, LBB constructs are considered more of a model than a tissue structure. Furthermore, LBB bioprinters are more expensive and complicated to use.

1.9 **Bio-printing of Micro-vascular Structures**

In the literature, a limited number of studies have demonstrated blood vessel fabrication via LBB technologies. In this section, studies that have used different technologies to generate micro-vascular structures has been reviewed.

Using the LIFT technology, branch-stem structures of HUVECs were printed on Matrigel by Wu and Ringeisen. Cell-cell arrangements were observed one day post printing but lacked stability (Figure 19A). The stability was improved by printing a upper layer of human umbilical vein smooth cells (HUVSMCs) above the HUVEC layer (P. Wu & Ringeisen, 2010). In this study, cell-cell arrangements were successful using LIFT technique. However, the

authors did not investigate the internal structure of the formed branch-stem architectures to interrogate lumen development.

Printing HUVECs on biopapers was also studied by Pirlo *et al*. Stackable porous poly-lactide-co-glycolide (PLGA) biopapers were loaded with collagen or Matrigel and were used as printing substrates. HUVECs were then printed on the biopapers into zigzag-staff patterns (Figure 19B). Although, HUVEC interactions and HUVEC network formation was observed (Pirlo, Wu, Liu, & Ringeisen, 2012), yet lumen formation was not investigated.

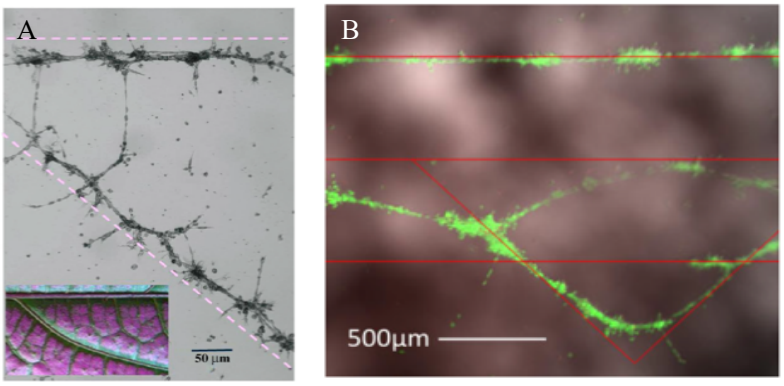

Figure 19. HUVEC branch/stem structure printed via LIFT 1 day post printing (P. Wu & Ringeisen, 2010). (B) Live/dead staining of LIFT printed HUVECs 24h after culture, red lines indicate the initial printed zigzag-staff pattern (Pirlo et al., 2012).

Kérourédan *et al*. studied HUVEC printed cells performed by LIFT on collagen type I hydrogel embedded MSCs. The addition of collagen I hydrogel overlay on the printed patterns containing vascular endothelial growth factor (VEGF), induced the formation of capillary-like structures. This study shows successful HUVEC patterning and network formation along the printed patterns (Figure 20A) (Kérourédan et al., 2019). However, formed networks were interwoven not offering precise control over each formed endothelial tube and also lumen development was not analyzed.

In another study, Gaebel *et al* printed HUVECs along with MSCs using LIFT on a polyster urethan urea (PEUU) cardiac patch. HUVEC gridlines were bordered with MSCs which studies have demonstrated that MSCs stimulate the angiogenesis process (Figure 20B). LIFT-tissue engineered cardiac patch demonstrated vessel formation with significant improvement of the infarcted hearts post implantation. The engineered cardiac patch can improve myocardial infarction treatment leading to functional preservation and wound healing (Gaebel et al., 2011).

Using a common modified form of LIFT (matrix-assisted pulsed-laser evaporation direct-write), Xiong *et al* printed both straight and Y-shape structures with alginate hydrogel bioink containing mouse fibroblast cells (Figure 21). The 3D Y-shaped fibroblast tubes possessed stability and cell viability was above 60% post-printing (Xiong, Zhang, Chai, Huang, & Chrisey, 2015).

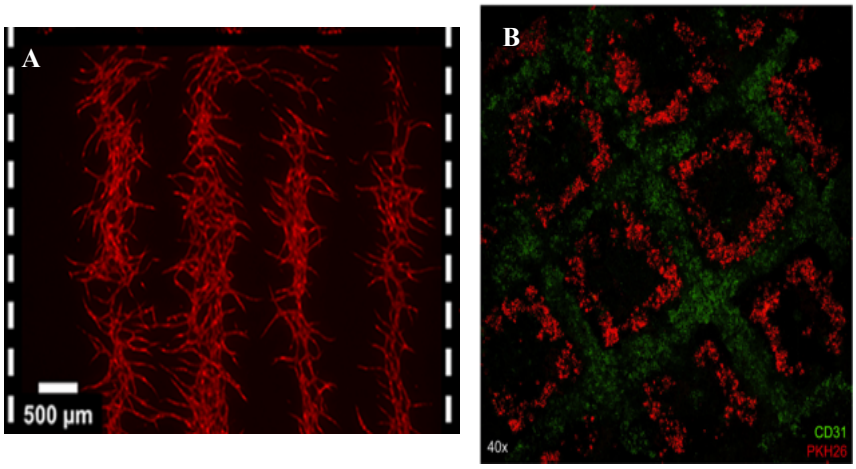

Figure 20. (A) Capillary-like network formation 3 days post LIFT printing (Kérourédan et al., 2019) (B) Shows HUVECs and MSCs arrangement by LIFT printing on the cardiac patch 24h post printing, MSCs were prestained with PKH26 and the patches were stained with polyclonal goat anti-Pecam1 24 hour after printing (Gaebel et al., 2011).

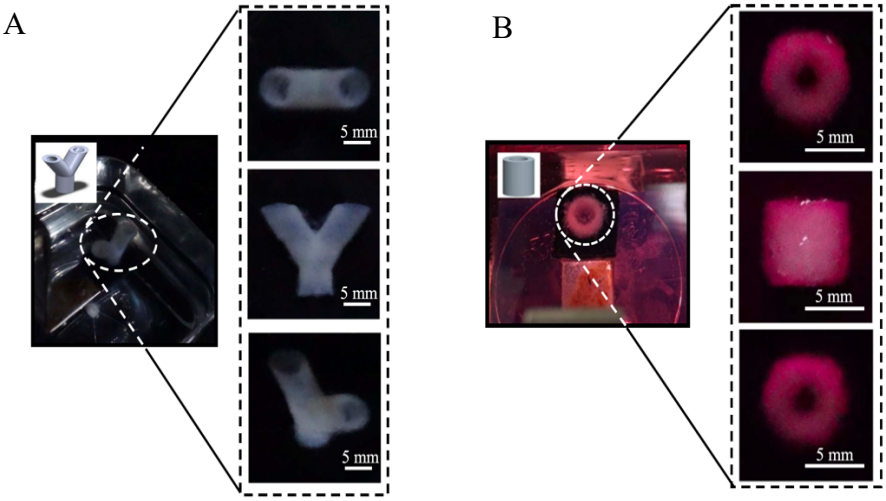

Figure 21. Representative images of Y-shaped alginate laser-printed tubes (A) Tubes printed using 8% alginate solution (B) Tubes printed using 2% alginate solution and mouse fibroblast cells (Xiong et al., 2015).

A near-infrared femtosecond laser was also used to produce 3D channels by heating gold nanorods embedded in collagen containing Bend3 mouse endothelial cells (Figure 22A). The heat was absorbed by gold nanorods causing in-situ denaturation of the surrounding collagen generating hollow 3D channels. Encapsulated endothelial cells in collagen migrated toward the 3D channels where they proliferated and possessed a 3D alignment allowing endothelial tube formation after 14 days (Figure 22B) (Kolin C. Hribar et al., 2015). Despite lumen development (Figure 22C), this model can be affected by several variables such as matrix stiffness, nonuniform cell migration and gold nanorod clearance procedure.

Digital light processing (DLP) 3D printing is a vat polymerization laser-based bioprinter technique which is advantageous due to its resolution, speed, flexibility and scalability. Zhu *et al* used a micro-scale continuous optical bioprinting (μCOB) based on DLP to design pre-vascularized tissue (Figure 23A). HUVEC and mesenchymal cells (liver hepatocellular HepG2 cells) were printed into the microvascular 3D designed channels (Figure 23). This process induced lumen-like structure formation by HUVEC cells in-vitro. When implanted in-vivo, anastomosis between the HUVEC network and host circulation with functional vessels containing red blood cells was detected (Zhu et al., 2017).

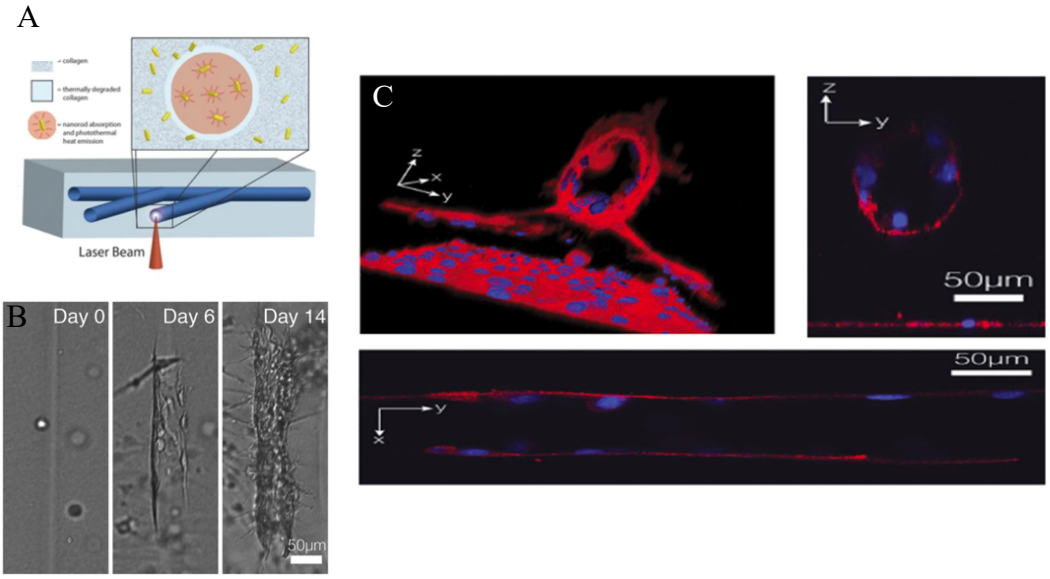

Figure 22. Endothelial tube formation by near-infrared femtosecond laser (A) Schematic of the patterning process and resulting cell response (B) Brightfield images of cell migration and tube formation (C) Confocal microscopy and 3D reconstruction of endothelial tube (Kolin C. Hribar et al., 2015).

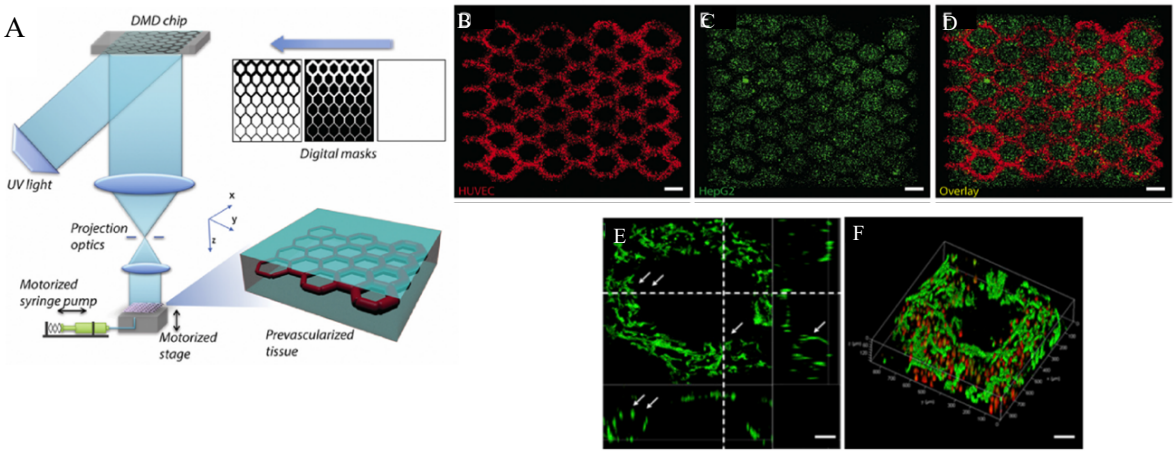

Figure 23. 3D printing of vascularized tissues (A) Schematic of bioprinting platform (B-D) Fluorescent images showing the bioprinting of 3D cell-laden tissue constructs HUVECs (red) are encapsulated in the intended channels and HepG2 (green) are encapsulated in the surrounding area (scale bar: 250 µm) (E) Cross section view demonstrates the HUVECs (green, stained with CD31) form lumen-like structures (marked by white arrows) along the printed microchannel (F) 3D reconstruction of HUVECs lining the microchannel wall (scale bar: 100 µm) (Zhu et al., 2017).

A design of complex vascular networks was printed on poly(ethylene glycol) diacrylate (PEGDA) using a stereolithography based laser bioprinter called dynamic optical projection stereolithography (DOPsL) (Figure 24) (Kolin C Hribar, Soman, Warner, Chung, & Chen, 2014). Further studies are required to implement vascular cells through the printed vascular pattern.

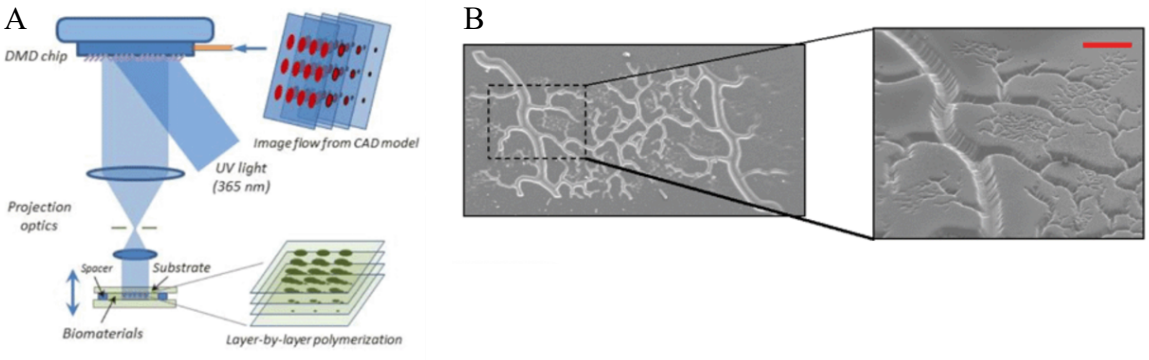

Figure 24. DOPsL printing of vascular network (A) Schematic of DOPsL (B) SEM image showing complex vascular network (scale bar: 100 µm) (Kolin C Hribar, Soman, Warner, Chung, & Chen, 2014).

To generate engineered bone grafts with micro vascularization, Fedorovich *et al* used an extrusion based multi-head tissue/organ bioprinter. In their study, heterogeneous structures containing goat endothelial progenitor cells (EPCs) and multi-potent stromal cells (MPSCs) were fabricated with the application of combined alginate and Matrigel-based bioink (Figure 25). Although bone formation and perfused blood vessels were detected six weeks post implantation, the constructs lacked sufficient mechanical stability (Fedorovich, Wijnberg, Dhert, & Alblas, 2011).

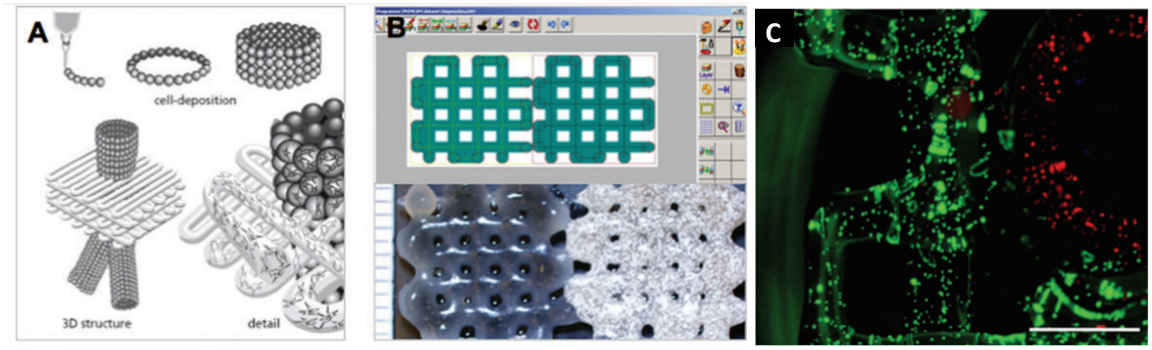

Figure 25. Printing heterogeneous constructs for vascularized bone tissue engineering (A) Schematic representation of the 3D fiber printing process (B) Model of the heterogeneous dual construct (top), printed graft (bottom); EPC-laden Matrigel part (left), MSC-laden Matrigel part including biphasic calcium phosphate (BCP) (right). (C) Fluorescently labeled populations of EPCs (red) and MSCs (green) (scale bar: 1 mm) (Fedorovich et al., 2011).

Using the same bioprinter technique, poly(caprolactone) (PCL) was constructed as a framework for liver tissue engineering due its supreme mechanical properties. PCL channels was loaded with collagen bioink consisting of three cell types, HUVECs, hepatocytes, and normal human lung fibroblasts. Co-cultured hepatocytes with non-parenchymal cells improved vascular formation and survival of hepatocytes (Figure 26). This study suggests that the fabricated 3D structure has a potential for liver tissue regeneration (J. W. Lee et al., 2016).

To form endothelialized microfluidic vessels, molding microstructures were applied on native collagen type I with injection molding techniques. HUVECs were seeded within the microstructures leading to successful microvessel formation along with lumen development. The interactions of this three-dimensional microvascular network with perivascular cells such as human umbilical arterial smooth muscle cells (HUASMCs) or human brain vascular pericytes (HBVPCs) seeded in collagen matrix was investigated (Figure 27). Angiogenesis in healthy and

pathological scenarios and thrombosis under quiescent and inflammatory conditions were analyzed, an indicative for the usefulness of this technique for the study of cardiovascular biology and pathophysiology (Zheng et al., 2012).

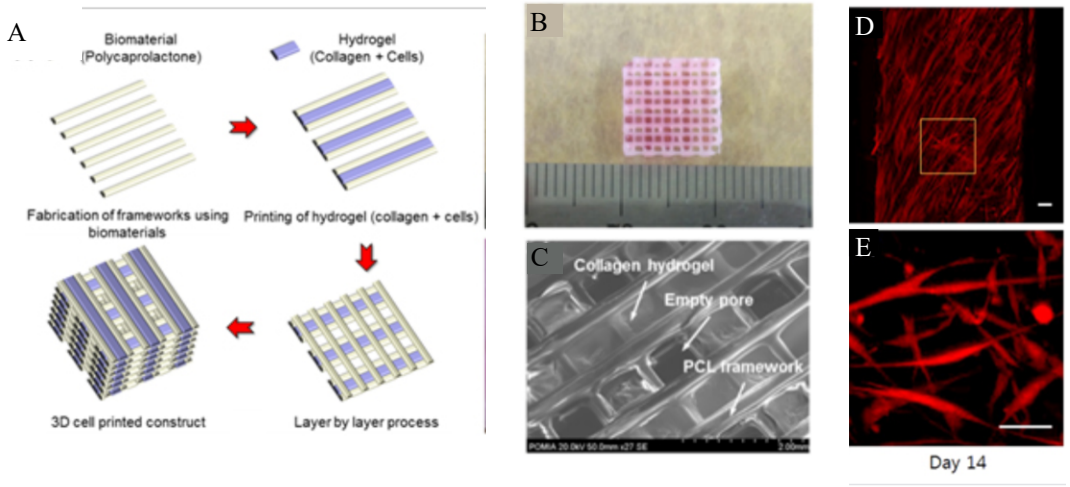

Figure 26. 3D cell printing construct for liver tissue engineering (A) Schematic of 3D cell printed scaffold fabrication process (B) Image of 3D cell printed construct (C) Scanning electron microscope (SEM) image of a freeze-dried 3D scaffold (D-E) Confocal microscopy image of capillary network formation by HUVECs in the printed collagen line at day 14 (scale bar: 50 μm) (J. W. Lee et al., 2016)

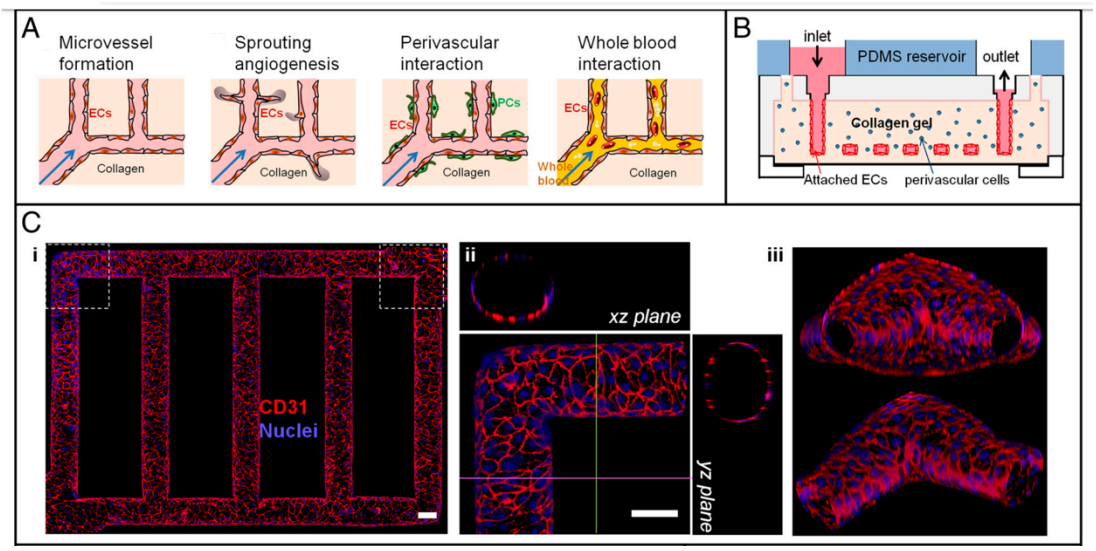

Figure 27. Microfluidic vessel networks (μVNs). (A) Schematic cross-sectional view of a section of μVN illustrating (B) Schematic of microfluidic collagen scaffolds after fabrication (C) Confocal microscopy images of endothelialized microfluidic vessels (D) Z-stack projection of horizontal sections of overall network (E) Corner view (F) branching sections Red, CD31; blue, nuclei (scale bar: 100 μm) (Zheng et al., 2012).

To overcome current limitations in thick tissue generation, Kolesky *et al*, constructed a thick (e.g., over 1 cm) vascularized bone tissue, printed on a 3D perfusable chip and with long term perfusion (>6-week), by applying indirection extrusion (Figure 28). First, a perfusion chip was printed using a silicone ink. Then, pluronic F127/thrombin blend fugitive ink and cell-laden bioinks were printed into the 3D perfusion chip. The cell-laden bioink contained human bone marrow-derived mesenchymal stem cells (hMSCs), fibrinogen and gelatin. To form an ECM matrix, a composite material including human neonatal dermal fibroblasts (HNDFs), gelatin, fibrinogen, thrombin and transglutaminase was then cast over the printed inks. After matrix solidification through cross-links of fibrin and gelatin, the sacrificial bioink was evacuated after liquifying by cooling. The hollow tubes were then perfused with HUVECs with an external pump to form vessels (Kolesky, Homan, Skylar-Scott, & Lewis, 2016). Not only this study featured the advantage of fabricating a thick vascularized tissue, but also confocal assessment demonstrated lumen development of the formed vascular network (Figure 28D).

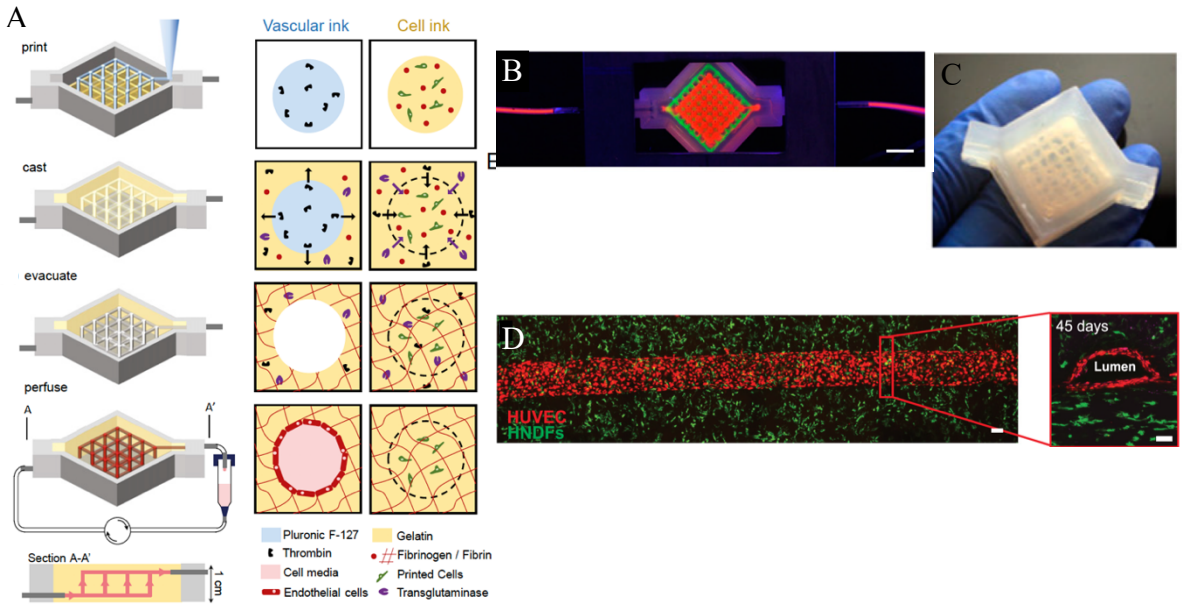

Figure 28. Three-dimensional vascularized tissue on a perfused chip (A) Schematic illustration of tissue fabrication process (B) Printed tissue construct within a perfusion chamber (C) Printed tissue construct removed from the perfusion chamber (D) Confocal microscopy of HUVECs (red) lining vascular network supported by HNDF-laden (green) matrix at 45 days of perfusion (scale bar:100 µm) (Kolesky et al., 2016).

2. Thesis Outline

Angiogenesis plays a pivotal role in blood vessel formation leading to tissue generation and viability maintenance. Therefore, new engineered tissues require angiogenesis and vascular network. Many research efforts in engineering of prevascularized tissue has relied on the spontaneous organization of ECs to form vascular networks on scaffolds. This type of organization leading to uncontrolled angiogenesis faces limitations such as the random organization of the vascular network and the spacing between vascular structures may be larger than 200 μm. Moreover, it does not offer clear locations for natural or surgical anastomosis which results in a delay in network perfusion to the vasculature of the patient.

To mimic the *in vivo* vascular network consisting of capillaries, precise artificial guidance within the microscale should be provided. This can be obtained by LBB techniques. The aim of this study is to guide HUVEC tube formation by printing HUVECs into precise patterns via LBB technologies to construct microvascular structures. In this research, two laser-based technologies, LIFT along with laser-induced side transfer (LIST), a recent technique developed in Dr. Boutopoulos's lab (Orimi et al., 2020) were studied and compared as high resolution printing techniques to deposit cells in precise patterns to guide HUVEC tube formation.

The hypothesis of this study is that pre-patterning of HUVECs by laser-bioprinting can guide the direction and structure of the angiogenesis process in-vitro.

The research objectives for this study are:

- Determining the most appropriate laser bio-printing technology
- Determining the optimum matrix for guiding laser-assisted angiogenesis
- To guide angiogenesis for the first time using a laser-assisted home-developed bioprinter

Prior to studies involving laser-bioprinting, ideal bioink formulations, printing substrate compositions (fibrin and Matrigel) were investigated to meet the aim of the study. Also, conventional HUVEC tube formation was studied by using fibroblasts as a second cell type to promote lumen formation.

3. Experimental Methods

3.1 Cell Culture and Maintenance

HUVECs are the major source of primary ECs for research in vascular biology. This is because human umbilical veins are more available compared to other blood vessel cell types. HUVECs are relatively easy to harvest and culture. They are widely used to study the development and pathologies of microvascular network *in vitro* (Cao et al., 2017).

HUVECs (PromoCell) were cultured in EndoGRO VEGF-medium (Millipore) with 1% Penicillin-Streptomycin Solution (Corning). The cells were grown in petri dishes coated with 0.1% bovine gelatin in sterile water and were cultured at 5% CO_2, 37 °C. Passages 3 and 4 cells were used for the experiments.

Fibroblast lung cells (IMR90 P20) were cultured in DMEM 1x medium (supplemented with 10% Fetal bovine serum and 1% Penicillin-Streptomycin, Corning) and at 5% CO_2, 37 °C. Passages 17 and 20 cells were used for the experiments.

3.2 Fibrin Solution Preparation

In this present study, fibrinogen solution is used for fibrin matrix preparation and as the bioink for cell suspension used for bioprinting applications. Fibrinogen solution (5 mg/mL^{-1}) was prepared by dissolving fibrinogen from bovine plasma (Sigma) in warm EndoGRO Basal medium (Millipore) at 37°C. The solution was placed on an orbital shaker for 15 minutes for complete dissolution. After sterile filtering, a final concentration of 50 $\mu g\ mL^{-1}$ aprotinin from bovine lung (Sigma Aldrich) was added to the solution.

3.3 Matrigel Substrate Preparation

Matrigel was thawed at room temperature and kept on ice. To prepare the Matrigel substrate for printing, 100 µl of Matrigel (Growth Factor Reduced, Phenol Red-free, LDEV-free, Corning) with 5 µl thrombin from bovine plasma (4.76 U/ml final concentration in the fibrin gel) (T7513-100UN, Sigma Aldrich) was pipetted on a 18x18 mm sterile cover glass. The

thrombin stock solution is composed at 100 U mL^{-1} using sterile 0.1% Bovine Serum Albumin (BSA) dissolved in distilled water, aliquoted and stored at -20°C. The Matrigel was then placed in the incubator (5% CO2 at 37°C) for 3 hours to form a gel.

3.4 HUVEC Network Formation Study on Fibrin Substrate Using Conventional Cell Seeding

Vascular ECs play a major role through angiogenesis *in vivo*. Angiogenesis is initiated by EC sprouting and followed by tube formation leading to vessel development. Measuring the ability of ECs to form tubes is one of the specific tests for angiogenesis (Madri, Pratt, & Tucker, 1988). Therefore, studying ECs behaviour and 3D network formation *in vitro* provides understanding about the angiogenesis process. In this study, fibrin gel was used as the ECM matrix for HUVECs since it increases tube formation and the developed tubes closely mimic the *in vivo* situation (Auerbach, Lewis, Shinners, Kubai, & Akhtar, 2003).Two studies were conducted to investigate endothelial tube formation on fibrin matrix. In the first study the HUVECs were cultured in 3D environment resuspended in fibrinogen and in the second study HUVECs were co-cultured with fibroblasts in a 2D environment.

For the first study, a fibrin layer was formed in a well surface (9.5 cm^2) by adding 1 ml of fibrinogen and 20 µl thrombin (0.99 U/ml final concentration in fibrin gel after adding second layer) and left at room temperature to solidify for 30 minutes. Thrombin converts fibrinogen enzymatically into fibrin. 1 x 10^6 HUVECs were counted and resuspended in 1 ml fibrinogen solution and added to the formed fibrin gel and left to solidify for 20 minutes (Figure 29). After solidification, fibrin gel was incubated. At day 8, HUVECs were stained with Calcein AM (0.402 µM) (400146, Cayman chemical) to acquire immunofluorescence images (Zeiss AxioObserver Z1 motorized inverted microscope, Germany).

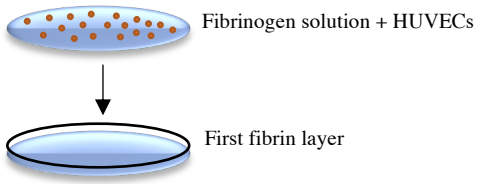

Figure 29. Schematic of 3D HUVEC cell seeding in fibrin.

Both LIFT and LIST laser-bioprinters employed in this study do not offer 3D printing. Therefore, a model was designed for 2D cell interactions on fibrin substrate corresponding with the available printing conditions. Previous studies have shown the role of fibroblasts in promoting endothelial tube and lumen formation (Newman, Nakatsu, Chou, Gershon, & Hughes, 2011). Therefore, for 2D HUVEC network formation on fibrin, the effect of adding fibroblasts on inducing HUVEC network formation was investigated. The effect of adding fibroblasts was studied in the forms of direct and indirect contact with HUVEC cells and a control was also considered by seeding HUVECs alone. The fibrin gel was prepared on a 18x18 mm cover glass, 2 µl of thrombin (3.84 U/ml final concentration in fibrin gel) was pipetted on an area of 100 mm^2. For gel formation, 50 µl of fibrinogen solution was added to the thrombin and left for 20 minutes in room temperature (gel thickness ~520 µm).

For the indirect contact condition, fibroblast cells were trypsinized and 50 x 10^3 cells were counted for the experiment. The cells were then cultured one day prior to the experiment in order to achieve cell attachment to the well surface (9.5 cm^2). 300 x 10^3 HUVECs were seeded on the fibrin gel (Figure 30a).

To study the direct contact of fibroblast cells, 300 x 10^3 HUVECs and 50 x 10^3 fibroblast cells were resuspended together in EndoGRO-VEGF complete medium and seeded on the fibrin gel (Figure 30b).

For the control, 300 x 10^3 HUVECs was cultured on the fibrin gel (Figure 30c). An overlay of fibrin was added on the seeded cells for all three conditions (overlay thickness ~150 µm) and allowed to solidify for 15 minutes. Each fibrin gel was then placed in each of the wells (6 well plate) and was kept in the incubator for 50 minutes prior to adding EndoGRO-VEGF complete medium. Medium of the samples was changed daily.

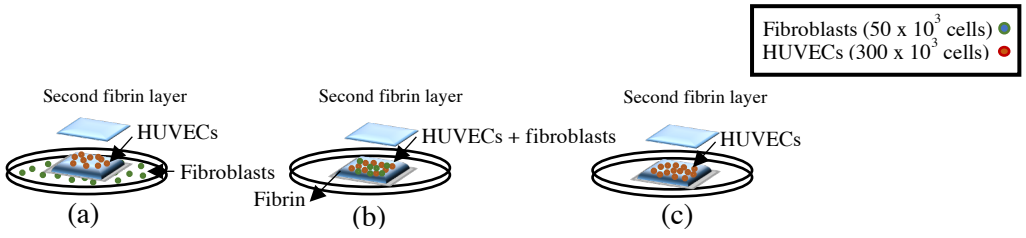

Figure 30. Schematic of HUVEC co-cultured with fibroblasts on fibrin (a) Indirect contact of fibroblast cells (b) Direct contact of fibroblast cells (c) Control.

3.5 HUVEC Network Formation Study on Matrigel Substrate Using Conventional Cell Seeding

Matrigel is a popular matrix for angiogenesis studies since it induces rapid endothelial tube formation (Auerbach et al., 2003). To compare HUVEC network formation on both types of fibrin and Matrigel matrices, a similar study was conducted an angiogenesis assay on fibrin substrate. Matrigel was thawed in room temperature and kept on ice before using. 50 µl of Matrigel was pipetted on the same area as mentioned previously (Matrigel thickness ~ 500 µm). To solidify, Matrigel was placed in the incubator for 2 hours prior to seeding HUVEC cells. The same procedure was repeated as in HUVEC network formation on fibrin (Figure 31).

Microscopy images of the samples were obtained at (Zeiss AxioObserver Z1 motorized inverted microscope, Germany) and the formed HUVEC network was analyzed at days 1, 3 and 6 using Angiogenesis Analyser ImageJ's plugin (": Angiogenesis Analyzer," 2012). To avoid misquantification, the areas with cell clumping were blocked from the quantification process by using the masking tool in ImageJ.

The total length between each set of nodes was measured and normalized by dividing it to the total measured area. Three series of experiments were conducted for quantification.

To study tube formation of HUVECs embedded within Matrigel, a similar set of experiments was studied on Matrigel with the addition of a Matrigel overlay on the seeded cells. The cell seeding procedure on Matrigel was followed as in previous studies. Overlay of a second layer of Matrigel was performed by using 15 µl of Matrigel and was incubated for 50 minutes to solidify (Figure 32) (overlay thickness ~150 µm).

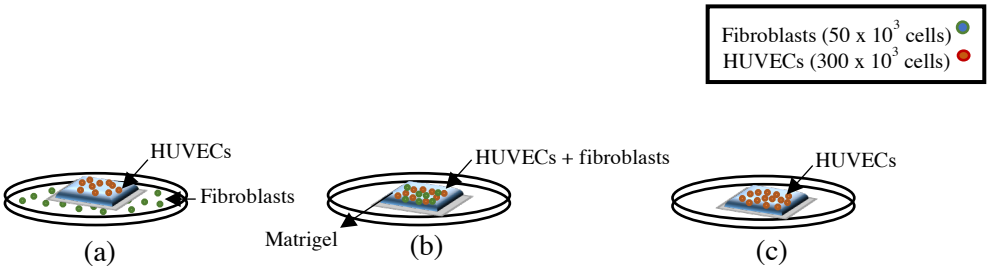

Figure 31. Schematic of HUVEC co-cultured with fibroblasts on Matrigel (a) Indirect contact of fibroblast cells (b) Direct contact of fibroblast cells (c) Control.

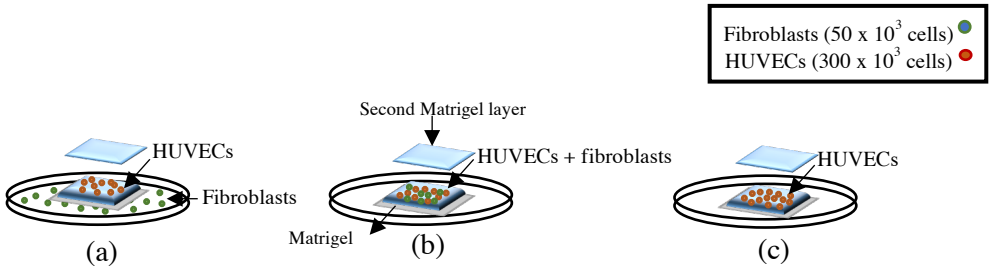

Figure 32. Schematic of HUVEC co-cultured with fibroblasts on Matrigel with overlay (a) Indirect contact of fibroblast cells (b) Direct contact of fibroblast cells (c) Control.

3.6 Laser-Induced Forward Transfer (LIFT)

Laser-induced forward transfer (LIFT) is a laser-based printing technique in which the donor substrate is coated with an energy absorbing layer such as gold or titanium. The laser pulse is focused on the bioink spreaded on the donor substrate leading to the evaporation of the bioink and formation of a bubble. The energy resulting from the formed bubble forces a droplet to eject from the bioink and depositing it on the receiving substrate (Figure 33).

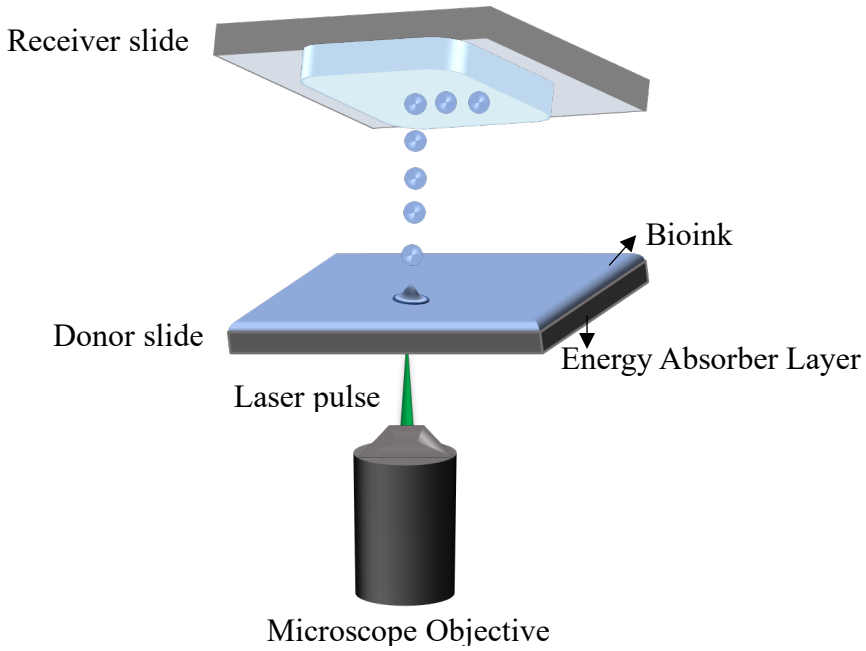

Figure 33. Schematic setup of LIFT.

The LIFT system employed in the present study, guides the laser beam from the laser source (Ultra compact pulsed Nd:YAG, Nano L series) through optic components to the camera port of a conventional microscope (Zeiss AxioObserver Z1 motorized inverted microscope, Germany) and irradiates the donor substrate via a microscope objective ("A-Plan" 5x/0.12 M27, Zeiss, Germany) (Figure 34). A donor substrate coated with a 40 nm titanium layer is used as donor substrate along with a set of cover glasses as placers for the receiver substrate (Figure 35a). As for the receiver substrate, 18x18 mm cover glasses coated with hydrogels (fibrin and Matrigel) were used (Figure 35b). Figure 35c represents a printed line by our LIFT system.

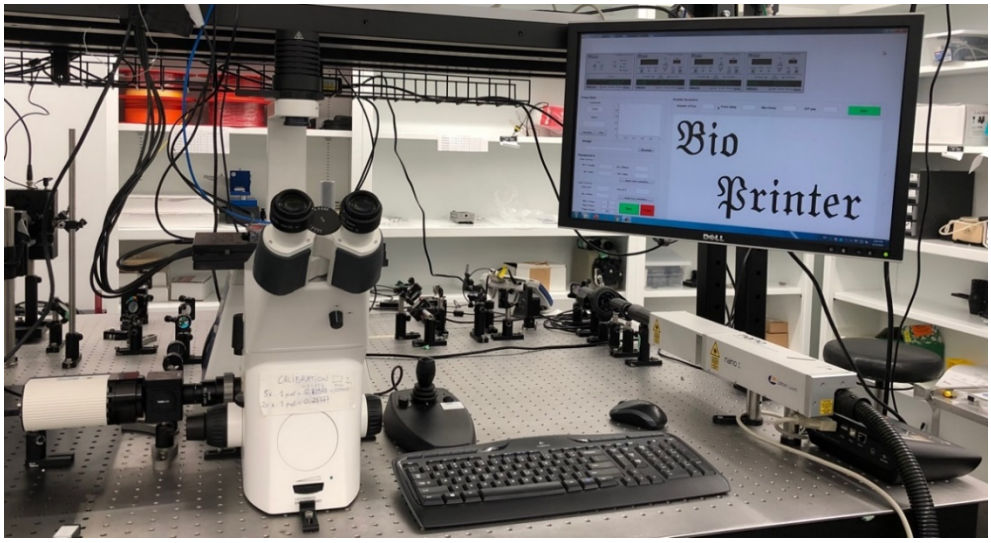

Figure 34. LIFT setup in lab.

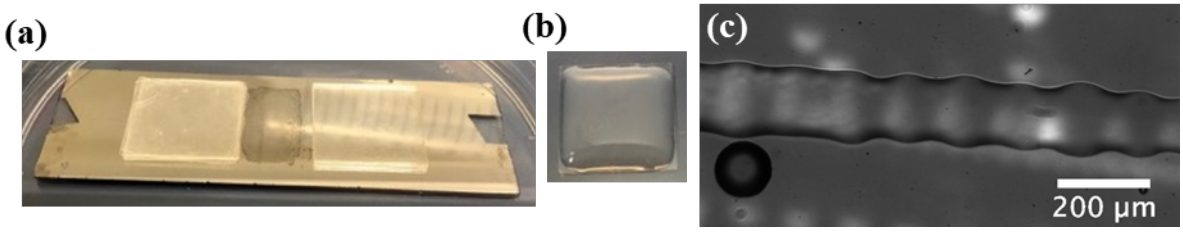

Figure 35. (a) Donor slide coated with a titanium layer and an area of bioink along with cover glass placers (b) Fibrin gel as a receiver substrate (c) Printed line via LIFT.

3.6.1 **Bioink Thickness Study**

Bioink film preparation plays an important role in LIFT printing and bioink film thickness is one of the main variables that affects the printing procedure and resolution.

Therefore, the effect of bioink film thickness on the droplet diameter was studied. Fibrinogen solution was prepared with the cell concentration of 100 x 10^6 cells/ml. 30% glycerol was added to the solution to prevent evaporation and to increase the spreadability (Guillotin et al., 2010). The amounts of 4, 6, 8 and 10 µl were spread on an area of 180 mm^2 to obtain bioink thicknesses of 22, 33, 44 and 55 µm respectively. The 18x18 mm coverglass was placed at a distance of 1.14 mm from the donor slide. Printing of cell containing droplets was performed using energies 15, 20, 25 and 30 µJ measured before the microscope objective. The printed droplets were then imaged (Zeiss AxioObserver Z1 motorized inverted microscope, Germany) and the diameter of each droplet was measured with Matlab.

3.6.2 **Printing HUVECs with LIFT**

The main goal of cell printing is the ability to pattern cells in desired designs. Therefore, to fulfill the aim of this study, LIFT was employed to print line patterns of HUVECs on Fibrin and Matrigel substrates to study angiogenesis guiding. To print HUVECs on fibrin, a bioink with 100 x 10^6 cells per ml with 5% Glycerol and 0.125% Methylcellulose was prepared. 6 µl was spread manually on an area of 180 μm^2 (bioink thickness ~ 33 µm). The distance between the donor and fibrin substrate was kept to approximately 1.9 mm by using cover glass stacks placed at each side to hold the receiver substrate. The energy used for the printing was within the range 20 to 25 µJ and 4 mm long lines were printed with the distance of 100 µm between the droplets. A fibrin overlay was then added on the printed cell patterns and after solidification, medium was added followed by incubation. Similar bioink solution composition was used to print on Matrigel (without thrombin). The printed droplets were then imaged (Zeiss AxioObserver Z1 motorized inverted microscope, Germany).

3.7 **Laser-Induced Side Transfer (LIST)**

Laser-Induced Side Transfer (LIST) (Ultra compact pulsed Nd:YAG, Nano L series) setup consisted of a motorized stage holding the printing substrate, a capillary (Vitrocom hollow square capillary,0.3mm inner diameter, 0.15mm wall thickness and 50 mm long) connected to a syringe pump supplied with the bioink and a 4X Olympus plan achromat objective which focuses the laser beam in the middle of the capillary. The laser pulse is focused at the capillary

leading to the evaporation of the bioink. The pressure generated from the bubble ejects a droplet from the capillary end toward the receiver substance (Figure 36, Figure 37).

Figure 38 shows sequences of bioink jet developments for different energies. The distance from the focal point to the end of the capillary is 500 μm and the capillary end is placed at a distance of 500-650 μm above the substance.

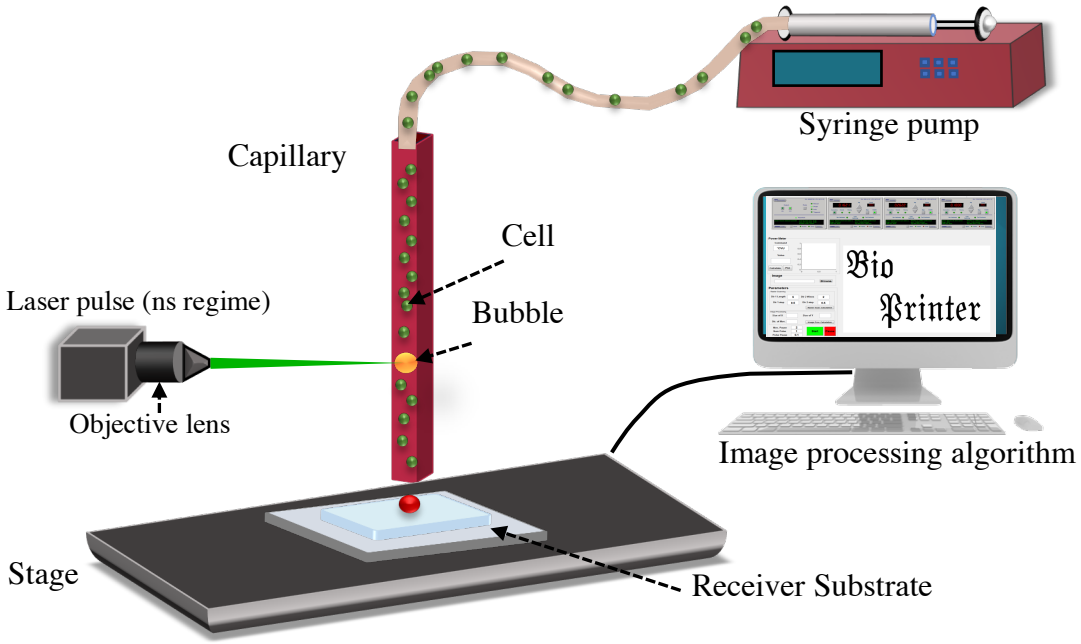

Figure 36. Schematic of LIST set-up.

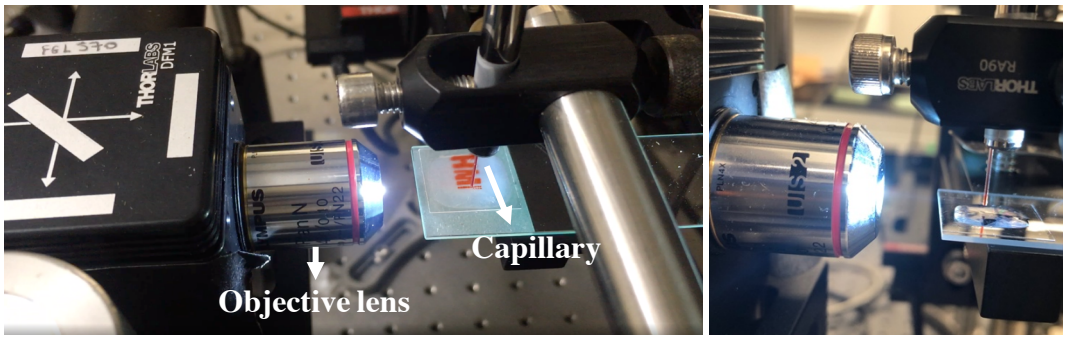

Figure 37. Image of capillary and objective lens from LIST set-up.

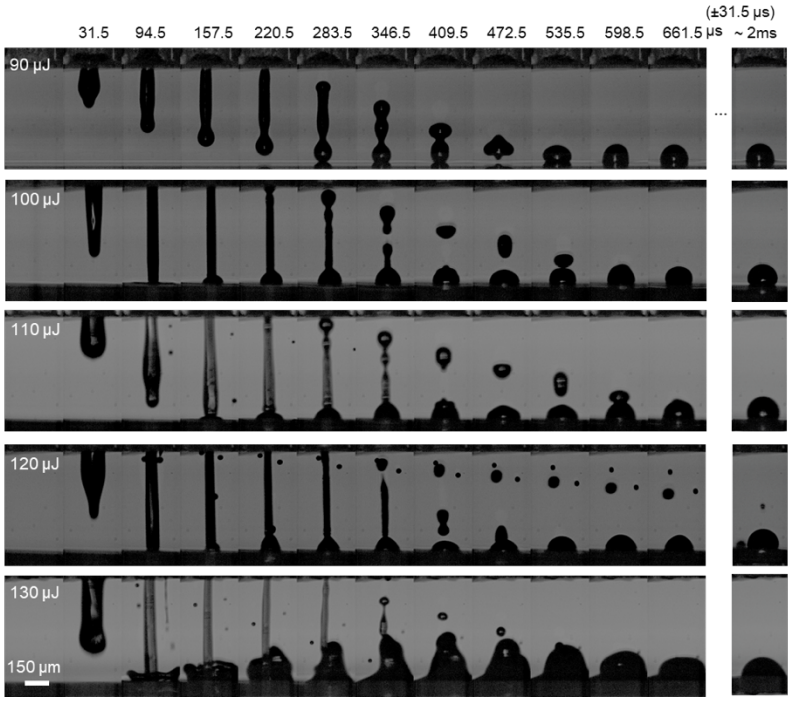

Figure 38. Sequences of snapshots showing micro-jet development for different laser energies (Orimi et al., 2020).

The bioink formulation used for the LIST setup differs from LIFT. The LIST printing technique requires red dye in the bioink as an energy absorber of the green laser beam. The red dye used for the bioink is Allura red AC which is a food dye. The energy absorbance of Allura red AC is around 504 nm. Due to the mechanism difference in LIFT and LIST techniques, the laser pulse energies reported throughout this study are not comparable.

3.7.1 Ink Preparation for LIST Printing

Bioink formulation used for LIST printings consist of HUVECs suspended in fibrinogen solution and red dye. HUVECs were treated with 0.05% Trypsin-EDTA (MilliporeSigma™) and neutralized with medium. After centrifuging at 1000 rpm for 5 minutes, the supernatant was removed, and the cells were suspended in medium for counting. HUVECs were centrifuged again and resuspended in the fibrinogen solution. Based on the quantity of the fibrinogen solution cell suspension, the red dye is added to reach a final concentration of 10 mM in the cell suspension.

3.7.2 Allura Red Dye Toxicity Test with Dye Exclusion Method

As Allura red dye is one of the main components of the bioink formulation used for LIST printing, the effect of this dye on HUVEC viability was investigated using a hemocytometer-based trypan blue dye exclusion assay. Trypan blue stains cells with damaged membrane in a distinctive blue color which can be observed under a microscope. In contrast, viable cells with intact membranes do not absorb trypan blue and remain uncoloured.

To prepare Allura red AC (A0943, TCI, America) as a solution, the Allura red dye powder is dissolved in distilled water and then sterile filtered

Two dye concentrations were tested 50 mM and 10 mM and a control condition with no dye. To verify the dye effect over the course of time, P3 HUVEC cells were counted and cultured one day prior to the experiment for cell attachment (6 well plate). For the cells to reach complete confluency at days 0, 1 and 3, 500 x 10^3, 250 x 10^3 and 150 x 10^3 cells were cultured per well respectively. The considered dye concentrations were added per each specific well and incubated for 50 minutes which is the approximate duration of cell exposition to the dye throughout the printing process. Each well was then washed with medium until complete dye removal. For the day 0 time point, the cells were incubated two hours after dye removal. The test was applied on each of the wells at their defined time point. The cells were treated with 0.05% trypsin and centrifuged. HUVECs were then resuspended in 50 µl EndroGro VEGF-medium and 50 µl trypan blue solution (4%, Thermofisher). To assess cell viability, cell suspensions were mixed with Trypan Blue (1:1) and microscopy images were acquired using a 10x objective. The images were quantified to define the cell viability percentage.

3.7.3 Allura Dye Effect on HUVEC Attachment and Network Formation

Since HUVEC tube formation is the main goal of this study, other than cell viability, a study was conducted to verify the effect of Allura red dye on HUVEC attachment to the Matrigel surface and HUVEC network formation. Six conditions were considered for this study (Table 3). Matrigel was used with thrombin and without thrombin for cell attachment comparison.

The bioink solutions were prepared as previously described with two 50 mM and 10 mM dye concentrations and one with no red dye as a control. For cell seeding on Matrigel surface,

20 x 10^3 cells were resuspended in 5 μm of the bioink solution. They were left at room temperature for 50 minutes before adding medium which is the approximate printing duration.

Table 3. Allura dye effect on HUVEC attachment and EC network formation study design.

Matrigel Substance	**Red Dye Concentration**		
+ Thrombin	50 mM	10 mM	Control
- Thrombin			

3.7.4 Printing HUVECs with LIST

For all the capillary-like structure studies in this thesis, HUVECs were printed using the energy of 110 μJ measured at the sample level (i.e. after the lens). The diameter of the printed droplets was measured 180-240 μm and the space between each droplet was 150-200 μm. The cells were printed in line patterns 10 mm long and 1.5 mm separation distance between the lines. After printing, the samples were incubated for 10 minutes prior to adding EndoGRO VEGF-medium for better cell attachment. The medium was exchanged after 30 minutes to remove the diffused red dye from the sample.

The cells were also printed in a mesh design with similar conditions. Lines of HUVECs were printed perpendicular to the first printed lines in order to form the mesh design. The samples were stained with Calcein AM (0.400 μM) (400146, Cayman chemical) and Hoechst 33342 (14.2 μM) (14533-100MG; Sigma-Aldrich) at day 2 to obtain immunofluorescence images. Calcein AM is used to determine viable cells and Hoechst 33342 stains all the cells (viable and dead cells).

3.7.5 HUVEC Viability Quantification Printed with LIST on Matrigel Substrate

The laser beam when focused in the capillary, produces heat to evaporate the bioink followed by droplet ejection. This produced heat can affect cell viability. Therefore, the effect of laser-induced heating on HUVEC viability was investigated by using three energies to print cells on Matrigel substrate with thrombin. The printing was performed using energies 100, 110

and 120 μJ in droplet form in line patterns, two lines were printed per energy. Control samples were prepared by pipetting bioink droplets on Matrigel surface. Due to the effect of Calcein AM staining on cell viability, a separate sample was considered for each timepoints at days 0, 1 and 3. Each sample was stained with Calcein AM (0.402 μM) and Hoechst 33342 (14.2 μM) (14533-100MG; Sigma-Aldrich) at its specified time point and imaged with immunofluorescence microscopy (Zeiss AxioObserver Z1 motorized inverted microscope, Germany). A Matlab code was used to quantify the cell viability percentage by overlaying Hoechst stained images by the absence of the corresponding cells in the Calcein stained images.

3.7.6 **Confocal Microscopy**

Transmission microscopy does not provide understanding of the internal cell organization and structure. To investigate intracellular junctions and capillary-like structures internally, confocal microscopy assessment was used. Time points one-, two- and three-days post printing were considered for follow up and comparison. Samples were fixed with 4% paraformaldehyde (PFA) for 20 minutes at room temperature. HUVECs were stained with Alexa Fluor 488 Mouse Anti-Human CD31 (1:100, BD Pharmingen ™) overnight at 4°C. Cell nuclei was stained using DAPI (0.56 μM) (D9532-5MG; MilliporeSigmaTM). In order to preserve the initial capillary-like structure and to prevent capillary collapse, Matrigels were not mounted on slides. As an alternative, samples were submerged in Phosphate-Buffer Saline (PBS) and confocal images were acquired with a 20x water immersion objective combined with an upright microscope (multi-photon Zeiss LSM880 system, Germany). Z-stacks with an interval of 0.2 μm were obtained and 3D structures were constructed using image analysis software (IMARIS, Bitplane, Switzerland).

3.7.7 **Frozen Section Procedure**

As confocal microscopy, frozen sectioning can also be used to verify internal structures by cutting cross sections of samples in the microscale and analyzing them with immunofluorescence microscopy. Frozen sections were generated to analyze the internal structure of the formed capillary-like structures at days 2 and 3 post printing. Since sectioning requires removing the Matrigel from the cover glass, the gel was prepared on disposable base

mold (24 x 24 x 5 mm, Fisherbrand) to facilitate Matrigel removal when frozen. The Samples were embedded in optimal cutting temperature medium (OCT) (Fisher Healthcare) and frozen at -80°C. The OCT block containing the Matrigel was cut with the microtome blade (Leica CM3050 S) into 20 μm sections and placed onto slides. The sections were fixed and stained with DAPI (Fluoroshield with DAPI, Sigma) as described previously. Immunofluorescence microscopy was performed on the sections and images were obtained (Zeiss AxioObserver Z1 motorized inverted microscope, Germany).

4. Results

4.1 HUVEC Network Formation Study on Fibrin Substrate using Conventional Cell Seeding

This study aimed to investigate HUVEC tube formation on fibrin matrix by comparing 2D and 3D cellular interactions and to verify the effect of fibroblasts on tube formation prior to laser bioprinting experiments. In the first section, cells were embedded within a 3D fibrin environment. After adding HUVECs suspended in fibrinogen solution to the first layer of the formed fibrin gel, the fibrinogen solidifies due to the existence of thrombin in the fibrin layer. This resulted in cell fixation in their current position and prevented their complete settlement on the first layer which allowed cell interaction in 3D. This interaction lead to network formation at day 8 (Figure 39).

In the fibrin model provided for 2D cell interaction, samples were followed throughout days 1 to 7 (Figure 40). HUVEC network formation can be observed for the indirect and control conditions from day 3. However, the formed networks for both conditions is immature which can be due to the fact that network formation in fibrin requires 3D cellular interaction rather than 2D (Nicosia & Ottinetti, 1990). Despite the lack of network formation, co-seeded fibroblasts and HUVECs demonstrated active cell growth in the direct contact setting.

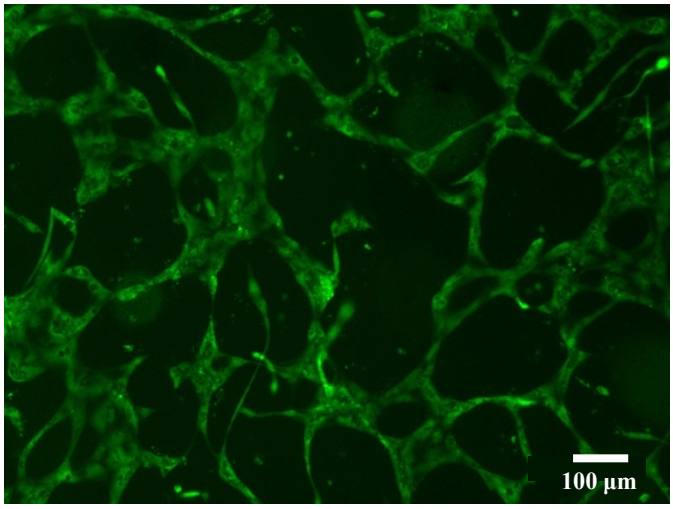

Figure 39. Immunofluorescence images of HUVEC network formation in 3D fibrin matrix day 8.

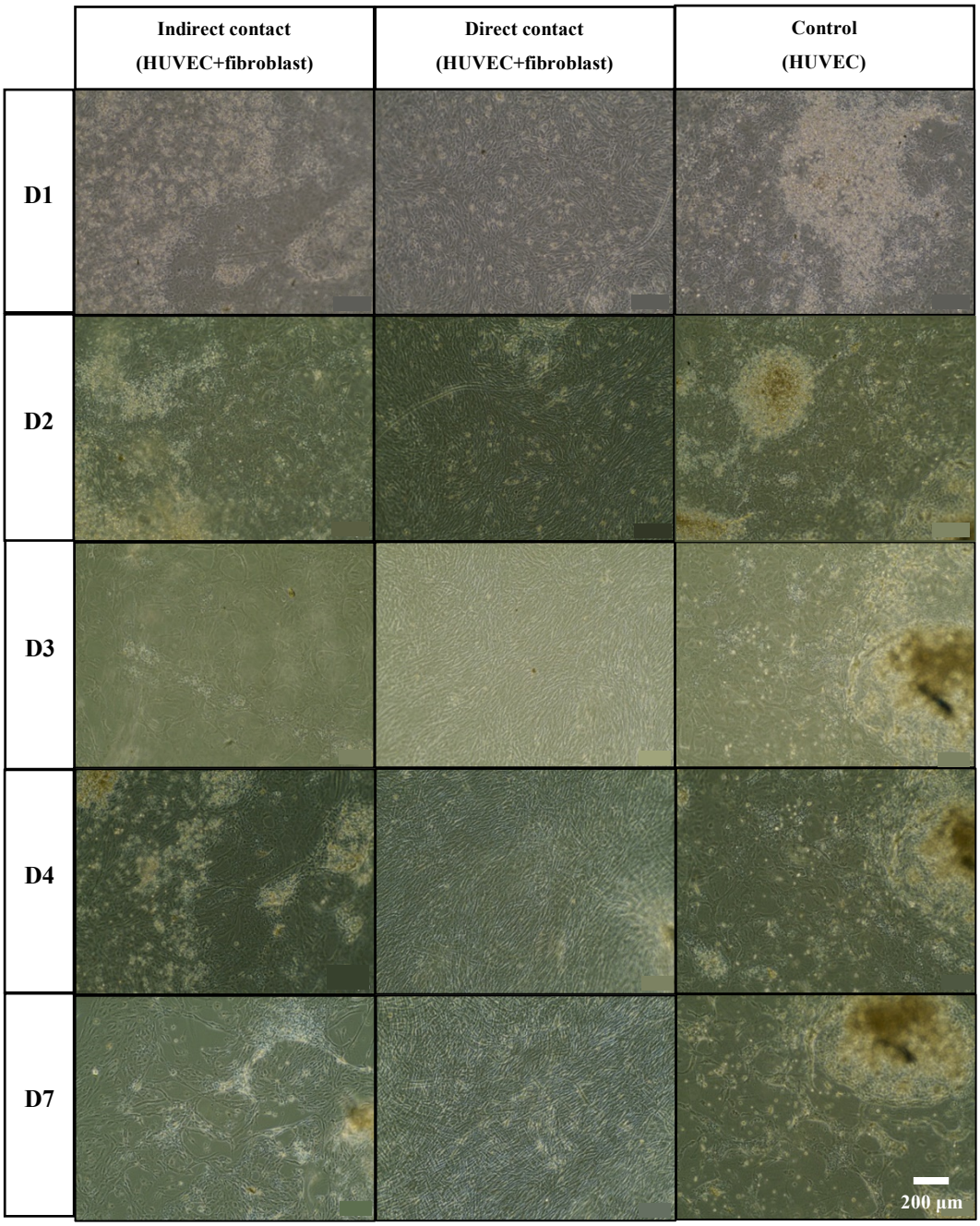

Figure 40. High magnification microscopy images of indirect, direct and control conditions of HUVEC network formation and regression on fibrin.

4.2 HUVEC Network Formation Study on Matrigel Substrate using Conventional Cell Seeding

To compare with fibrin matrix, HUVEC tube formation was also studied on Matrigel surface by direct and indirect contact of fibroblasts with HUVECs and HUVECs seeded alone as a control. The experiments were repeated three times and followed over the course of 8 days to verify the effect of fibroblasts on HUVEC network formation.

Figure 42 demonstrates HUVEC network formation in the indirect contact condition. A uniform network was formed throughout the Matrigel surface while the control formed a network with more cells aggregated within the central and networks formed at the surroundings (Figure 43). Both the indirect contact and control formed networks at day 1 and regression process was initiated at day 2. In contrast, with the direct contact, both cell types accumulated into a single patch with no network formation one day after cultivation (Figure 41). Figure 44 shows high magnification microscopy images of the formed networks for all three conditions.

The addition of a Matrigel overlay on the seeded cells resulted in abnormal network formation in the indirect contact and control conditions (Figure 45). As for the direct contact, tube-like structures were formed at days 1 and 2. At day 5 the fibroblasts from these structures overgrew HUVECs, creating patches of elongated fibroblasts.

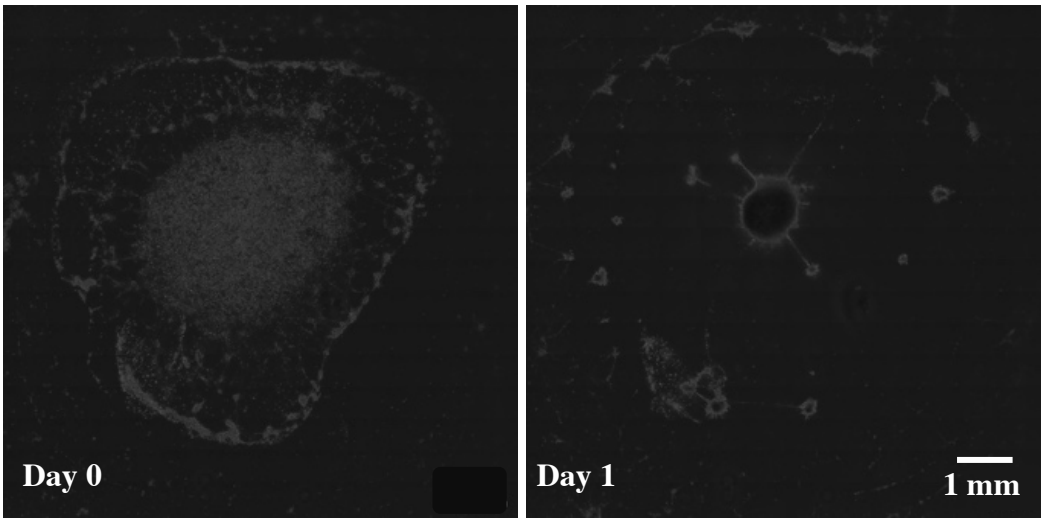

Figure 41. Direct contact condition of HUVEC network formation study on Matrigel.

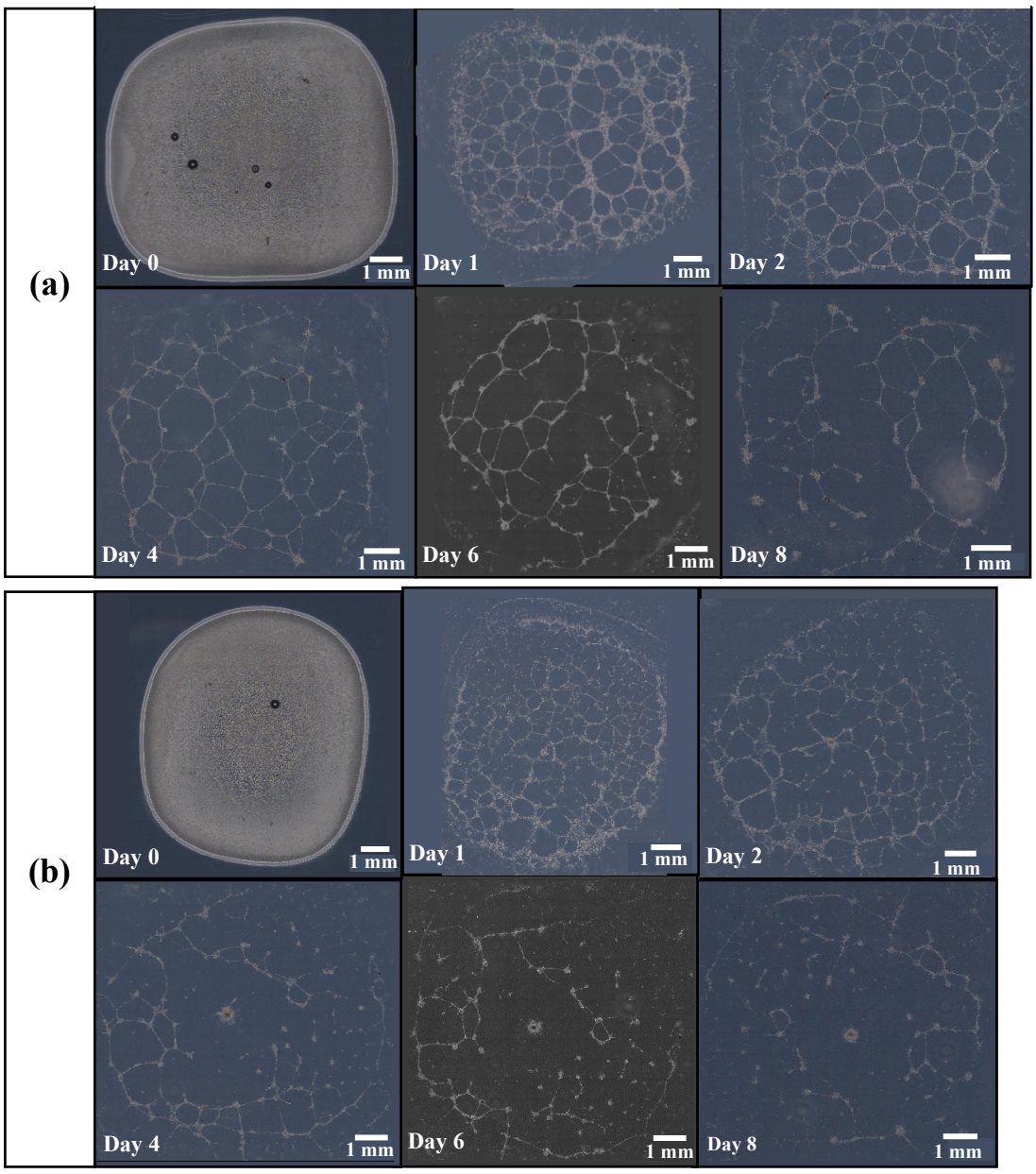

Figure 42. Two series (a and b) of indirect contact HUVEC network formation and regression on Matrigel surface.

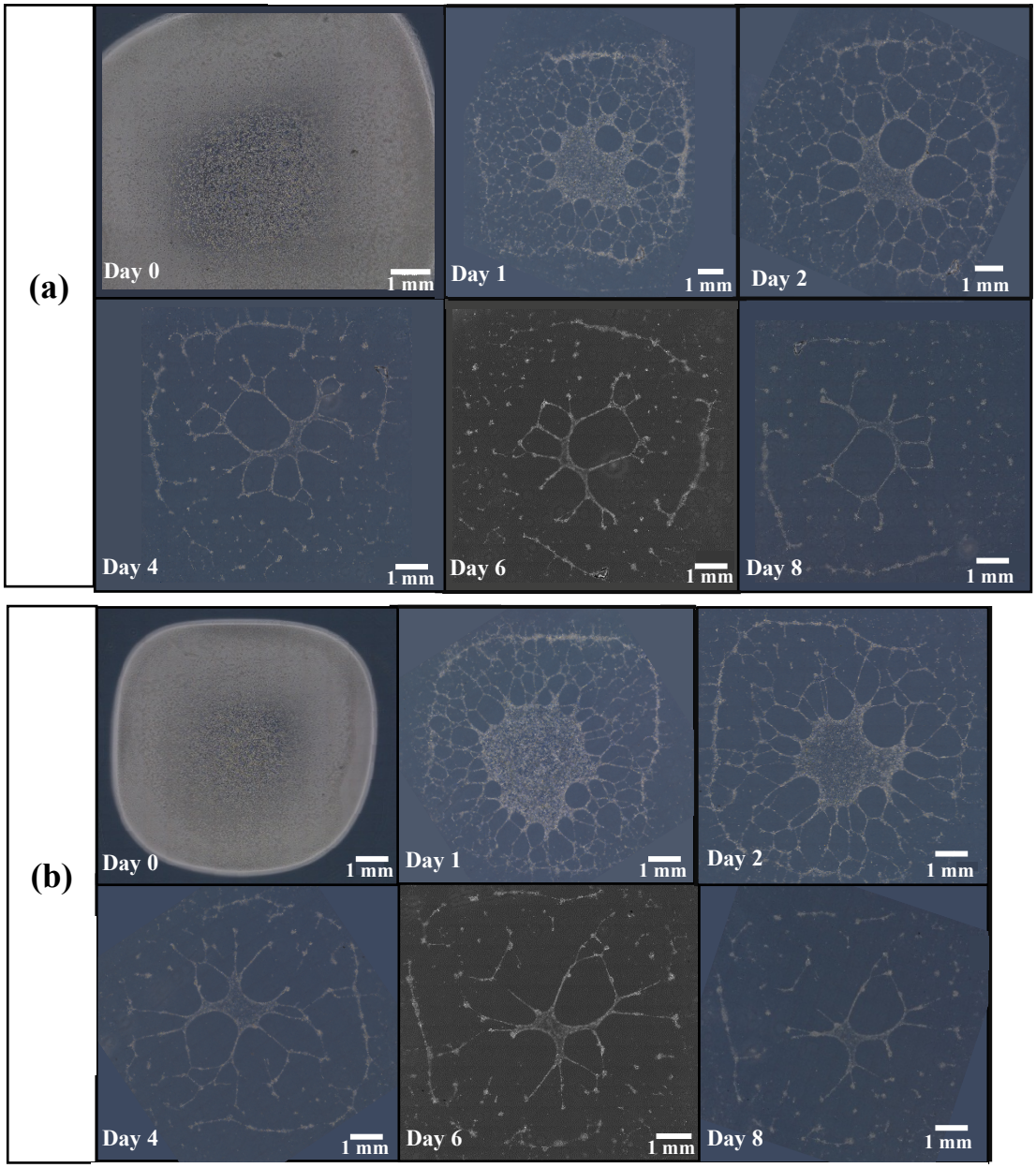

Figure 43 . Two series (a and b) of control HUVEC network formation and regression on Matrigel surface.

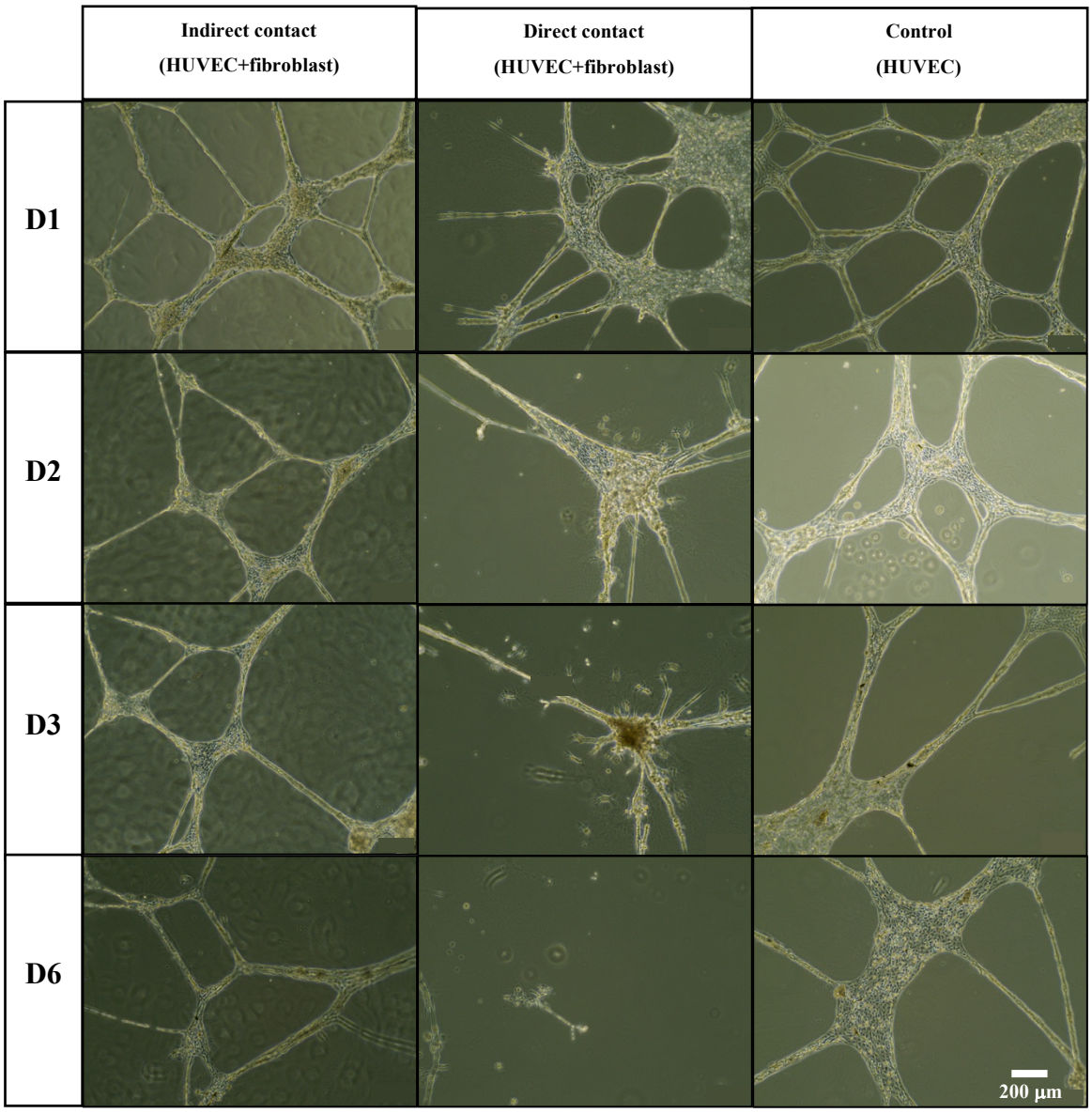

Figure 44. High magnification microscopy images of indirect, direct and control of HUVEC network formation and regression on Matrigel.

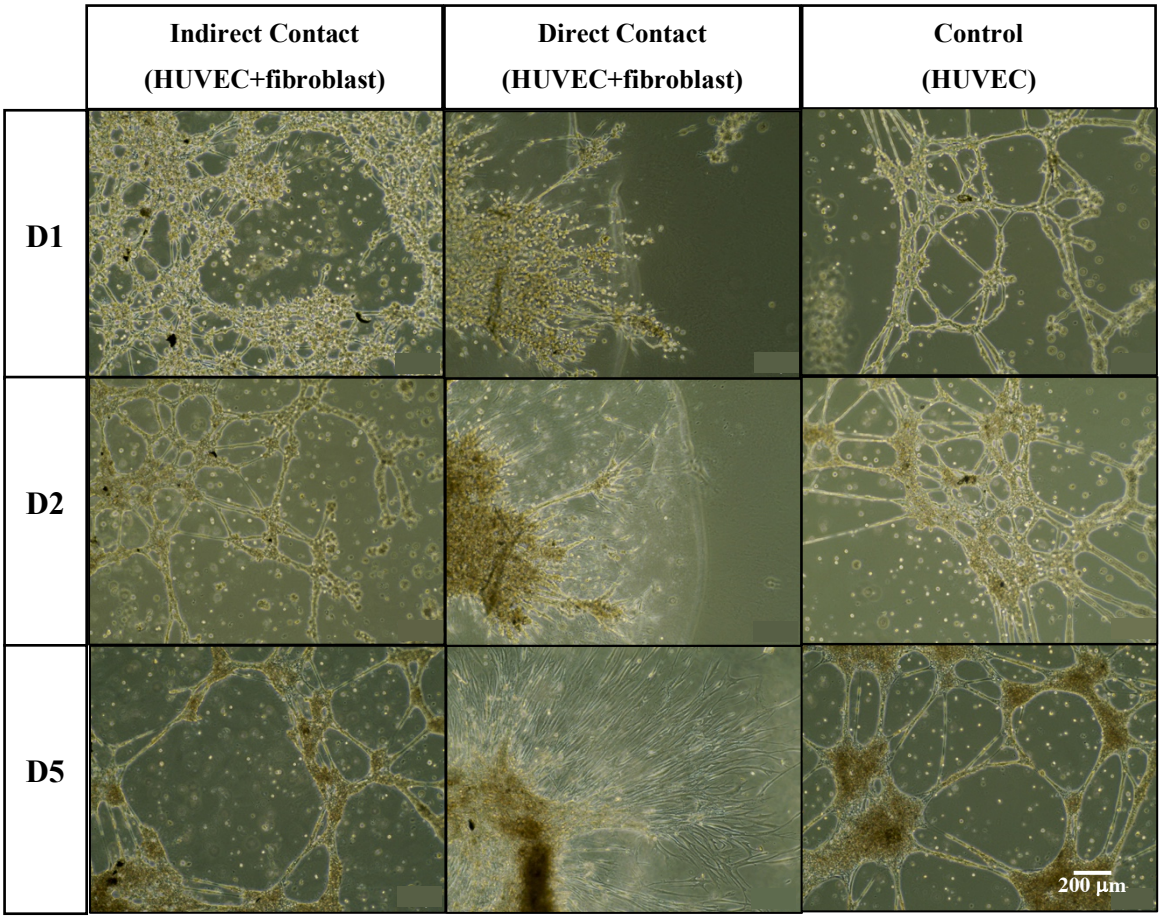

Figure 45. High magnification microscopy images of indirect, direct and control conditions of HUVEC network formation study on Matrigel with an overlay.

To measure the total segment length of the HUVEC network, the cell aggregated patches in the control was excluded using the masking tool in ImageJ (Figure 46).

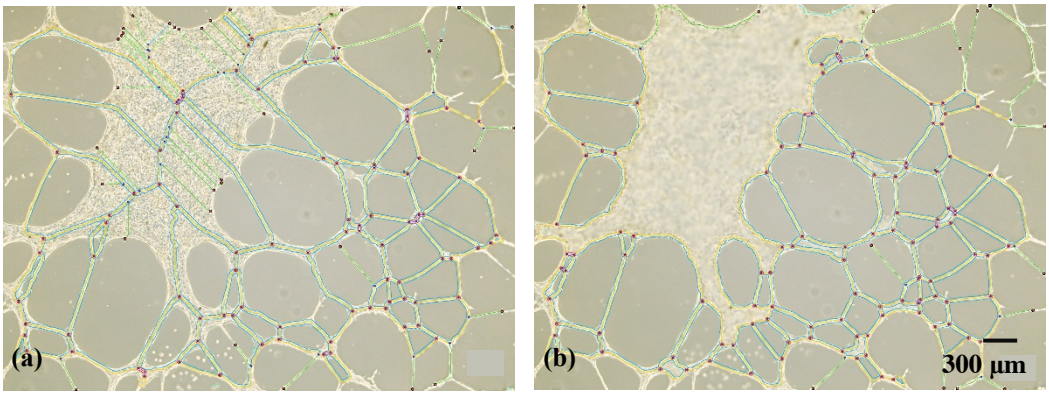

Figure 46. The total segment length of the cords was measured (blue routes). (a) Quantification without masking (b) Quantification with masking.

The quantification results (Figure 47) show that the total segment length per area in the indirect contact condition at days 1, 2 and 6 was 2.86 x 10^{-3}, 2.25 x 10-3 and 9.99 x 10^{-4} μm^{-1}, respectively. While the control condition possessed 2.17 x 10^{-3}, 1.51 x 10^{-3} and 6.16 x 10^{-4} μm^{-1} total segment length per area, for days 1, 2 and 6, respectively. Comparisons of sample means were performed using the two-way ANOVA test, the difference between the indirect contact and control conditions were not large enough to be statistically significant. It seems that the indirect contact condition might increase the total segment length per area compared to the control at all three time points. With more data the difference might have been significant. There is a trend that shows the total segment length per area decreases from days 1 to 6 for the indirect condition. While for the control, the difference is significant for days 1 and 2 compared to day 6 which is an indicative that the absence of fibroblasts accelerates the regression process.

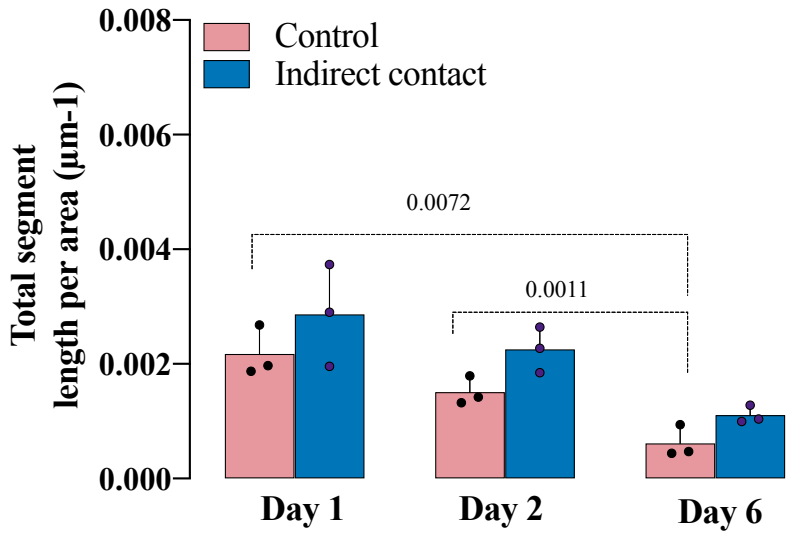

Figure 47. The total segment length per area for indirect contact and control. Error bars represent standard deviation (N=3), the two-way ANOVA test was used for comparison. Data analysis showed no significant difference between the two conditions. The difference for days 1 and 2 compared to day 6 for the control condition was significant.

4.3 Laser-Induced Forward Transfer (LIFT)

4.3.1 Bioink Thickness Study

The bioink with the thickness 22 µm had successful droplet ejections for all four energies however the droplets lack uniformity and circular shape and were generated along with satellites

(Figure 48). The quantified droplet diameters per energy (Figure 52) indicates that as the printing energy increases the droplet diameter, increases showing a linear relationship between the printing energy and the droplet diameter.

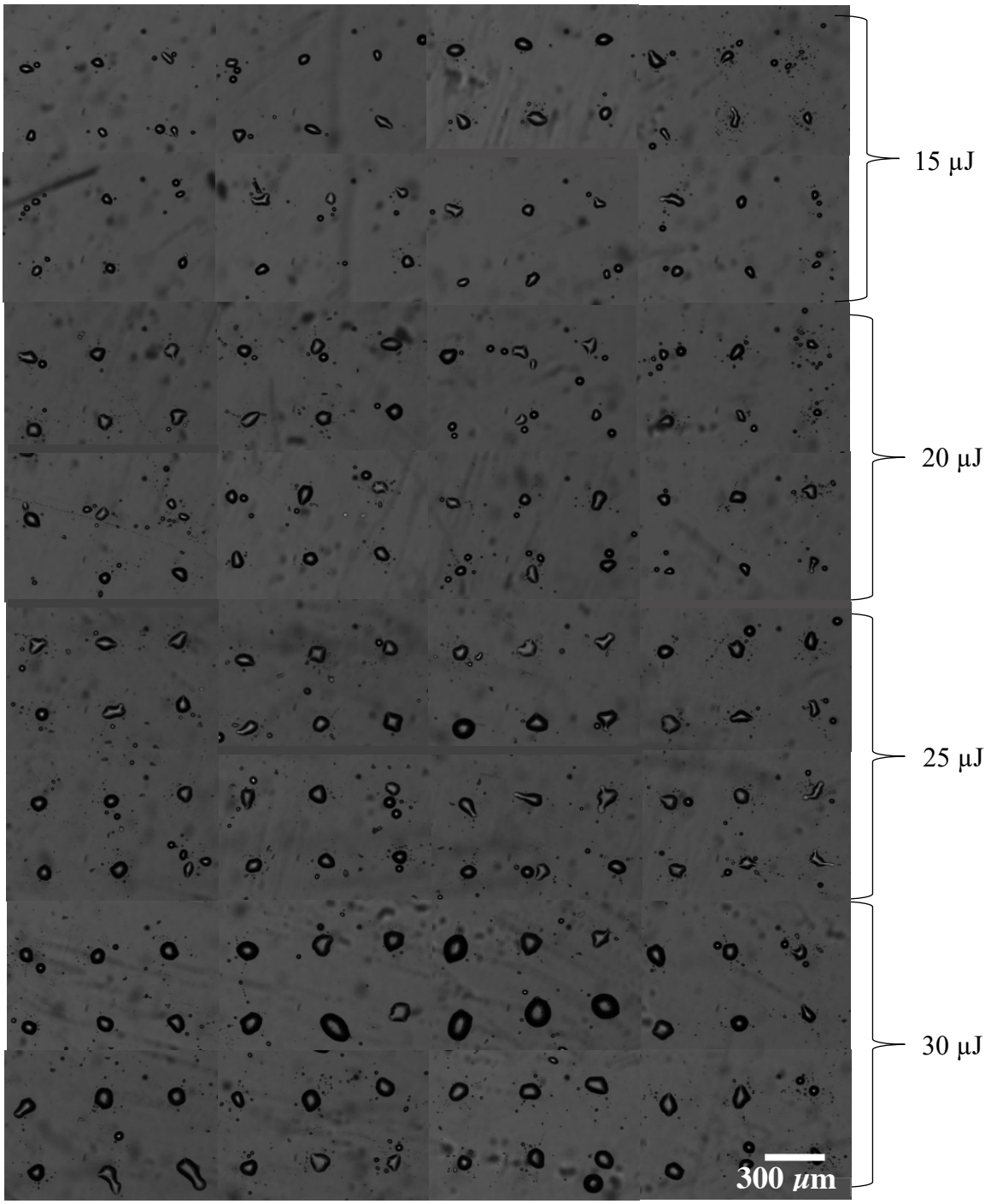

Figure 48. Printed droplets with 22 µm bioink thickness.

As for the 33 µm thickness, a more uniform shape of the droplets is displayed with less formed satellites (Figure 49). Unlike the 22 µm thickness, some of the droplets were not ejected successfully from the bioink toward the receiver slide. Circular shape of droplets was observed for the energies 20, 25 and 30 µJ. Energy increase is accompanied by droplet diameter enhancement (Figure 52).

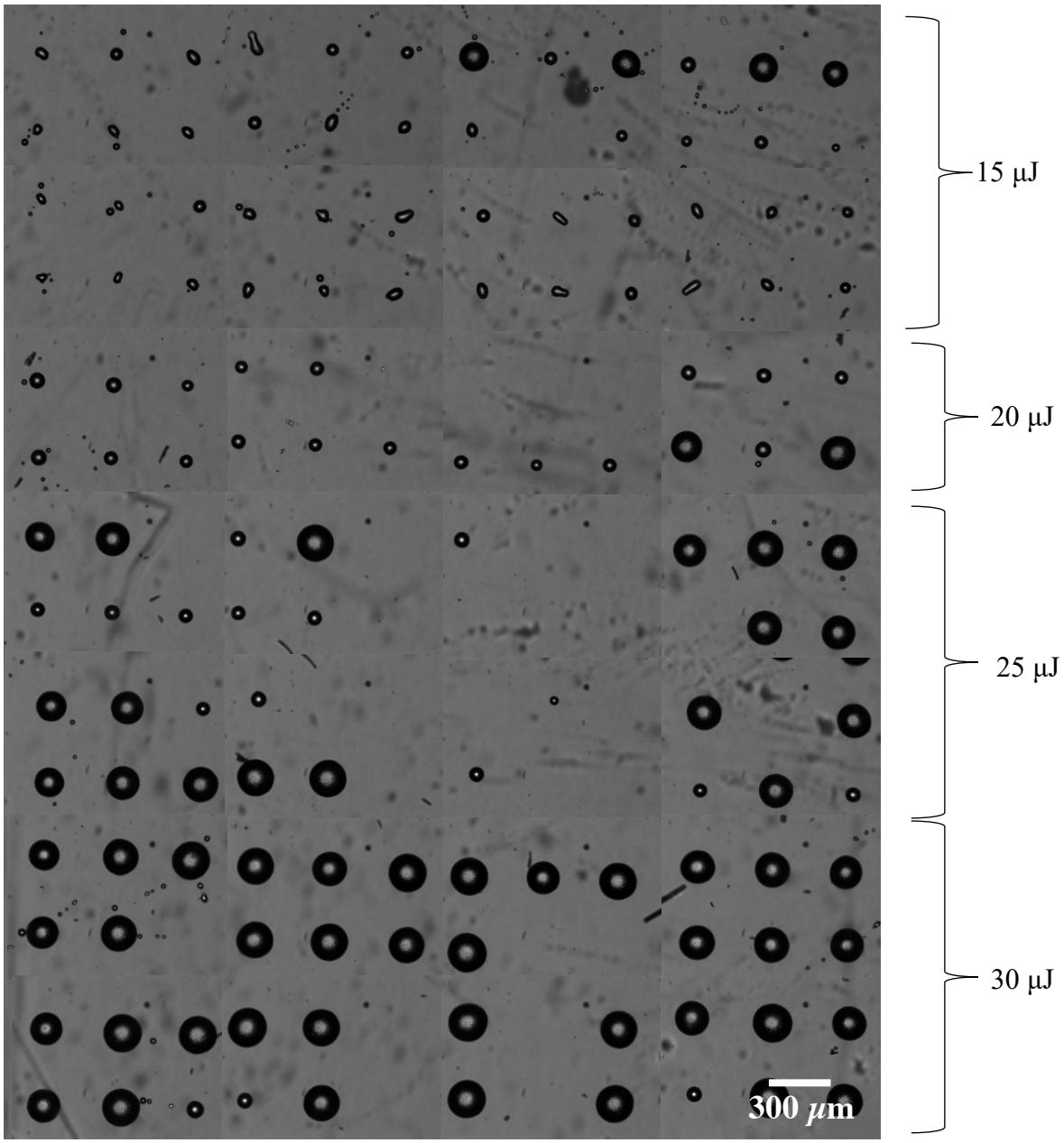

Figure 49. Printed droplets with 33 µm bioink thickness.

Performing printing with the energy 15 µJ led to complete droplet ejection failure for the 44 µm thickness (Figure 50).

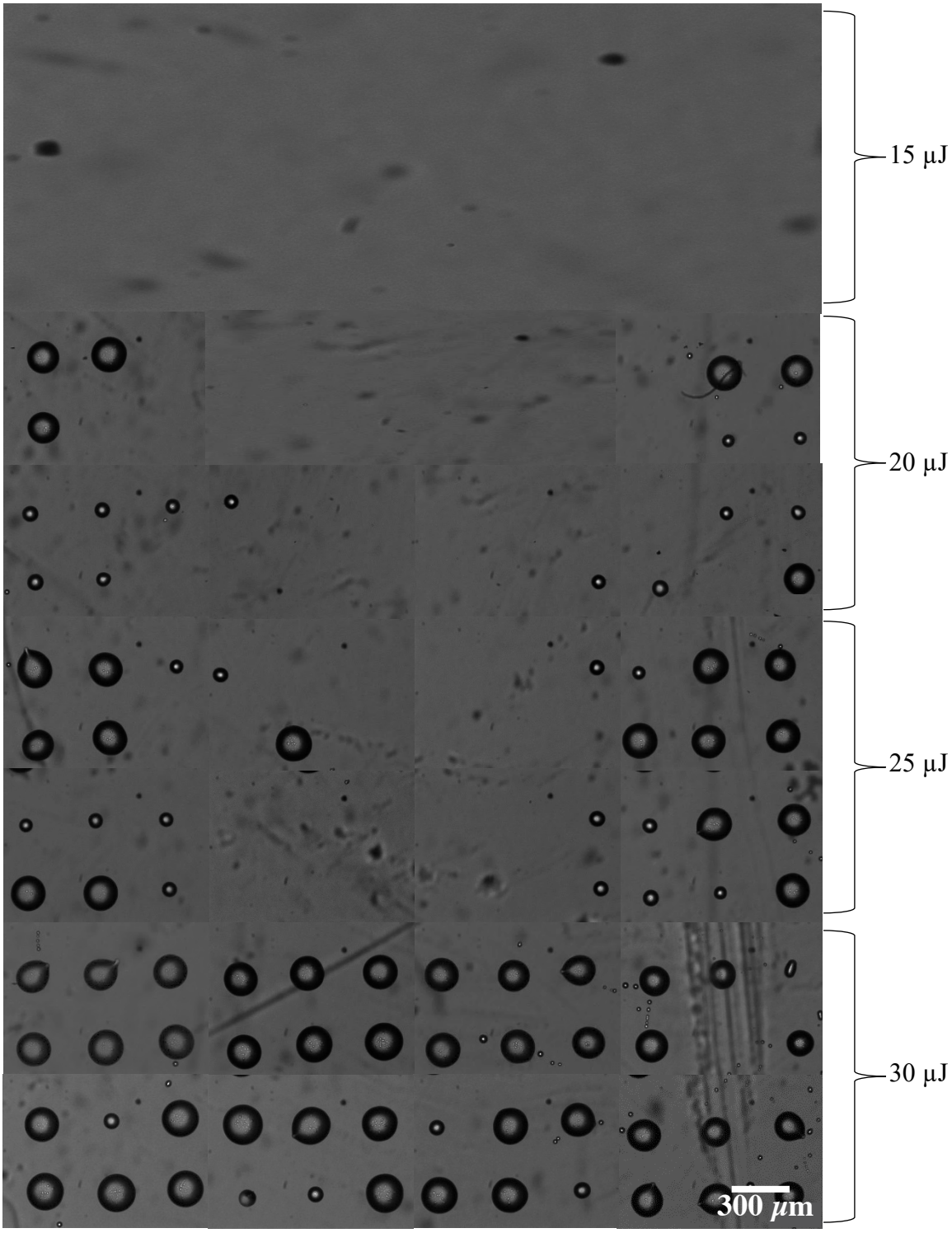

Figure 50. Printed droplets with 44 µm bioink thickness.

There is a trend that shows droplet diameter increase in printings performed with higher energies (Figure 52). The laser beam was unable to eject droplets thoroughly for the 55 µm thickness even in the higher energy range (Figure 51 and Figure 52).

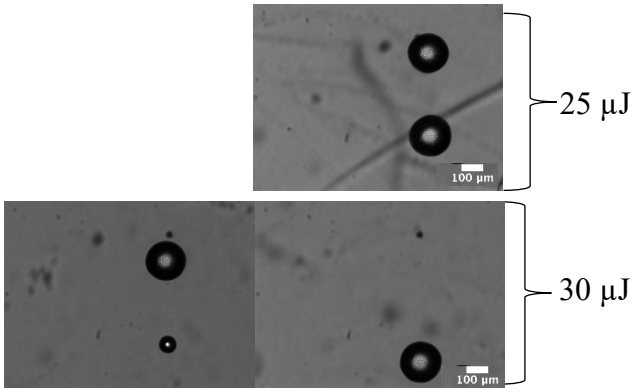

Figure 51. Printed droplets with 55 µm bioink thickness.

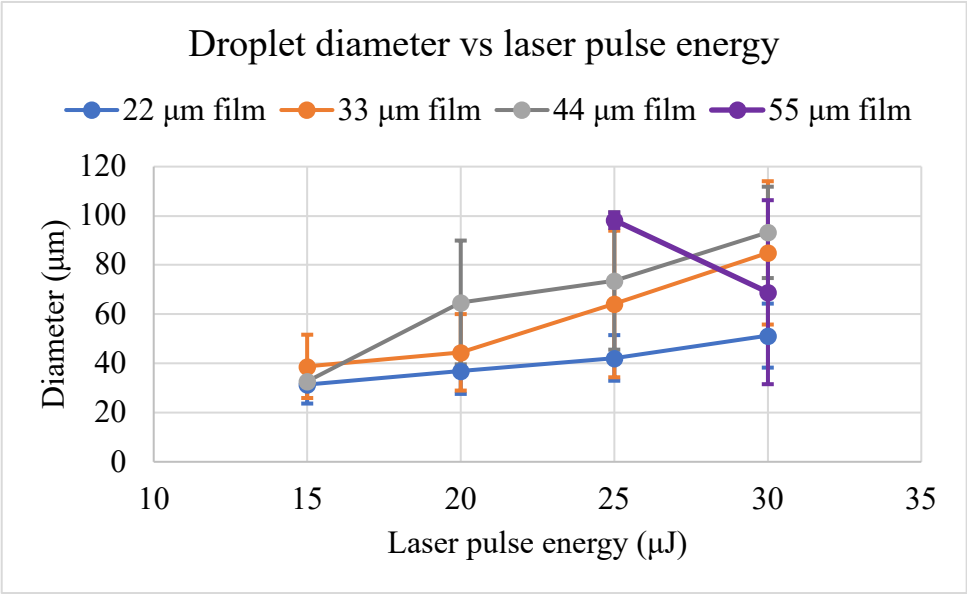

Figure 52. The average droplet diameter per thickness (N=1).

4.3.2 **Printing HUVECs with LIFT**

To study HUVEC tube guidance by LIFT bioprinting, HUVEC cells were patterned into lines on a fibrin substrate using the energy ranges 20-25 µJ to perform printing (Figure 53a). The printed HUVECs maintained their attachment to the fibrin substrate one day post printing (Figure 53b) and proliferate at day 2 leading to connections between cells in the other printed lines (Figure 53c). Calcein staining at day 2 shows cell viability and their tendency to form

connections with other cells (Figure 54). Despite the formed cell connections, no HUVEC network formation occurred. Furthermore, printing performed on the Matrigel substrate (without thrombin) resulted in complete cell detachment from the gel surface one day after printing (Figure 55).

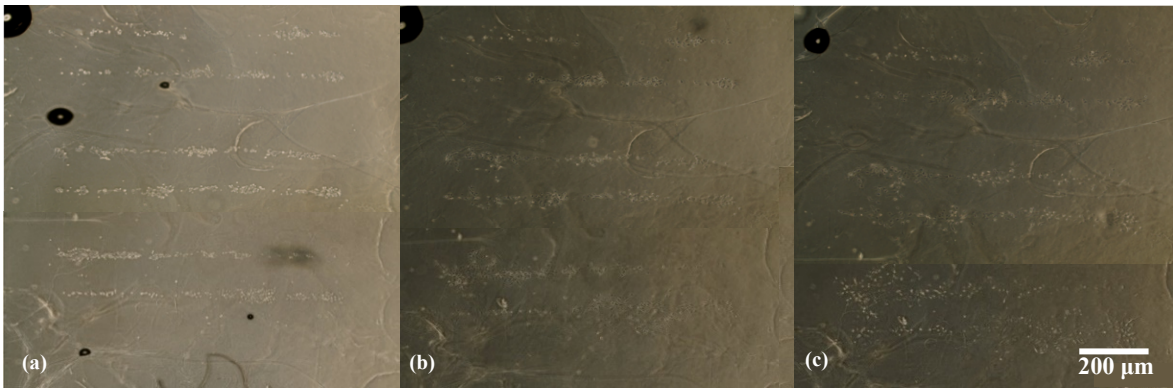

Figure 53. Printed HUVECs on fibrin substrate with LIFT (a) day 0 (b) day 1 (c) day 2.

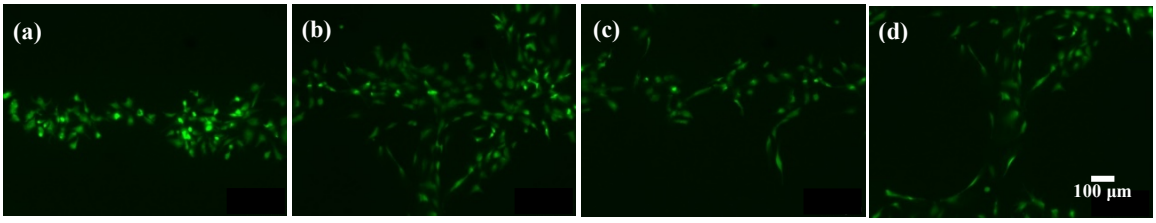

Figure 54. Day 2 Calcein staining of HUVECs on fibrin substrate with LIFT (a-c) printed lines (d) connection between two printed lines.

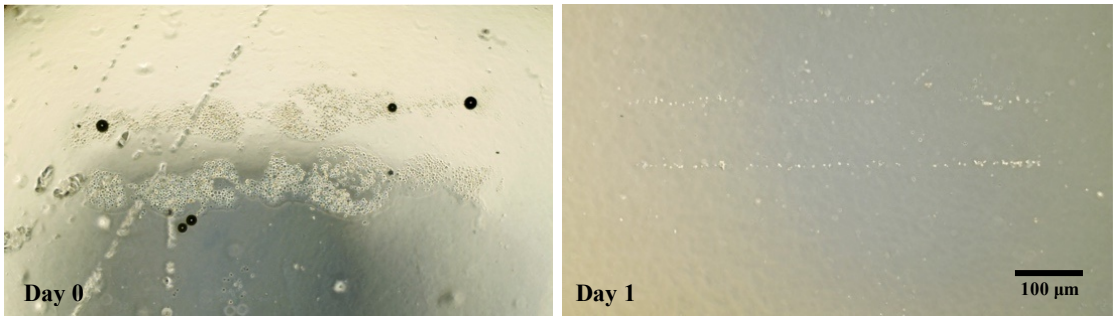

Figure 55. Printed HUVECs with LIFT on Matrigel substrate.

4.4 Laser-Induced Side Transfer (LIST)

Following several technical difficulties on LIST printing of HUVECs such as the difficulty to obtain a uniform bioink film, low printing duration due to bioink evaporation and the requirement for bioink additives, I opted to use LIST in anticipation of improved printing results. Figure 56 demonstrates LIST printed HUVECs in droplet form on fibrin substrate at day 0. Indeed, it can be observed that LIST allows uniform printing of circular droplets, high number of successful ejected droplets and high number of cells compared to LIFT (Figure 57).

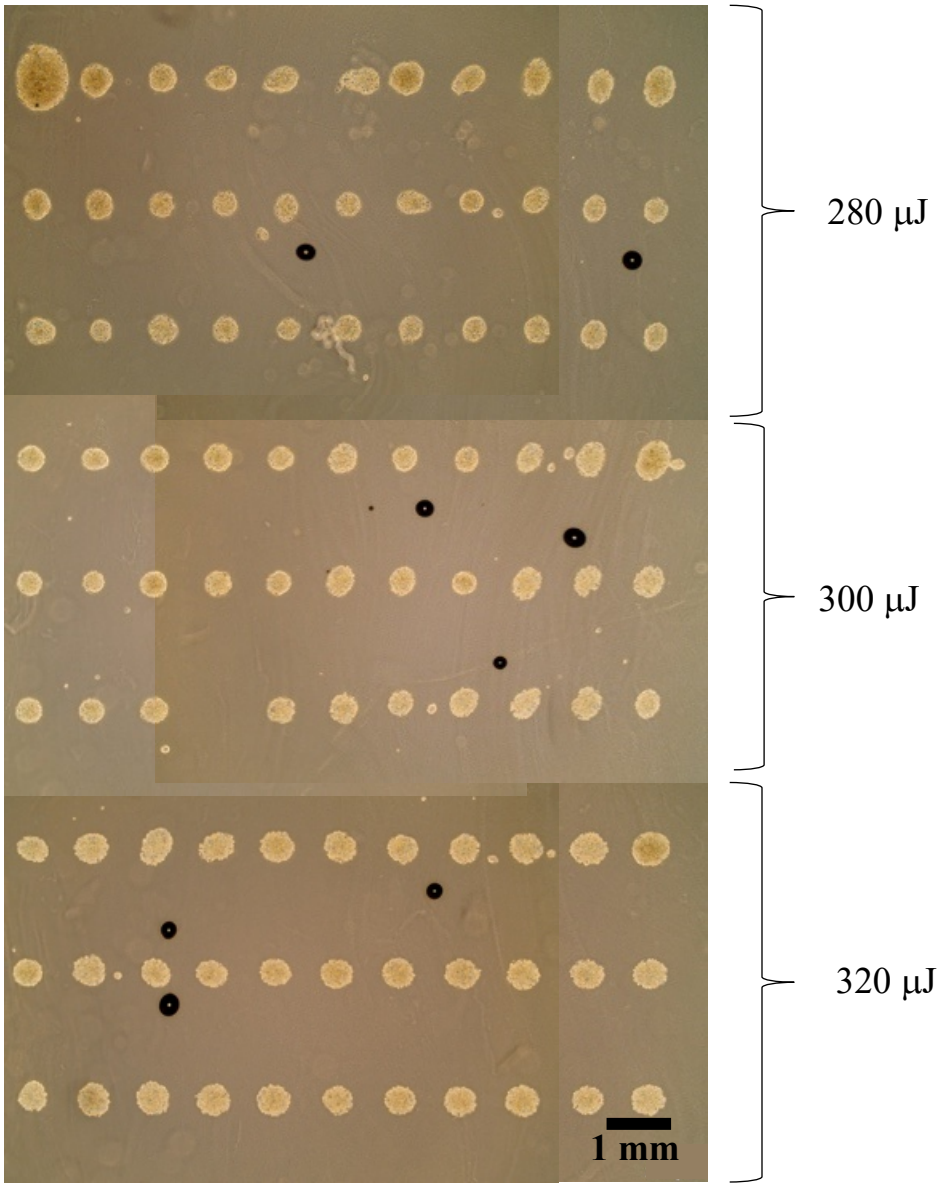

Figure 56. Droplet printing of HUVECs on fibrin substrate using LIST technique day 0.

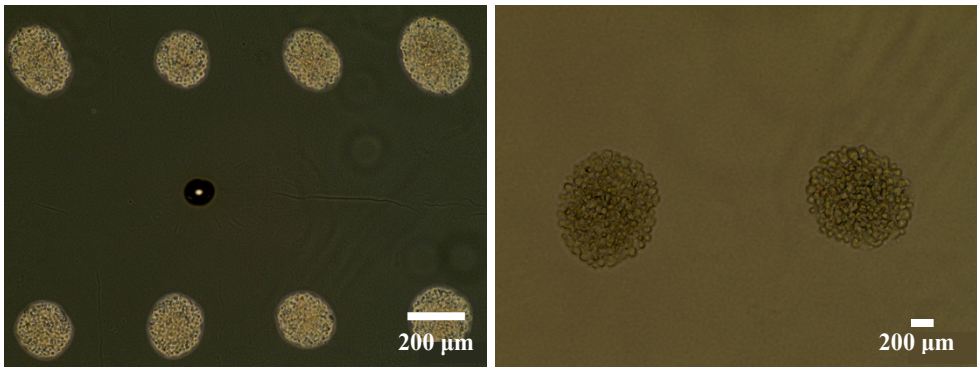

Figure 57. Droplet printing of HUVEC cells on fibrin substrate using LIST technique day 0 (a) 10x magnification (b) 20x magnification.

4.4.1 **Allura Red Dye Toxicity Test with Dye Exclusion Method**

The bioink used in the LIST setup requires a red dye to absorb the laser pulse energy and generate a bubble for droplet ejection. Therefore, we evaluated the Allura red dye effect on HUVEC viability. Figure 58 displays the quantification results for 50 mM and 10 mM red dye concentrations. Comparisons of sample means were performed by two-way ANOVA test.

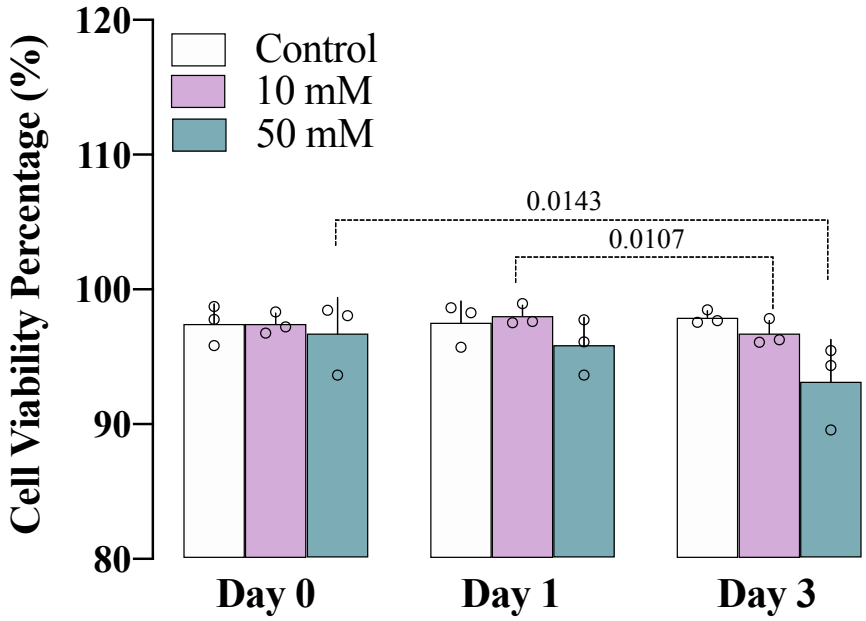

Figure 58. HUVEC viability percentage for dye concentrations of 50 mM, 10 mM and a control condition. Error bars represent standard deviation (N=3), two-way ANOVA test was used for comparison. Data analysis showed no significant difference between the dye concentrations. The 50 mM concentration shows significant difference between days 0 and 3 and the difference between days 1 and 3 for the 10 mM was also significant.

The sample treated at 50 mM has 96.65% viability at day 0 which decreases significantly to 93.07% at day 3. While the 10 mM possesses 97.97% cell viability at day 1 with a significant decrease to 96.67% at day 3. The difference between the dye concentrations and the control were not large enough to be statistically significant. The results for the dye exclusion test shows that there is trend of higher toxicity level of 50 mM concentration for the HUVECs compared to the 10 mM concentration.The 50 mM concentration toxicity seems to decrease HUVEC viabilty through short (day 0) and long term (day 3), whereas, the cell viability percentage of the 10 mM concentration is not significantly different with the control making it appropriate for bioink usage. Data were reported as mean values with error bars representing the standard deviation (N=3).

4.4.2 Allura Dye Effect on HUVEC Attachment and HUVEC Network Formation study

Other than dye effect on cell viability, its effect on HUVEC attachment and HUVEC network formation was examined on Matrigel substrates with and without thrombin (Figure 59). Comparison between images with the 50 mM and 10 mM dye demonstrate that both dye concentrations decrease cell attachment in the absence of thrombin. High number of cell detachment was observed at day 0 right after adding medium for the bioink with 50 mM dye concentration. Cells were detached one day after cell seeding with the bioink 10 mM dye bioink leading to incomplete HUVEC network formation for both concentrations compared to the control. The 50 mM bioink also affected the type of the network structure formed on the Matrigel containing thrombin.

HUVECs were successfully attached to Matrigel containing thrombin surfaces and maintained their attachment up to day 2. The network structure formed on all the Matrigels containing thrombin exhibit different network structure which possess narrow cords with smaller meshes compared to the control Matrigel with no thrombin. To summarize, Allura red dye affects HUVEC cell attachment to Matrigel and in high concentrations affects the network structure (50 mM). The addition of thrombin to Matrigel substrates influences the formed network type. This results from the polymerization process of fibrinogen into fibrin which fixes the cells in position and reduces their mobility to form networks.

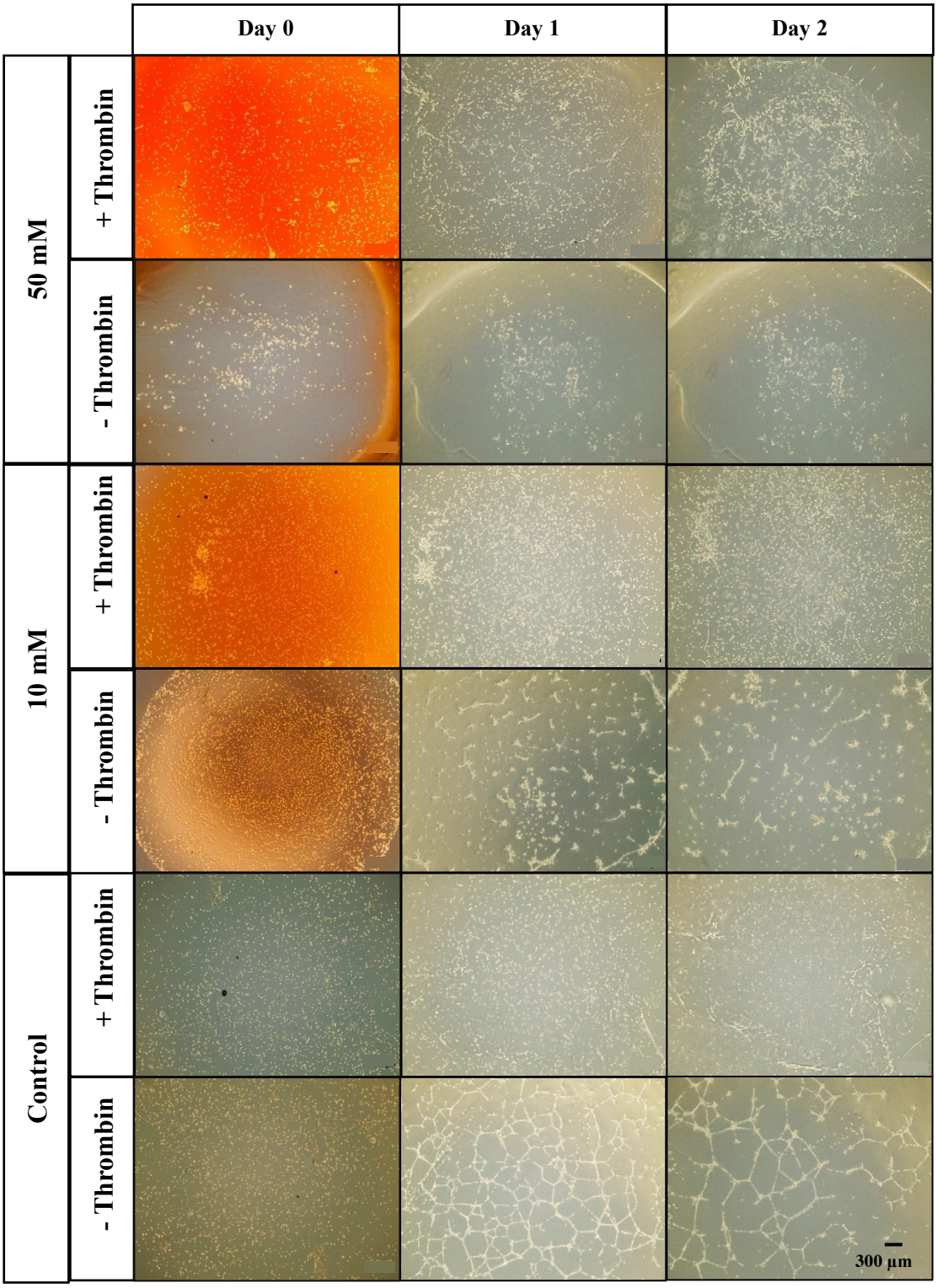

Figure 59. Bioink study with 50 mM and 10 mM concentrations on Matrigel substrates with and without thrombin.

4.4.3 HUVEC Viability Quantification Printed with LIST on Matrigel Substrate

Since LIST is a recent developed technology by our lab, HUVEC viability was investigated using three different energies. Figure 60 represents a section of the microscopy images for days 0, 1 and 3 that were used for quantification to obtain the cell viability percentage. Figure 61 shows the process of cell viability quantification with Matlab code.

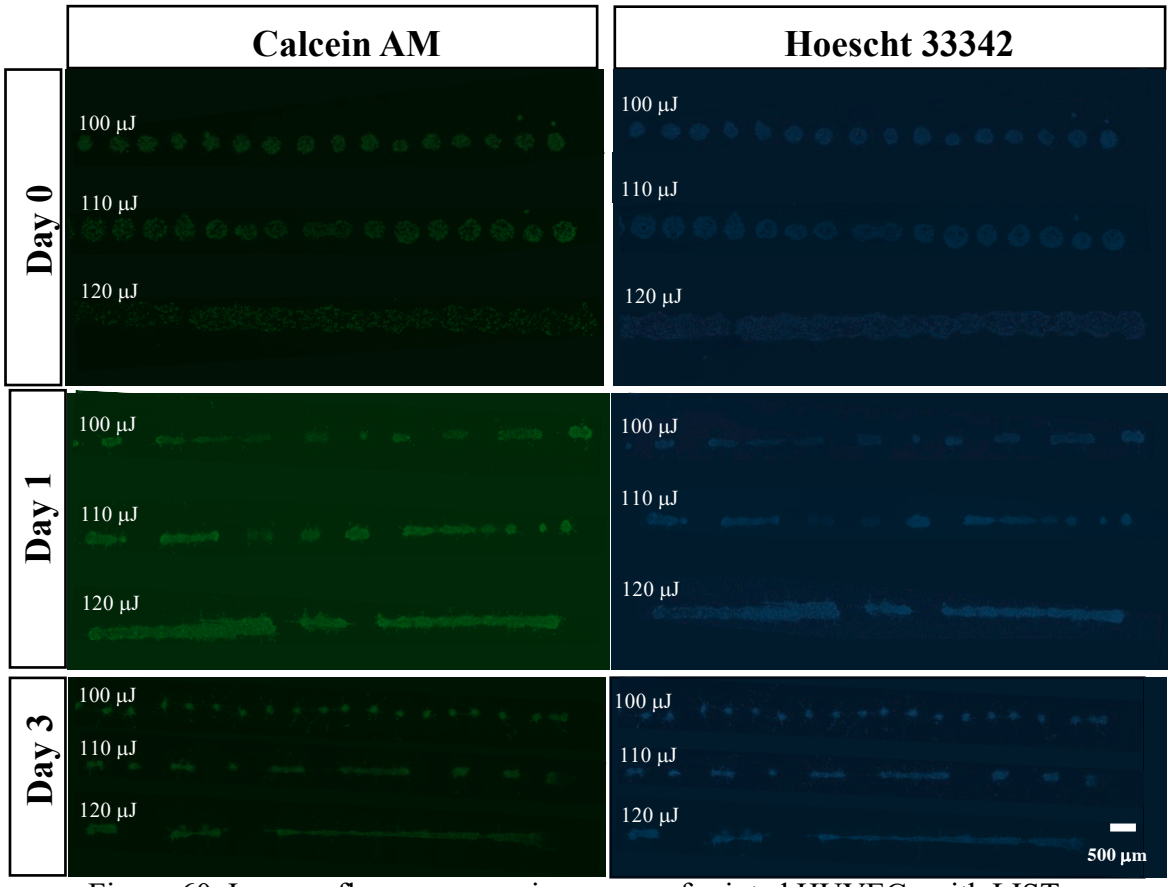

Figure 60. Immunofluorescence microscopy of printed HUVECs with LIST.

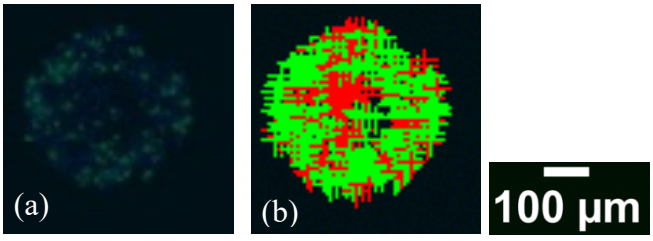

Figure 61. (a) Calcein AM and Hoescht 33342 stained image overlay (b) Live cells labeled with green and dead cells labeled with red.

Figure 62 exhibits the quantified results for the HUVEC viability percentage at days 0, 1 and 3 for printing performed with energies 100, 110 and 120 µJ. The results show a trend of a reverse relationship for day 0 between the energy and cell viability which is due to the immediate laser pulse effect on HUVECs. The immediate laser pulse effect on HUVECs leads to cell death during the printing process. Higher energies eject larger droplets leading to higher number of cells throughout the printing. Therefore, the remaining live cells proliferate and grow resulting in cell viability increase as the energy increases for days 1 and 3. The results show that cell viability might increase 3 days after printing. This is due to the higher number of cells printed for the energy 120 µJ at day 0 which live cells proliferate and the cell viability increases at day 3. Due to time limitation caused by laboratory constraints, the experiment repetition was not applied in order to add errors bars. Therefore, the low cell viability of the control for day 1 can be representative of the experimental error (N=1).

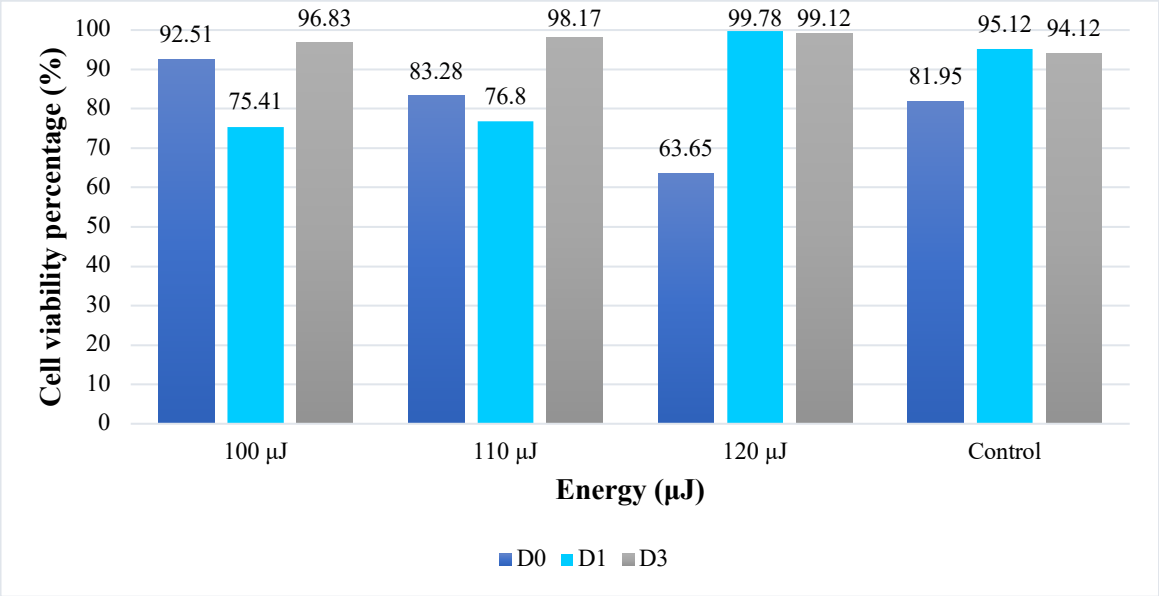

Figure 62. HUVEC cell viability percentage of printed cells with LIST on Matrigel substrate. Due to time limitation caused by laboratory constraints, the experiment repetition was not applied in order to add errors bars (N=1).

4.4.4 LIST HUVEC Printing on Fibrin Substrate

Guiding HUVEC tube formation on fibrin via LIST was studied, HUVECs were patterned into lines on fibrin substrate using LIST technique (Figure 63a). No HUVEC tube formation occurred along the printed HUVEC lines which was a result of the cells inability to preserve their initial printed pattern one day after printing (Figure 63b). The cells demonstrated high cell growth and unorganized distribution throughout the fibrin surface 3 days post printing (Figure 63c). This study can be compared to the conventional seeding of HUVECs on fibrin where the second layer of fibrin was added on the seeded HUVECs and shows similar results: cells proliferated two-dimensionally rather than forming networks.

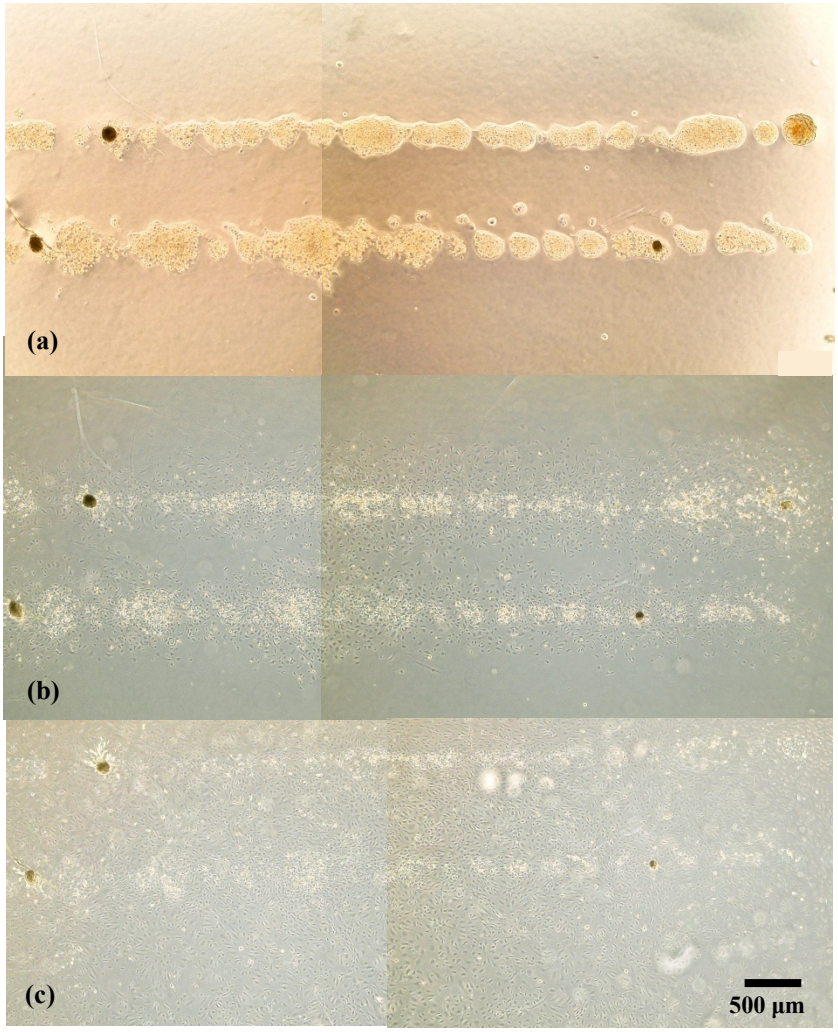

Figure 63. HUVECs printed with LIST on fibrin substrate. (a) day 0, (b) day 1 (c) day 3.

4.4.5 LIST HUVEC Printing on Matrigel Substrate

To investigate guiding tube formation on Matrigel via LIST printing, HUVECs were printed on a Matrigel substrate (without thrombin) using a bioink containing 18 x 10^6 cells/ml (Figure 64a). HUVECs adhesion was not maintained one day after the printing leading to cell detachment from the Matrigel surface (Figure 64b). This finding is in contrary to the observations of the conventional seeding study on Matrigel which the cells remained attached. Furthermore, the attached cells formed networks on the Matrigel surface. This can be explained by the fact that HUVECs require intercellular connections to remain attached to the Matrigel surface. In this printing the number of cells might not have been adequate to provide the required connections leading to cell detachment.

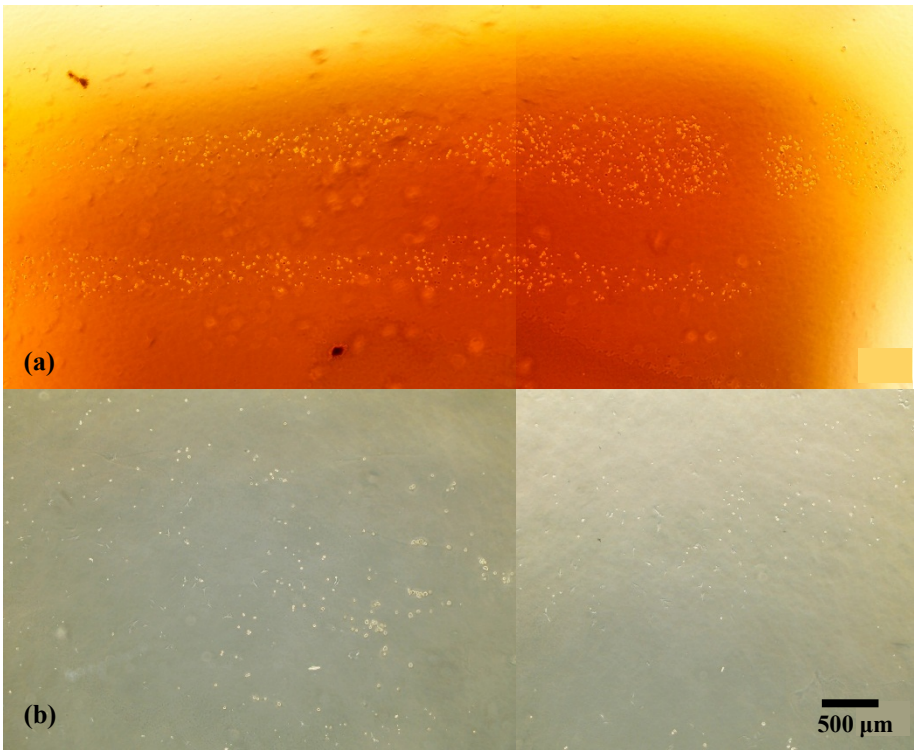

Figure 64. Printing HUVEC cells with LIST on Matrigel substrate without thrombin, bioink concentration 18 x 10^6 cells/ml. (a) day 0, (b) day 1.

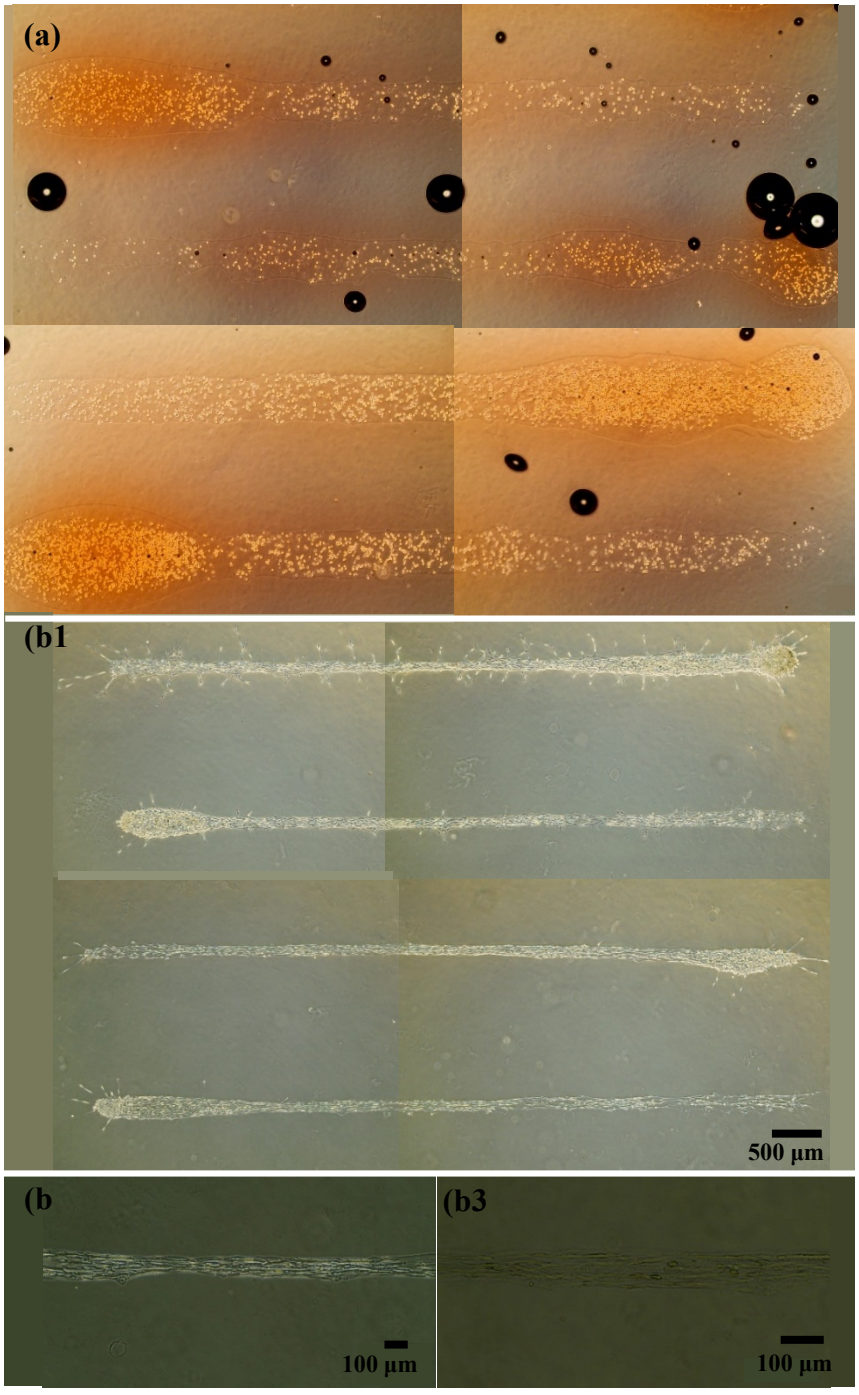

Figure 65. Printing HUVECs with LIST on Matrigel substrate with thrombin, bioink concentration 18 x 10^6 cells/ml. (a) day 0, (b) day 1.

The addition of thrombin to the Matrigel substrate allowed the cells to remain attached to the surface one day after printing. The HUVECs formed connections with adjacent cells constructing capillary-like structures along the patterned lines (Figure 65).

To investigate HUVEC attachment to the Matrigel surface when having high number of cellular interactions, an experiment was conducted performing printing on Matrigel with and without thrombin using bioink with similar cell concentration of 37.5 x 10^6 cells/ml for both substrates.

HUVECs remained attached on the surface of Matrigel without thrombin one day after printing, which is indicative of the role of intercellular connections in cell attachment. The capillary-like structure formation on Matrigel surface with thrombin demonstrates a more uniform structure with less side branching from the main cell printing pattern which was prohibited due to the existence of thrombin (Figure 66). In contrast, the Matrigel without thrombin created capillary-like structures with branches along the sides (Figure 67). Some of these branches connected to the branch from other structures. This is referred as anastomosis which HUVEC tubes connect with each other. Contrary, thrombin immobilizes HUVECs preventing further tube branching and anastomosis.

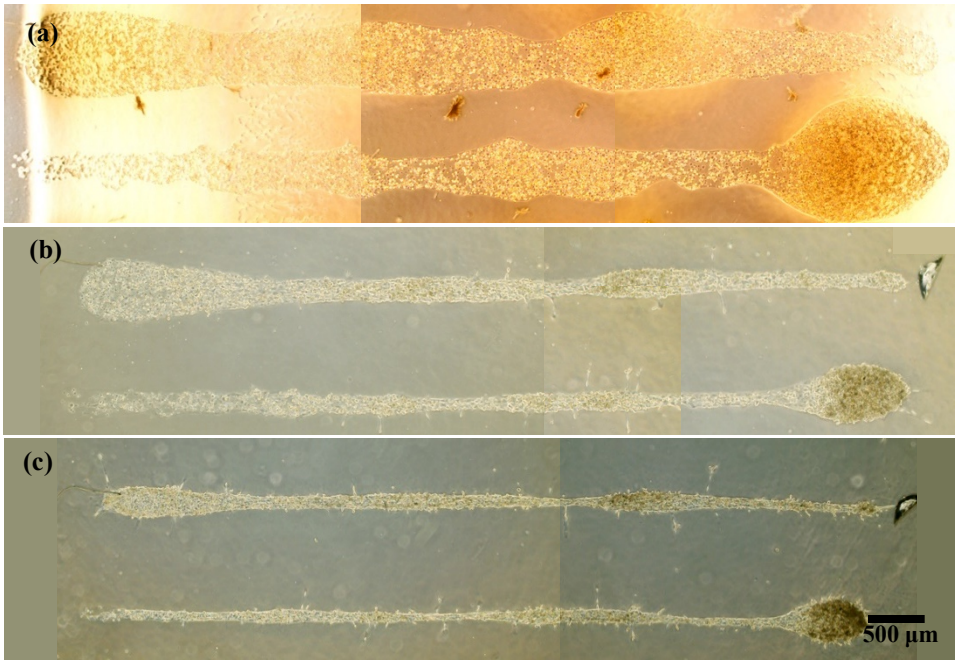

Figure 66. HUVECs printed with LIST on Matrigel substrate containing thrombin and bioink cell concentration 37.5 x 10^6 cells/ml. (a) day 0 (b) day 1 (c) day 2.

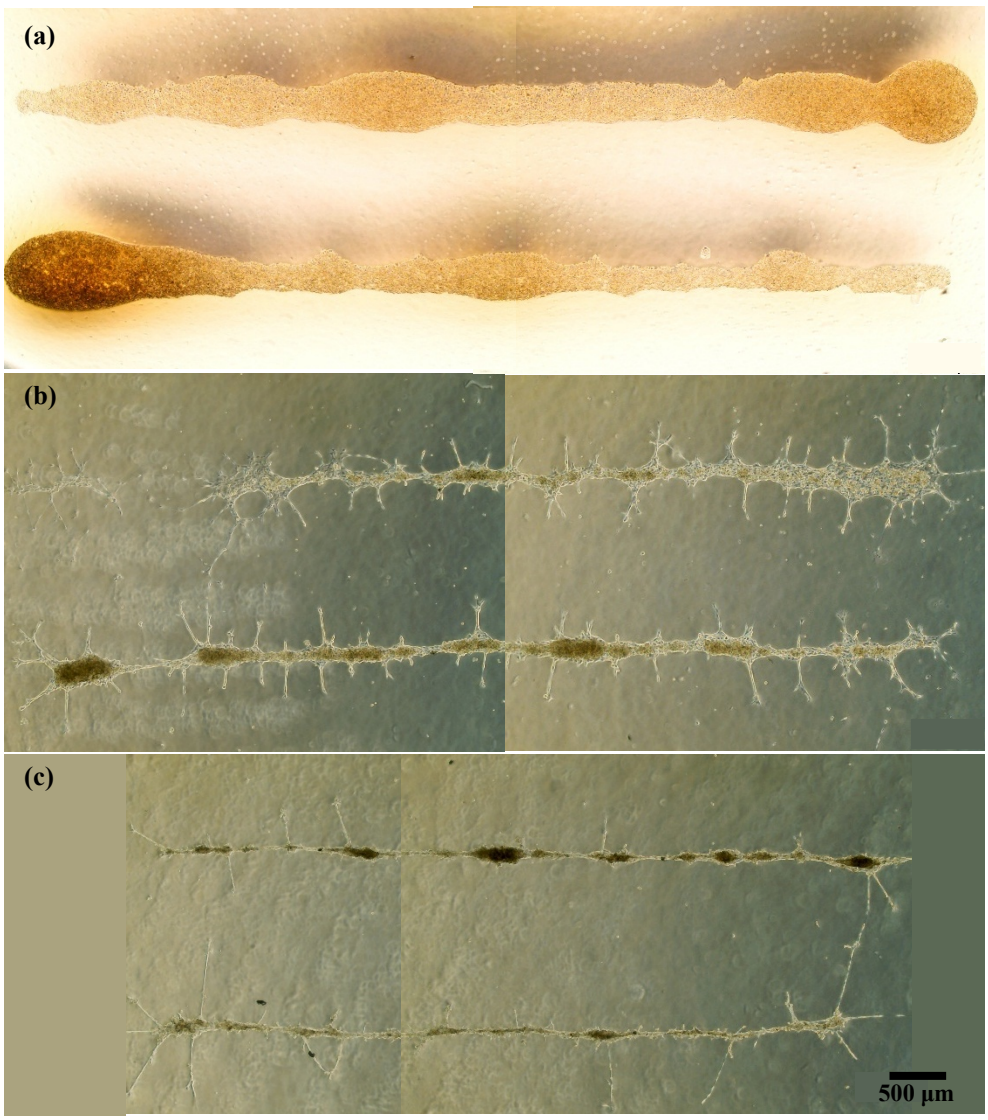

Figure 67. HUVECs printed with LIST on Matrigel without thrombin and bioink cell concentration 37.5 x 10^6 cell/ml. (a) day 0 (b) day 1 (c) day 2.

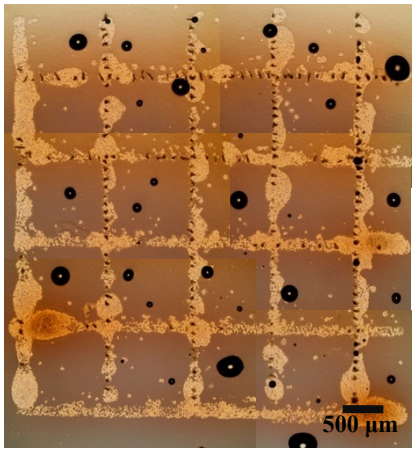

Figure 68. Printed mesh pattern of HUVECs on Matrigel substrate with

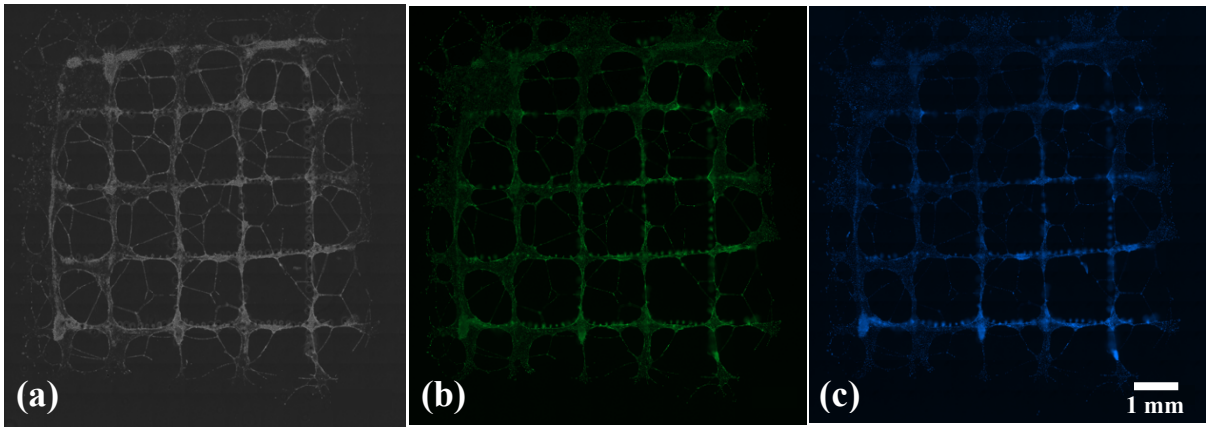

Figure 69. Immunofluorescence microscopy of HUVEC mesh printing on Matrigel substrate with thrombin at day 2. (a) Transmission image (b) Calcein AM staining (c) Hoescht 33342.

To evaluate complex pattern printing, HUVECs were patterned as a mesh on Matrigel substrate with thrombin (Figure 68).

Immunofluorescence microscopy of the mesh printing pattern stained with Calcein AM and Hoescht 33342 at day 2 showed structure formations and network connections (Figure 69). The connection networks between HUVECs in two perpendicular lines can be explained by the anastomosis process within two angiogenic sprouting events (Diaz-Santana, Shan, & Stroock, 2015). The occurred anastomosis in this sample can be the result of situating HUVECs in near distances especially within the mesh corners, leading to tube connection with the HUVEC in the neighboring line. This study demonstrates that within low distances of printed HUVEC lines, angiogenic cues can overcome the ability of thrombin in immobilizing HUVECs.

4.4.6 Thickness Quantification of Capillary-like structures

To evaluate the structure formation throughout time, the thickness was quantified for days 1, 2 and 3 (Figure 70). The results demonstrated that the average structure thickness for days 1, 2 and 3 evolves from 113,9, to 92.62 and to 70,85 µm, respectively (Figure 71). One-way ANOVA test was used for mean comparison. The difference was not large to be considered significant. The trend shows that the thickness of the capillary-like structures decreases from days 1 to 3, an indicative for structure regression.

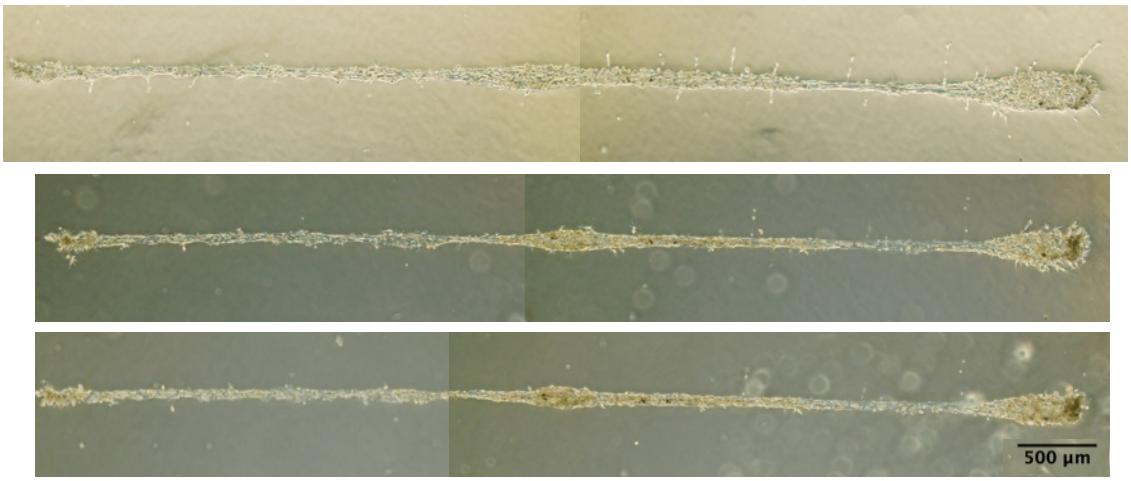

Figure 70.Thickness study of capillary-like formations from day 1 to 3.

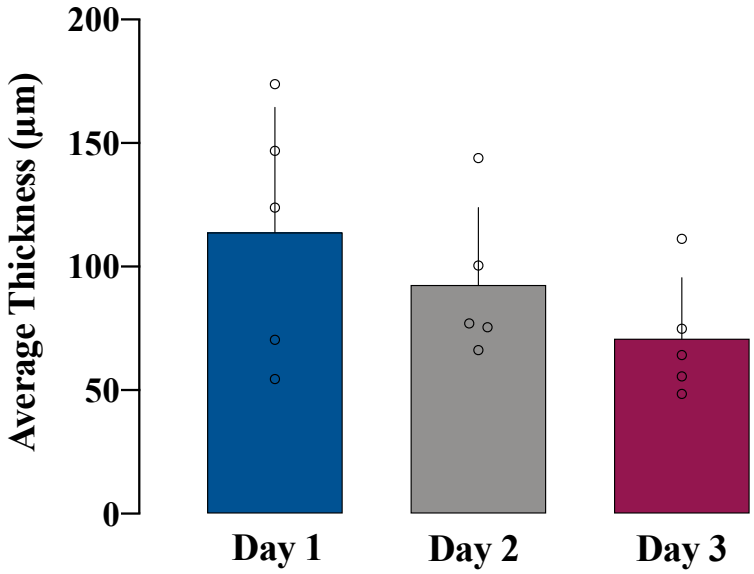

Figure 71. Average thickness of capillary-like structures for days 1, 2 and 3. Error bars represent standard deviation (N=5), one-way ANOVA test was used for mean comparison. Data analysis showed no significant difference.

4.4.7 Confocal Imaging of Capillary-like Formations

The formed capillary-like structures were analyzed by obtaining Z-stack images with confocal microscopy to investigate the inner structure. HUVECs were printed on Matrigel substrate with thrombin and three samples were prepared for three different time points. Each sample was fixed and stained at its specific time point. Confocal microscopy showed that stained HUVECs and cell junction proteins have formed multicellular structures.

Images obtained for day 1 sample demonstrated partially formed capillary-like structures with wide continuous opening along the structure (Figure 72(a1, a2)). Z-stack images reveal void areas within the structure (Figure 72(a3)). Day 2 confocal microscopy assessment showed complete development of the structures (Figure 73 (a1, a2)) and non-continuous void areas in different levels throughout the structure (Figure 73(a3)). The regression process of the structures initiates at day 3 leading to structure collapse (Figure 74(a1, a2)) and void area shrinkage (Figure 74 (b3)).

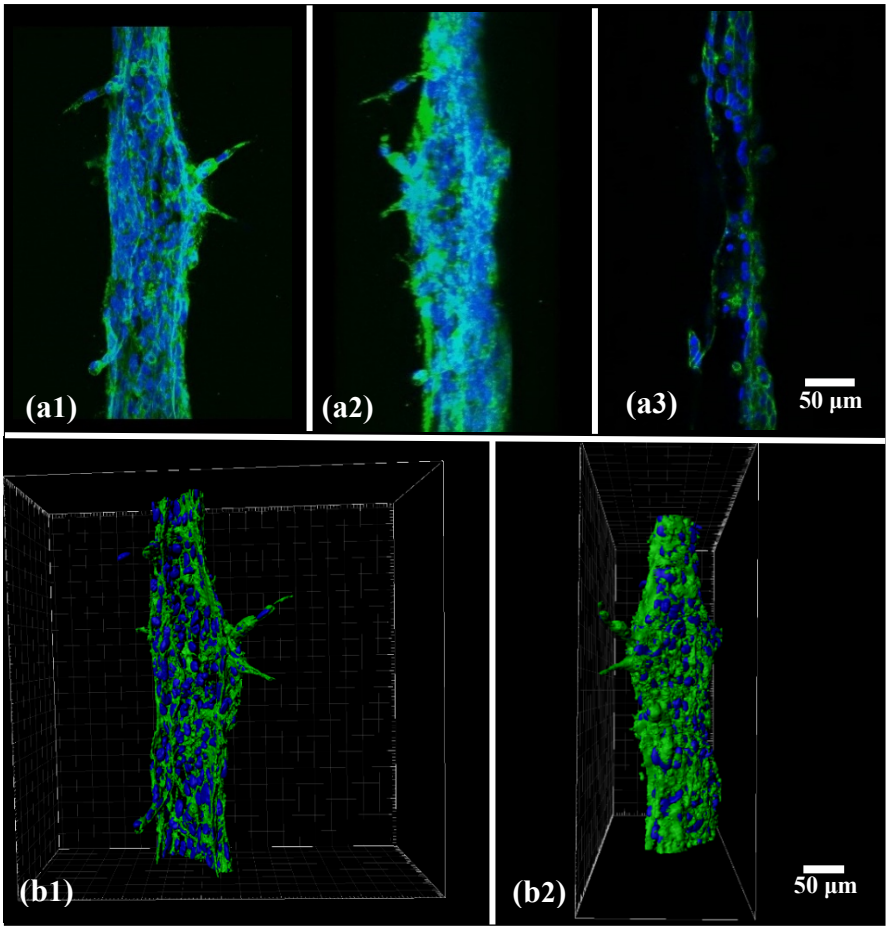

Figure 72. Confocal microscopy of capillary-like structures stained with CD31 and DAPI at day 1 (a1) 3D object of structure front view (a2) 3D object of structure side view (a3) Single plane of Z-stack, numbered void areas were quantified (b1) Imaris reconstruction of structure front view (b2) Imaris reconstruction of structure side view.

The ideal time point in this case for the capillary-like structures would be day 2 due to complete structure formation and due to the observation of internal void areas. The void areas were analyzed by measuring the length, width and the depth of each individual. The average length, width and depth for the void areas were measured as 242,56 ± 99,46, 30,58 ± 15,09 and 143 ± 47,71 µm, respectively (Number of void areas measured=6).

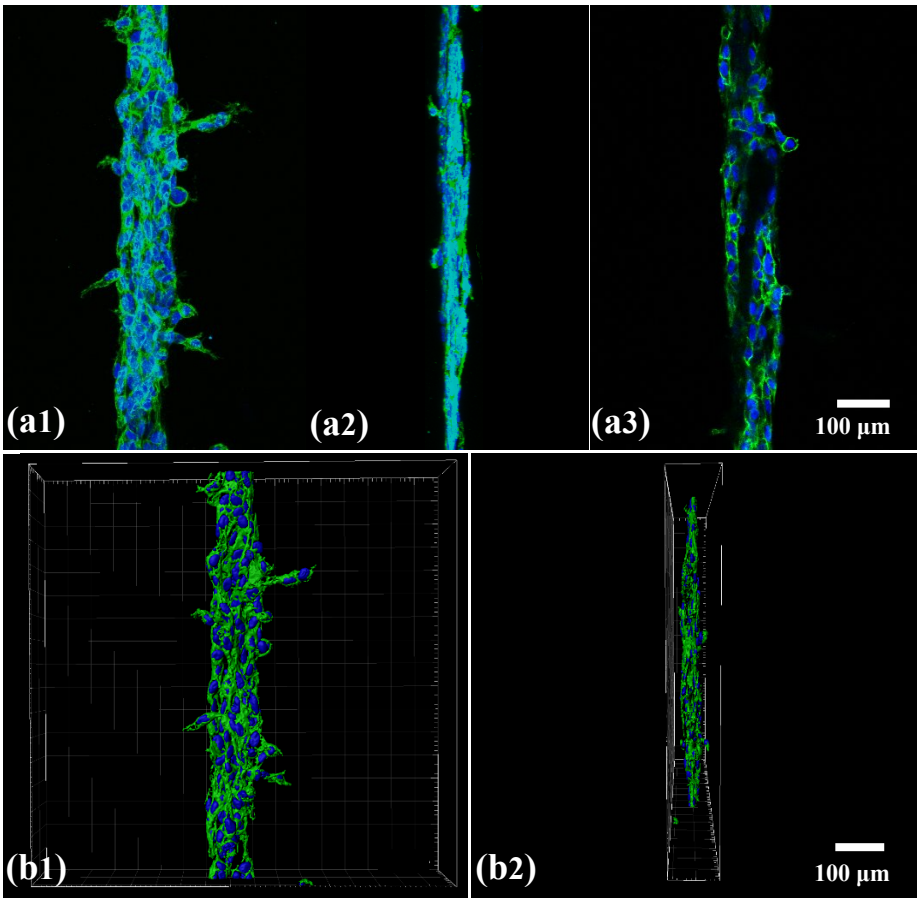

Figure 73. Confocal microscopy of capillary-like structures stained with CD31 and DAPI at day 2 (a1) 3D object of structure front view (a2) 3D object of structure side view (a3) Single plane of Z-stack (b1) Imaris reconstruction of structure front view (b2) Imaris reconstruction of structure side view.

Day 3 void area was not measurable due to structure collapse and regression resulting in void areas with openings which was not considered for quantification. The quantified dimensions can be an indicative for lumen development with further improvement studies such as applying a second cell type such as fibroblasts or PCs to stabilize the formed structure.

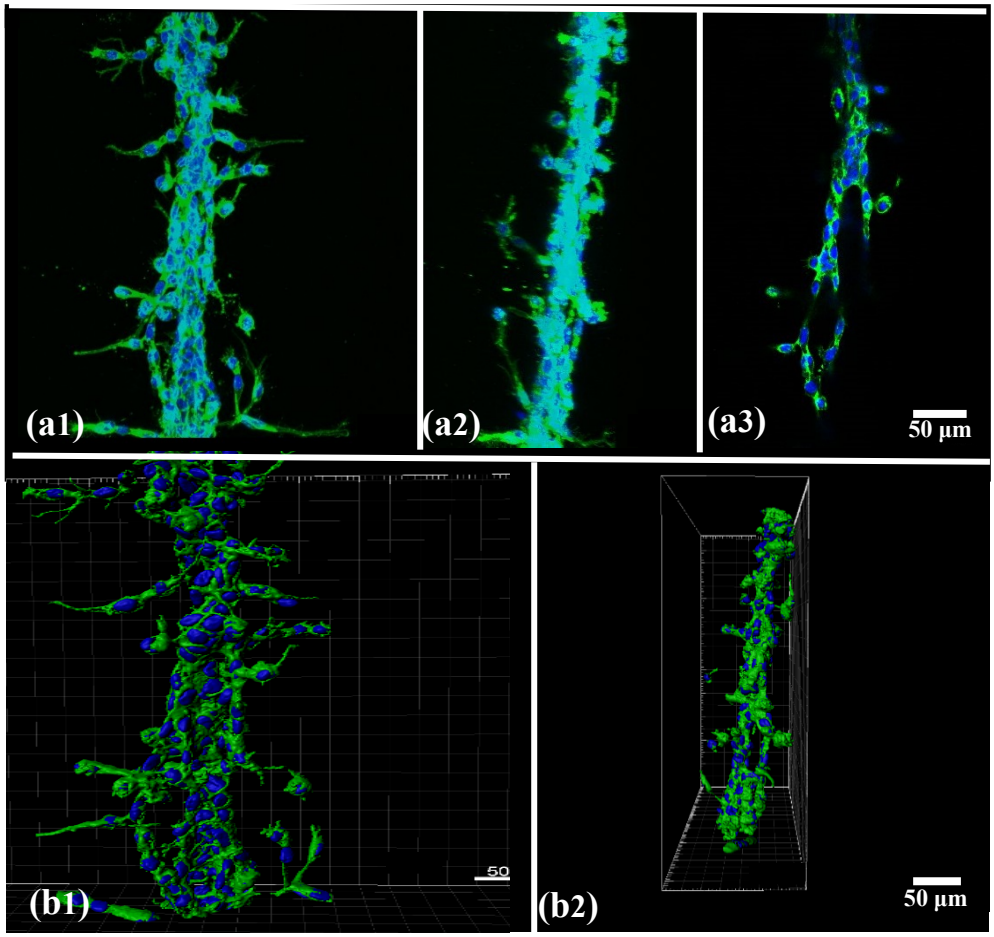

Figure 74. Confocal microscopy of capillary-like structures stained with CD31 and DAPI at day 3 (a1) 3D object of structure front view (a2) 3D object of structure side view (a3) Single plane of Z-stack (b1) Imaris reconstruction of structure front view (b2) Imaris reconstruction of structure side view.

4.4.8 Evaluation of the Presence of Lumen using Frozen Sections

Figure 75 and Figure 76 each demonstrate 3 sections per sample. Immunofluorescence microscopy images of frozen sections enabled internal capillary-like structure visualization. Hollow areas surrounded by cells might be detected in day 2 images (Figure 75 (a1), (a3), (a4), (b3), (b6), (c1)) while some sections showed incomplete hollow areas with an opening (Figure 75 (a5), (b3), (b5), (c4), (c6)). Day 2 sections seem to indicate the existence of non-continuous void areas throughout the capillary-like structures. Initiated regression process and structure collapse at day 3 might have resulted in less sections with assumed complete (Figure 76 (b1), (c1), (c2), (c3), (c5)) and incomplete void areas (Figure 76 (a3), (b4)) compared to day 2 which can be considered as an indicative for our findings in confocal microscopy. Due to the very thin

(20 µm) and delicate nature of the sections, obtaining the sections faced a complex procedure. Therefore, decreasing the possibility to have higher numbers of sections to achieve a conclusive statement and also quantification.

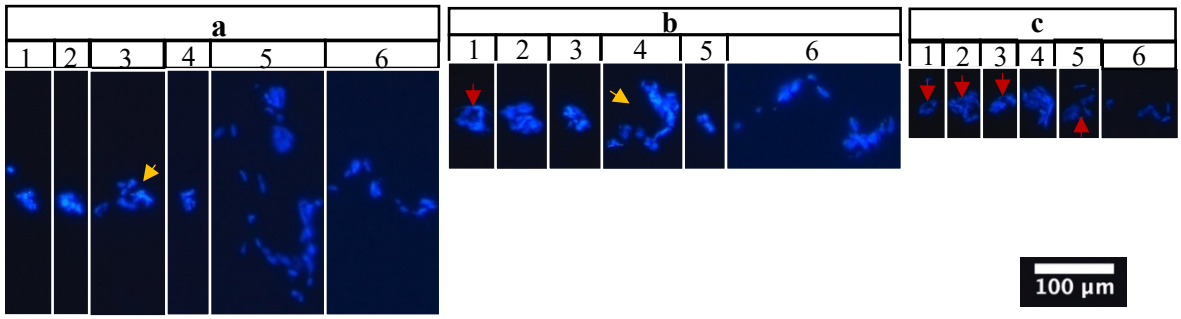

Figure 75. Immunofluorescence images of day 2 frozen sections (a-c) Each represent an individual section of a sample consisting of 6 capillary-like structures (red arrows show complete void areas and yellow areas show incomplete void areas).

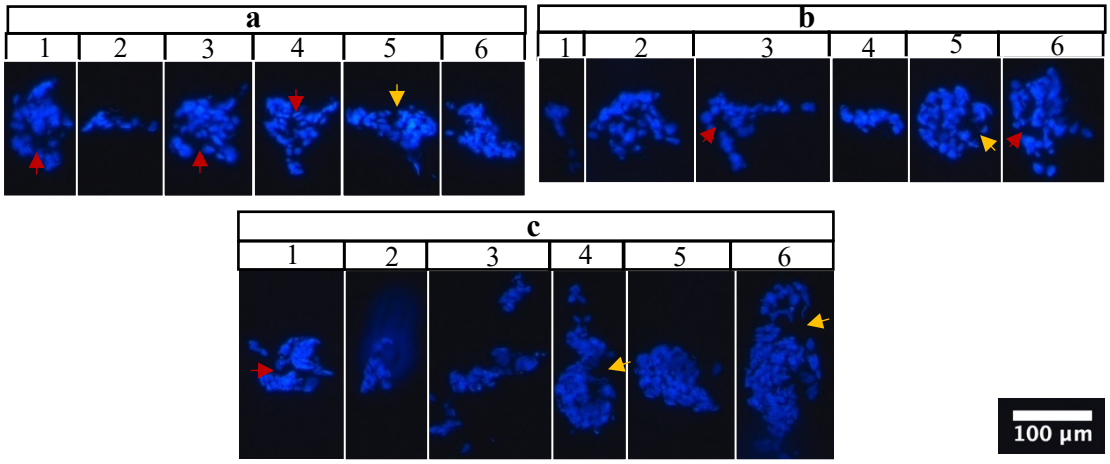

Figure 76. Immunofluorescence images of day 3 frozen sections (a-c) Each represent an individual section of a sample consisting of 6 capillary-like structures (red arrows show complete void areas and yellow areas show incomplete void areas).

5. Discussion

LIFT offers high printing resolution up to 10 µm allowing precise deposition of cells. Extrusion and inkjet bioprinters provide printing resolution in the sub millimeter and print cell aggregates rather single cells (Guillotin et al., 2010).

The present study consists of two series of experiments involved in the pre-bioprinting stage and the bioprinting process which evaluated the two laser-based techniques, LIFT and LIST. Through the pre-bioprinting stage, factors such as biomaterial composition, bioink formulation, HUVEC network formation and printing optimization conditions were investigated to identify ideal printing procedures. HUVEC conventional seeding was studied on fibrin and Matrigel cultured with and without fibroblasts. A parametric study was performed on the bionk thickness film of the LIFT donor substrate to identify and optimize optimal printing conditions. Since Allura red dye is an essential requirement for the bioink application in the LIST setup, HUVEC death rate was tested on cells exposed to 10- and 50-mM dye concentration. Furthermore, the dye effect on the cell attachment on Matrigel with or without thrombin was verified. Prior to patterning HUVECs with LIST, assessment of printing process influence on HUVEC viability at days 0, 1 and 3 was obtained. In the bioprinting process, HUVECs were patterned with both LIFT and LIST techniques on fibrin and Matrigel substrates to observe pattern preservation and HUVEC tube formation. Printed samples with capillary-like structures were analyzed by confocal microscopy, 3D image reconstruction and frozen sectioning.

Since vascular HUVEC is the main building blocks of the angiogenesis process, prior to the cell printing experiments, a series of calibration experiments were conducted to investigate HUVEC behaviour on two types of ECMs, fibrin and Matrigel. In our fibrin models, we studied HUVEC cellular interaction in both 2D and 3D. In the 2D model fibroblasts were incorporated by directly and indirectly contacting HUVECs to investigate the effect of fibroblast-derived factors on endothelial tube formation. The key role of fibroblasts in angiogenesis has been well-recognized. Studies have shown that fibroblast-derived factors promote HUVEC sprouting and lumen formation (Newman et al., 2011). Cellular interaction in 3D resulted in tube formation at day 8 while in 2D incomplete networks were observed for the indirect and control conditions from day 3. This could be explained by the fact that HUVECs require interactions within 3D to

form endothelial tubes in the fibrin hydrogel. Moreover, significant effect of fibroblasts on network formation in the indirect contact was not observed compared to the control. While in the direct condition, fibroblasts prevented any sort of HUVEC structure formation and both cell types proliferated on the surface.

Matrigel, a tumor extract containing basement membrane components, allows the association of cells in 3D and formation of structures similar to the related tissue source (Kleinman & Martin, 2005). Endothelial network formation on Matrigel was reported in previous studies (Kubota, Kleinman, Martin, & Lawley, 1988). Therefore, we used it as a matrix to induce endothelial tube formation. In contrast to the fibrin matrix, seeded HUVECs on a single layer of Matrigel formed tubular structures in both indirect contact (Figure 42) and control conditions (Figure 43) one day after cultivation. While in the direct contact, instead of forming network structures, the cells aggregated into a single patch at day 1 (Figure 41). HUVEC tube formation was quantified by measuring the tube length between two nodes within a network. The total segment length per area of the indirect contact and the control conditions at day 1 were 2.86×10^{-3} μm^{-1} and 2.17×10^{-3} μm^{-1}, respectively (Figure 47). The formed networks regressed through time, leading to the total segment length per area of 9.99×10^{-4} μm^{-1} for the indirect contact and 6.16×10^{-4} μm^{-1} for the control. This might be an indication for the effect of fibroblast-derived factors on HUVEC tube formation, and not the fibroblast cell itself and the unrequired necessity for co-culturing fibroblasts directly with HUVEC cells. To benefit from the fibroblast secreted factors, the designed model should allow the factors to reach the HUVECs and promote tube formation. Moreover, it can be observed that not only does direct co-cultured with fibroblasts not promote endothelial tube formation, but also inhibits the 2D growth of HUVEC cells on Matrigel which is in contrast with direct co-cultured fibroblast and HUVECs on fibrin gel (Figure 40).

To obtain an additional 3D environment, a similar study was conducted on Matrigel with the difference that a Matrigel overlay was added on top of the seeded cells. This led to abnormal network formation of the HUVECs in both indirect and control conditions which were not considered for quantification (Figure 45). This can be a result of the extra Matrigel layer which immobilized the cells and prevented their movement to form endothelial tube structures. In the direct contact after forming a patch of cells at day 1, fibroblast sprouting from the cell patch was

observed at day 6. The 3D Matrigel environment promoted fibroblast sprouting while fibrin promoted 2D fibroblast growth along with HUVECs. This could be explained by the fact that since HUVEC growth was inhibited, the fibroblasts over grew and were able to freely form sprout-like structures.

Printing resolution with LIFT depends on several factors such as the laser energy, laser pulse frequency, the distance between the donor and receiver substrates, bioink thickness, bioink viscosity along with wettability. Therefore, we investigated the effect of cell containing bioink film thickness and laser energy factors to adjust printing conditions. Four bioink thicknesses, 22, 33, 44 and 55 µm were studied using laser energies 15, 20, 25 and 30 µJ to print individual droplets. It was observed through a set of experiments that the number of printed droplets might increase with the bioink thickness decrease and the laser energy increase. Despite the higher number of droplets produced in low bioink thicknesses, droplet nonuniformity is clearly observed through different energy ranges (Figure 48, Figure 49). Whereas, higher thicknesses such as 44 and 55 µm have less droplet ejection but improved droplet features (Figure 50, Figure 51) which can benefit precise pattern designing to obtain high resolution printing performance. This is due to the ability of achieving a uniform bioink film when spreading thick bioinks manually, while attaining a thin uniform bioink film faces difficulties such as rapid drying in the periphery. It is clearly observed that high energies favor droplet ejection in higher thicknesses. However, the ejected droplets required high energy (25 and 30 µJ). Other than successful droplet ejection, high energy prints droplets with higher droplet areas which is suitable for printing high number of cells if required. Regardless of all the mentioned advantages, increasing laser energies for cell printing, decreases cell viability (Catros, Guillotin, Bačáková, Fricain, & Guillemot, 2011). Therefore, a balance should be established between the bioink thickness and the energy used to pursue all the printing goals. The 33 µm thickness combined with energy range 20-25 µJ was considered as an optimized printing condition for further experiments.

Patterned HUVEC lines via LIFT and LIST on fibrin substrate with an additional fibrin overlay formed intercellular connections at day 2 rather forming endothelial tubes (Figure 53, Figure 54). In the literature, to date no study demonstrated the formation of capillary-like structures on fibrin hydrogel using laser-based bioprinter.

Printed HUVECs via LIFT on Matrigel detached one day post printing which can be due to the fact that HUVECs require high number intercellular connections to remain attached (Figure 55). Whereas, manual studies on Matrigel possessing high intercellular connections demonstrated cell attachment leading to network formation.

In this work, LIFT was used in studies such as printing condition optimization and HUVEC printing. Despite LIFT's advantages such high resolution for cell printing, allowing printing of viscous bioinks and high printing speed, we encountered several limitations through our study. When increasing the cell concentration of the bioink (100-200 x 10^6 cells/ml), the wettability duration of the bioink film decreases, limiting the required time to perform printing. Moreover, the bioink should be spreadable on the surface of the donor substrate which is inhibited due to surface tension. Additives such as glycerol and Methylcellulose can improve both wetabillity and spreadibility of the bioink, respectively. However, glycerol is toxic for cells which can decrease cell viability (Catros et al., 2011). Other LIFT limitation is the difficulty to obtain a uniform bioink film on the donor substrate resulting in inconstancy of the printed pattern and final cell concentration on the receiver substrate. Therefore, due to LIFT limitations, we decided to use the recently developed LIST technology (Orimi et al., 2020). LIST eliminates the requirement to obtain a uniform bioink film since it uses a hollow microcapillary as the bioink donor. Compared to LIFT with 65% successful cell-containing droplet ejection, LIST features up to 98% droplet ejection which allows uniform printing using different energy ranges (Figure 56). Printing resolution in LIFT is higher between 10 and 140 μm, while for LIST is between 165 and 325 μm which can be improved with changing the size of the capillary. It seems that LIST might also offer high cell viability above 90% for printed HUVECs three days post-printing (Figure 62).

In the LIFT setup, a titanium or gold layer which coats the donor substrate absorbs the energy of the laser beam while in LIST the energy absorber is a red dye. The analyzed cell viability of the Allura red dye in 10 mM and 50 mM concentrations demonstrated above 90% for both concentrations at days 0, 1 and 3 (Figure 58). The red dye effect on HUVEC attachment and network formation on Matrigel with and without thrombin was also investigated. It was observed that the red dye affected cell attachment to Matrigel surface for both concentrations as cells detached at day 0 for the 50 mM and at day 1 for the 10 mM (Figure 59). Contrary, Matrigel

containing thrombin kept the cells attached, the fibrinogen solution used to resuspend the HUVECs polymerizes when comes into contact with thrombin in the Matrigel substrate. Thus, solidifying the fibrinogen in place and immobilizing the cells leading to different network formation compared to the control networks without thrombin. It was also observed that the 50 mM concentration on the Matrigel with no thrombin affected the type of the formed network. Since the 10 mM dye concentration possessed higher cell viability percentage, higher cell attachment and normal network formation compared to the 50 mM, it was considered as the optimal concentration for cell printing experiments.

Bioink formulation consisted of fibrinogen solution for all cell printing experiments. The bioink cell concentration was optimized through a set of experiments. To prevent cell detachment when performing HUVEC printing on Matrigel with low cell concentrations (18 x 10^6 cells/ml) (Figure 64), Matrigel containing thrombin was used as a substrate. Eventually, LIST was able to print HUVECs that formed capillary-like structures (Figure 65). It was observed that due to intercellular connections, high cell concentrations (37.5 x 10^6 cells/ml) formed capillary-like structures on both Matrigel with (Figure 66) and without thrombin (Figure 67). The capillary-like structures formed on Matrigel without thrombin exhibited side branching along the structure while the structures on the Matrigel with thrombin lack these branches. These branches also anastomose with other HUVEC branches from the neighboring line. However, anastomose was also observed in the mesh pattern design despite the existence of thrombin. This can be explained by the fact that since HUVECs were located within near distances, such as the mesh corners, angiogenic factors overcome the solidified fibrinogen and form anastomoses. Other than cell attachment, thrombin plays the maintenance role of the printed patterns and stabilizes the structures post formation. It also offers the ability to print with low cell concentrations which is not applicable on Matrigel due to cell detachment. Therefore, in this study we considered Matrigel containing thrombin as an ideal printing substrate since the goal of this study is to apply low cell concentrations to construct narrow capillary-like structures (Figure 65). This was based on the goal that tissue regeneration requires precise and defined vascular structures to begin with. As seen in the mesh design, HUVEC tubes still possess the ability to connect with other tubes which is an indicative that thrombin does not abnormally

prevent branching but can only restrict it (Figure 69). However, depending on the desired application, branched capillary-like structures can be suitable for drug screening platforms.

The quantified thickness for the capillary-like structures at days 1, 2 and 3 shows that the average thickness seems to decrease throughout time which can be an indicative for the unstable state of the structures (Figure 70, Figure 71).

Capillary-like structures at days 1, 2 and 3 were analyzed with confocal microscopy. The immunofluorescence images showed that day 1 structures are partially formed missing a section of the structure wall throughout the construct (Figure 72 (a1, a2)). The capillary formation. procedure was completed at day 2 resulting in a uniform structure (Figure 73 (a1, a2)). At day 3 the structures initiated their early regression process leading to structure collapse (Figure 74 (a1, a2)). Day 2 Z-stack images showed non-continuous void areas (Figure 73(a3)) measured to 242,56 ± 99,46 μm long while at day 3 the void areas decrease in dimensions not allowing quantification (Figure 74(a3)). Both days 2 (Figure 75) and 3 (Figure 76) frozen sections might correspond to the Z-stacks, demonstrating sections with circular void areas and decrease in the size of these void areas in the day 3 frozen sections.

In the literature a limited number of studies have employed LIFT technology to print vascular structures. In studies, printed HUVECs formed cord structures rather than capillary structures and their lumen development was not investigated (Pirlo et al., 2012; P. Wu & Ringeisen, 2010). In another study, capillary-like structures were generated in the form of an interwoven network instead of a single and distinct structure which as previous studies, lumen development was also not studied (Kérourédan et al., 2019). As for studies employing other printing techniques, lumen formation was verified but the extend of the formed lumen throughout the structure was not investigated (Kolesky et al., 2016; Zhu et al., 2017).

This study was able to guide HUVECs to generate precise capillary-like structures with the average thickness of 92,62 μm (day 2). Furthermore, other than printing lines, we also demonstrated the capability of this technique for successful printing of a more complex mesh pattern (Figure 68).

6. Future works

Matrigel allows the formation of microvascular structures in 2D cultures while fibrin matrix requires a 3D culture (Nicosia & Ottinetti, 1990). Matrigel induces rapid microvascular network formation (after 24 hours). However, the formed microvascular structures are immature and have reduced luminal size (Nicosia & Ottinetti, 1990). In this study, the formed capillary structures can be further stabilized by recruiting a second cell type in the form of co-printing or co-culturing with the printed HUVECs. Fibroblasts (Nicosia & Ottinetti, 1990) or PCs (Garner, 1994) are necessary to stabilize the newly formed capillary-like structures. In this case, these cell types can aid lumen development and prevent early structure regression at day 3.

Since LIST is a novel technique it will require further optimization to improve stable printing conditions and allow printing repeatability.

7. Conclusion

In this study, we compared LIFT and LIST laser-based bioprinters and we demonstrated the role of fibroblasts cells as promoters of endothelial network formation. LIST is a more efficient laser-bioprinter compared to LIFT, providing precise deposition of cells and uniform printing patterns. LIST technology allows to pre-organize HUVECs in order to guide the formation of microvascular structures *in vitro*. The important outcome of this work was the successful guidance of capillary-like structure formation via LIST. This represents a major step in achieving the main process for engineered angiogenesis *in vitro*. With further improvements, this model can be a platform for drug screening and in the upcoming future, can be applied to vascularize complex engineered tissues.

The effect of fibroblast cells on printed capillary-like structures was not investigated in this study due to time limitation caused by laboratory access constraints.

8. References

Adams, R. H., & Alitalo, K. (2007). Molecular regulation of angiogenesis and lymphangiogenesis. *Nature reviews Molecular cell biology, 8*(6), 464-478.

. : Angiogenesis Analyzer. (2012): Carpentier G. ImageJ contribution.

Antoshin, A., Churbanov, S., Minaev, N., Deying, Z., Yuanyuan, Z., Shpichka, A., & Timashev, P. (2019). LIFT-bioprinting, is it worth it? *Bioprinting*, e00052.

Atala, A. (2011). Tissue engineering of human bladder. *British medical bulletin, 97*(1), 81-104.

Atala, A., Kasper, F. K., & Mikos, A. G. (2012). Engineering complex tissues. *Science translational medicine, 4*(160), 160rv112-160rv112.

Auerbach, R., Lewis, R., Shinners, B., Kubai, L., & Akhtar, N. J. C. c. (2003). Angiogenesis assays: a critical overview. *49*(1), 32-40.

Augustin, H. G., Kozian, D. H., & Johnson, R. C. (1994). Differentiation of endothelial cells: analysis of the constitutive and activated endothelial cell phenotypes. *Bioessays, 16*(12), 901-906.

Bancroft, G. N., Sikavitsas, V. I., van den Dolder, J., Sheffield, T. L., Ambrose, C. G., Jansen, J. A., & Mikos, A. G. (2002). Fluid flow increases mineralized matrix deposition in 3D perfusion culture of marrow stromal osteoblasts in a dose-dependent manner. *Proceedings of the National Academy of Sciences, 99*(20), 12600-12605.

Barallobre-Barreiro, J., Loeys, B., Mayr, M., Rienks, M., Verstraeten, A., & Kovacic, J. C. (2020). Extracellular Matrix in Vascular Disease, Part 2/4: JACC Focus Seminar. *Journal of the American College of Cardiology, 75*(17), 2189-2203.

Bellin, M., Marchetto, M. C., Gage, F. H., & Mummery, C. L. (2012). Induced pluripotent stem cells: the new patient? *Nature reviews Molecular cell biology, 13*(11), 713-726.

Bender, J. G., Cooney, E. M., Kandel, J. J., & Yamashiro, D. J. (2004). Vascular remodeling and clinical resistance to antiangiogenic cancer therapy. *Drug Resistance Updates, 7*(4-5), 289-300.

Berillis, P. J. T. O. C., & Journal, V. (2013). The role of collagen in the aorta's structure. *6*(1).

Bian, L., Hou, C., Tous, E., Rai, R., Mauck, R. L., & Burdick, J. A. (2013). The influence of hyaluronic acid hydrogel crosslinking density and macromolecular diffusivity on human MSC chondrogenesis and hypertrophy. *Biomaterials, 34*(2), 413-421.

Bianco, P., & Robey, P. G. (2001). Stem cells in tissue engineering. *Nature, 414*(6859), 118-121.

Bidanda, B., & Bártolo, P. J. (2007). *Virtual prototyping & bio manufacturing in medical applications*: Springer.

Blasi, F., & Carmeliet, P. (2002). uPAR: a versatile signalling orchestrator. *Nature reviews Molecular cell biology, 3*(12), 932-943.

Blau, H. M., & Daley, G. Q. (2019). Stem Cells in the Treatment of Disease. *New England Journal of Medicine, 380*(18), 1748-1760. doi:10.1056/NEJMra1716145

Bohandy, J., Kim, B., & Adrian, F. (1986). Metal deposition from a supported metal film using an excimer laser. *Journal of Applied Physics, 60*(4), 1538-1539.

Bosman, F. T., & Stamenkovic, I. (2003). Functional structure and composition of the extracellular matrix. *The Journal of Pathology: A Journal of the Pathological Society of Great Britain and Ireland, 200*(4), 423-428.

Brown, L. F., Yeo, K., Berse, B., Yeo, T.-K., Senger, D. R., Dvorak, H. F., & Van De Water, L. (1992). Expression of vascular permeability factor (vascular endothelial growth factor) by

epidermal keratinocytes during wound healing. *The Journal of experimental medicine, 176*(5), 1375-1379.

Cao, Y., Gong, Y., Liu, L., Zhou, Y., Fang, X., Zhang, C., . . . Li, J. (2017). The use of human umbilical vein endothelial cells (HUVECs) as an in vitro model to assess the toxicity of nanoparticles to endothelium: a review. *Journal of Applied Toxicology, 37*(12), 1359-1369.

Carmeliet, P. (2003). Angiogenesis in health and disease. *Nature medicine, 9*(6), 653-660.

Carrow, J. K., Kerativitayanan, P., Jaiswal, M. K., Lokhande, G., & Gaharwar, A. K. (2015). Polymers for bioprinting. In *Essentials of 3D Biofabrication and Translation* (pp. 229-248): Elsevier.

Catros, S., Guillotin, B., Bačáková, M., Fricain, J.-C., & Guillemot, F. (2011). Effect of laser energy, substrate film thickness and bioink viscosity on viability of endothelial cells printed by Laser-Assisted Bioprinting. *Applied Surface Science, 257*(12), 5142-5147.

Chang, R., Emami, K., Wu, H., & Sun, W. (2010). Biofabrication of a three-dimensional liver micro-organ as an in vitro drug metabolism model. *Biofabrication, 2*(4), 045004.

Chernysh, I. N., Nagaswami, C., Purohit, P. K., & Weisel, J. W. (2012). Fibrin clots are equilibrium polymers that can be remodeled without proteolytic digestion. *Scientific reports, 2*(1), 1-6.

Cines, D. B., Pollak, E. S., Buck, C. A., Loscalzo, J., Zimmerman, G. A., McEver, R. P., . . . Schwartz, B. S. (1998). Endothelial cells in physiology and in the pathophysiology of vascular disorders. *Blood, The Journal of the American Society of Hematology, 91*(10), 3527-3561.

Datta, P., Ayan, B., & Ozbolat, I. T. (2017). Bioprinting for vascular and vascularized tissue biofabrication. *Acta biomaterialia, 51*, 1-20.

Datta, P., Barui, A., Wu, Y., Ozbolat, V., Moncal, K. K., & Ozbolat, I. T. (2018). Essential steps in bioprinting: From pre-to post-bioprinting. *Biotechnology advances, 36*(5), 1481-1504.

Davis, G. E., & Senger, D. R. (2005). Endothelial extracellular matrix: biosynthesis, remodeling, and functions during vascular morphogenesis and neovessel stabilization. *Circulation research, 97*(11), 1093-1107.

De Angelis, E., Moss, S. H., & Pouton, C. W. J. A. d. d. r. (1996). Endothelial cell biology and culture methods for drug transport studies. *18*(2), 193-218.

Derakhshanfar, S., Mbeleck, R., Xu, K., Zhang, X., Zhong, W., & Xing, M. (2018). 3D bioprinting for biomedical devices and tissue engineering: A review of recent trends and advances. *Bioactive materials, 3*(2), 144-156.

Devillard, R., Pages, E., Correa, M. M., Keriquel, V., Remy, M., Kalisky, J., . . . Guillemot, F. (2014). Cell patterning by laser-assisted bioprinting. In *Methods in cell biology* (Vol. 119, pp. 159-174): Elsevier.

Diaz-Santana, A., Shan, M., & Stroock, A. D. (2015). Endothelial cell dynamics during anastomosis in vitro. *Integrative Biology, 7*(4), 454-466.

DiMasi, J. A., Grabowski, H. G., & Hansen, R. W. (2015). The cost of drug development. *New England Journal of Medicine, 372*.

Eble, J. A., & Niland, S. (2009). The extracellular matrix of blood vessels. *Current pharmaceutical design, 15*(12), 1385-1400.

Edelberg, J. M., Aird, W. C., Wu, W., Rayburn, H., Mamuya, W. S., Mercola, M., & Rosenberg, R. D. (1998). PDGF mediates cardiac microvascular communication. *The Journal of clinical investigation, 102*(4), 837-843.

Fedorovich, N. E., Wijnberg, H. M., Dhert, W. J., & Alblas, J. (2011). Distinct tissue formation by heterogeneous printing of osteo-and endothelial progenitor cells. *Tissue Engineering Part A, 17*(15-16), 2113-2121.

Feinberg, A. W., Feigel, A., Shevkoplyas, S. S., Sheehy, S., Whitesides, G. M., & Parker, K. K. (2007). Muscular thin films for building actuators and powering devices. *Science, 317*(5843), 1366-1370.

Ferrara, N., Gerber, H.-P., & LeCouter, J. (2003). The biology of VEGF and its receptors. *Nature medicine, 9*(6), 669-676.

Folkman, J. (1992). shing Y. *Angiogenesis. J Biol Chem, 267*, 10931-10934.

Gaebel, R., Ma, N., Liu, J., Guan, J., Koch, L., Klopsch, C., . . . Mark, P. (2011). Patterning human stem cells and endothelial cells with laser printing for cardiac regeneration. *Biomaterials, 32*(35), 9218-9230.

Gaengel, K., Genové, G., Armulik, A., & Betsholtz, C. (2009). Endothelial-mural cell signaling in vascular development and angiogenesis. *Arteriosclerosis, thrombosis, and vascular biology, 29*(5), 630-638.

Garner, A. (1994). Pathobiology of ocular diseases. In *Vascular Diseases*: Dekker New York.

Gelain, F., Bottai, D., Vescovi, A., & Zhang, S. (2006). Designer self-assembling peptide nanofiber scaffolds for adult mouse neural stem cell 3-dimensional cultures. *PloS one, 1*(1).

Genetic Engineering and Biotechnology News, L. H. (2017). Advancing 3D Cell Culture for Biomedical Research Using Primary Cells. Retrieved from https://www.genengnews.com/magazine/297/advancing-3d-cell-culture-for-biomedical-research-using-primary-cells/

Gerhardt, H., Golding, M., Fruttiger, M., Ruhrberg, C., Lundkvist, A., Abramsson, A., . . . Shima, D. (2003). VEGF guides angiogenic sprouting utilizing endothelial tip cell filopodia. *The Journal of cell biology, 161*(6), 1163-1177.

Greif, D. M., Kumar, M., Lighthouse, J. K., Hum, J., An, A., Ding, L., . . . Offermanns, S. (2012). Radial construction of an arterial wall. *Developmental cell, 23*(3), 482-493.

Gudapati, H., Dey, M., & Ozbolat, I. (2016). A comprehensive review on droplet-based bioprinting: Past, present and future. *Biomaterials, 102*, 20-42.

Guillemot, F., Souquet, A., Catros, S., & Guillotin, B. (2010). Laser-assisted cell printing: principle, physical parameters versus cell fate and perspectives in tissue engineering. *Nanomedicine, 5*(3), 507-515.

Guillotin, B., Souquet, A., Catros, S., Duocastella, M., Pippenger, B., Bellance, S., . . . Amédée, J. (2010). Laser assisted bioprinting of engineered tissue with high cell density and microscale organization. *Biomaterials, 31*(28), 7250-7256.

Harkness, M. L., Harkness, R., & McDonald, D. (1957). The collagen and elastin content of the arterial wall in the dog. *Proceedings of the Royal Society of London. Series B-Biological Sciences, 146*(925), 541-551.

He, P., Zhao, J., Zhang, J., Li, B., Gou, Z., Gou, M., . . . trauma. (2018). Bioprinting of skin constructs for wound healing. *6*(1).

He, Y., Yang, F., Zhao, H., Gao, Q., Xia, B., & Fu, J. (2016). Research on the printability of hydrogels in 3D bioprinting. *Scientific Reports, 6*, 29977.

Holzl, K., Lin, S., Tytgat, L., Van Vlierberghe, S., Gu, L., & Ovsianikov, A. Bioink properties before, during and after 3D bioprinting. Biofabrication. 2016; 8 (3): 032002. In.

Hölzl, K., Lin, S., Tytgat, L., Van Vlierberghe, S., Gu, L., & Ovsianikov, A. (2016). Bioink properties before, during and after 3D bioprinting. *Biofabrication, 8*(3), 032002.

Horváth, L., Umehara, Y., Jud, C., Blank, F., Petri-Fink, A., & Rothen-Rutishauser, B. (2015). Engineering an in vitro air-blood barrier by 3D bioprinting. *Scientific Reports, 5*, 7974.

Hribar, K. C., Meggs, K., Liu, J., Zhu, W., Qu, X., & Chen, S. (2015). Three-dimensional direct cell patterning in collagen hydrogels with near-infrared femtosecond laser. *Scientific Reports, 5*(1), 17203. doi:10.1038/srep17203

Hribar, K. C., Soman, P., Warner, J., Chung, P., & Chen, S. (2014). Light-assisted direct-write of 3D functional biomaterials. *Lab on a Chip, 14*(2), 268-275.

Hughes, C. S., Postovit, L. M., & Lajoie, G. A. (2010). Matrigel: a complex protein mixture required for optimal growth of cell culture. *Proteomics, 10*(9), 1886-1890.

Huh, D., Hamilton, G. A., & Ingber, D. E. (2011). From 3D cell culture to organs-on-chips. *Trends in cell biology, 21*(12), 745-754.

Ibrahim T. Ozbolat, W. P., Veli Ozbolat,. (2016). Application areas of 3D bioprinting. *Drug Discovery Today, 21*(8), 1257-1271. doi:https://doi.org/10.1016/j.drudis.2016.04.006.

Järveläinen, H., Sainio, A., Koulu, M., Wight, T. N., & Penttinen, R. (2009). Extracellular matrix molecules: potential targets in pharmacotherapy. *Pharmacological reviews, 61*(2), 198-223.

Kassem, M., Abdallah, B. M., Yu, Z., Ditzel, N., & Burns, J. S. (2004). The use of hTERT-immortalized cells in tissue engineering. *Cytotechnology, 45*(1-2), 39-46.

Kérourédan, O., Bourget, J.-M., Rémy, M., Crauste-Manciet, S., Kalisky, J., Catros, S., . . . Devillard, R. (2019). Micropatterning of endothelial cells to create a capillary-like network with defined architecture by laser-assisted bioprinting. *Journal of Materials Science: Materials in Medicine, 30*(2), 28.

Klebe, R. J. (1988). Cytoscribing: a method for micropositioning cells and the construction of two- and three-dimensional synthetic tissues. *Experimental cell research, 179*(2), 362-373.

Kleinman, H. K., & Martin, G. R. (2005). *Matrigel: basement membrane matrix with biological activity.* Paper presented at the Seminars in cancer biology.

Koch, L., Kuhn, S., Sorg, H., Gruene, M., Schlie, S., Gaebel, R., . . . Ma, N. (2010). Laser printing of skin cells and human stem cells. *Tissue Engineering Part C: Methods, 16*(5), 847-854.

Kolesky, D. B., Homan, K. A., Skylar-Scott, M. A., & Lewis, J. A. (2016). Three-dimensional bioprinting of thick vascularized tissues. *Proceedings of the National Academy of Sciences, 113*(12), 3179-3184.

Kubota, Y., Kleinman, H. K., Martin, G. R., & Lawley, T. J. (1988). Role of laminin and basement membrane in the morphological differentiation of human endothelial cells into capillary-like structures. *The Journal of cell biology, 107*(4), 1589-1598.

Lee, D. W., Choi, Y.-S., Seo, Y. J., Lee, M.-Y., Jeon, S. Y., Ku, B., . . . Nam, D.-H. (2014). High-throughput screening (HTS) of anticancer drug efficacy on a micropillar/microwell chip platform. *Analytical chemistry, 86*(1), 535-542.

Lee, J. W., Choi, Y.-J., Yong, W.-J., Pati, F., Shim, J.-H., Kang, K. S., . . . Cho, D.-W. (2016). Development of a 3D cell printed construct considering angiogenesis for liver tissue engineering. *Biofabrication, 8*(1), 015007.

Li, Y.-C., Zhu, K., & Young, T.-H. (2017). Induced pluripotent stem cells, form in vitro tissue engineering to in vivo allogeneic transplantation. *Journal of thoracic disease, 9*(3), 455.

Lindblom, P., Gerhardt, H., Liebner, S., Abramsson, A., Enge, M., Hellström, M., . . . Nyström, H. C. (2003). Endothelial PDGF-B retention is required for proper investment of pericytes in the microvessel wall. *Genes & development, 17*(15), 1835-1840.

Little, C. J., Bawolin, N. K., & Chen, X. (2011). Mechanical properties of natural cartilage and tissue-engineered constructs. *Tissue Engineering Part B: Reviews, 17*(4), 213-227.

Lodish, H., Berk, A., Matsudaira, P., Kaiser, C., Krieger, M., Scott, M., . . . Darnell, J. (2003). Molecular Cell Biology. WH Freeman and Company.

Ma, L., Gao, C., Mao, Z., Zhou, J., Shen, J., Hu, X., & Han, C. (2003). Collagen/chitosan porous scaffolds with improved biostability for skin tissue engineering. *Biomaterials, 24*(26), 4833-4841.

Ma, X., Liu, J., Zhu, W., Tang, M., Lawrence, N., Yu, C., . . . Chen, S. (2018). 3D bioprinting of functional tissue models for personalized drug screening and in vitro disease modeling. *Advanced drug delivery reviews, 132*, 235-251.

Madden, L. R., Nguyen, T. V., Garcia-Mojica, S., Shah, V., Le, A. V., Peier, A., . . . Nguyen, D. G. (2018). Bioprinted 3D primary human intestinal tissues model aspects of native physiology and ADME/Tox functions. *IScience, 2*, 156-167.

Madri, J. A., Pratt, B. M., & Tucker, A. M. J. T. J. o. c. b. (1988). Phenotypic modulation of endothelial cells by transforming growth factor-beta depends upon the composition and organization of the extracellular matrix. *106*(4), 1375-1384.

Mandrycky, C., Wang, Z., Kim, K., & Kim, D.-H. (2016). 3D bioprinting for engineering complex tissues. *Biotechnology advances, 34*(4), 422-434.

Mazurek, R., Dave, J. M., Chandran, R. R., Misra, A., Sheikh, A. Q., & Greif, D. M. (2017). Vascular cells in blood vessel wall development and disease. In *Advances in Pharmacology* (Vol. 78, pp. 323-350): Elsevier.

Medvedev, S., Shevchenko, A., & Zakian, S. (2010). Induced pluripotent stem cells: problems and advantages when applying them in regenerative medicine. *Acta Naturae (англоязычная версия), 2*(2 (5)).

Mei, L., Hu, D., Ma, J., Wang, X., Yang, Y., & Liu, J. (2012). Preparation, characterization and evaluation of chitosan macroporous for potential application in skin tissue engineering. *International journal of biological macromolecules, 51*(5), 992-997.

Merceron, T. K., & Murphy, S. V. (2015). Hydrogels for 3D bioprinting applications. In *Essentials of 3D biofabrication and translation* (pp. 249-270): Elsevier.

Miri, A. K., Khalilpour, A., Cecen, B., Maharjan, S., Shin, S. R., & Khademhosseini, A. (2019). Multiscale bioprinting of vascularized models. *Biomaterials, 198*, 204-216.

Morin, K. T., & Tranquillo, R. T. (2013). In vitro models of angiogenesis and vasculogenesis in fibrin gel. *Experimental cell research, 319*(16), 2409-2417.

Murphy, S. V., & Atala, A. (2014). 3D bioprinting of tissues and organs. *Nature biotechnology, 32*(8), 773.

Newman, A. C., Nakatsu, M. N., Chou, W., Gershon, P. D., & Hughes, C. C. (2011). The requirement for fibroblasts in angiogenesis: fibroblast-derived matrix proteins are essential for endothelial cell lumen formation. *Molecular biology of the cell, 22*(20), 3791-3800.

Nichol, J. W., & Khademhosseini, A. (2009). Modular tissue engineering: engineering biological tissues from the bottom up. *Soft matter, 5*(7), 1312-1319.

Nicosia, R. F., & Ottinetti, A. (1990). Modulation of microvascular growth and morphogenesis by reconstituted basement membrane gel in three-dimensional cultures of rat aorta: a comparative study of angiogenesis in matrigel, collagen, fibrin, and plasma clot. *In vitro cellular & developmental biology, 26*(2), 119-128.

Novosel, E. C., Kleinhans, C., & Kluger, P. J. J. A. d. d. r. (2011). Vascularization is the key challenge in tissue engineering. *63*(4-5), 300-311.

O'brien, F. J. (2011). Biomaterials & scaffolds for tissue engineering. *Materials today, 14*(3), 88-95.
O'Connell, M. K., Murthy, S., Phan, S., Xu, C., Buchanan, J., Spilker, R., . . . Taylor, C. A. (2008). The three-dimensional micro-and nanostructure of the aortic medial lamellar unit measured using 3D confocal and electron microscopy imaging. *Matrix Biology, 27*(3), 171-181.
O'farrell, F. M., & Attwell, D. J. N. R. C. (2014). A role for pericytes in coronary no-reflow. *11*(7), 427-432.
Orimi, H. E., Kolkooh, S. S. H., Hooker, E., Narayanswamy, S., Larrivée, B., & Boutopoulos, C. (2020). Drop-on-demand cell bioprinting via Laser Induced Side Transfer (LIST). *Scientific reports, 10*(1), 1-9.
Otrock, Z. K., Mahfouz, R. A., Makarem, J. A., & Shamseddine, A. I. (2007). Understanding the biology of angiogenesis: review of the most important molecular mechanisms. *Blood Cells, Molecules, and Diseases, 39*(2), 212-220.
Ozbolat, I. T. (2015). Bioprinting scale-up tissue and organ constructs for transplantation. *Trends in biotechnology, 33*(7), 395-400.
Ozbolat, I. T., Peng, W., & Ozbolat, V. (2016). Application areas of 3D bioprinting. *Drug Discovery Today, 21*(8), 1257-1271.
Ozbolat, I. T., & Yu, Y. (2013). Bioprinting toward organ fabrication: challenges and future trends. *IEEE Transactions on Biomedical Engineering, 60*(3), 691-699.
Paquet, C., Larouche, D., Bisson, F., Proulx, S., Simard-Bisson, C., Gaudreault, M., . . . Duranceau, L. (2010). Tissue engineering of skin and cornea: development of new models for in vitro studies. *Annals of the New York Academy of Sciences, 1197*(1), 166-177.
Park, J.-H., Yoon, J.-K., Lee, J. B., Shin, Y. M., Lee, K.-W., Bae, S.-W., . . . Youn, Y.-N. (2019). Experimental tracheal replacement using 3-dimensional bioprinted artificial trachea with autologous epithelial cells and chondrocytes. *Scientific reports, 9*(1), 1-11.
Peak, C. W., Cross, L., Singh, A., & Gaharwar, A. K. (2016). Microscale technologies for engineering complex tissue structures. In *Microscale Technologies for Cell Engineering* (pp. 3-25): Springer.
Peng, W., Unutmaz, D., & Ozbolat, I. T. (2016). Bioprinting towards physiologically relevant tissue models for pharmaceutics. *Trends in biotechnology, 34*(9), 722-732.
Pepper, M. E., Seshadri, V., Burg, T., Booth, B. W., Burg, K. J., & Groff, R. E. (2011). *Cell settling effects on a thermal inkjet bioprinter.* Paper presented at the 2011 Annual International Conference of the IEEE Engineering in Medicine and Biology Society.
Perry, T. E., Kaushal, S., Sutherland, F. W., Guleserian, K. J., Bischoff, J., Sacks, M., & Mayer, J. E. (2003). Bone marrow as a cell source for tissue engineering heart valves. *The Annals of thoracic surgery, 75*(3), 761-767.
Pirlo, R. K., Wu, P., Liu, J., & Ringeisen, B. (2012). PLGA/hydrogel biopapers as a stackable substrate for printing HUVEC networks via BioLP™. *Biotechnology and bioengineering, 109*(1), 262-273.
Potente, M., Gerhardt, H., & Carmeliet, P. (2011). Basic and therapeutic aspects of angiogenesis. *Cell, 146*(6), 873-887.
Rimann, M., & Graf-Hausner, U. (2012). Synthetic 3D multicellular systems for drug development. *Current opinion in biotechnology, 23*(5), 803-809.
Risau, W. (1997). Mechanisms of angiogenesis. *Nature, 386*(6626), 671-674.

Sakar, M. S., Neal, D., Boudou, T., Borochin, M. A., Li, Y., Weiss, R., . . . Asada, H. H. (2012). Formation and optogenetic control of engineered 3D skeletal muscle bioactuators. *Lab on a Chip, 12*(23), 4976-4985.

Sanchez-Adams, J., & Athanasiou, K. A. (2012). Dermis isolated adult stem cells for cartilage tissue engineering. *Biomaterials, 33*(1), 109-119.

Sasmal, P., Datta, P., Wu, Y., & Ozbolat, I. T. (2018). 3D bioprinting for modelling vasculature. *Microphysiological systems, 2*.

Shaikh, F. M., Callanan, A., Kavanagh, E. G., Burke, P. E., Grace, P. A., & McGloughlin, T. M. (2008). Fibrin: a natural biodegradable scaffold in vascular tissue engineering. *Cells Tissues Organs, 188*(4), 333-346.

Shin, Y., Han, S., Jeon, J. S., Yamamoto, K., Zervantonakis, I. K., Sudo, R., . . . Chung, S. (2012). Microfluidic assay for simultaneous culture of multiple cell types on surfaces or within hydrogels. *Nature protocols, 7*(7), 1247-1259.

Smith, A. G. (2001). Embryo-derived stem cells: of mice and men. *Annual review of cell and developmental biology, 17*(1), 435-462.

Snyder, J., Hamid, Q., Wang, C., Chang, R., Emami, K., Wu, H., & Sun, W. (2011). Bioprinting cell-laden matrigel for radioprotection study of liver by pro-drug conversion in a dual-tissue microfluidic chip. *Biofabrication, 3*(3), 034112.

Stratman, A. N., Malotte, K. M., Mahan, R. D., Davis, M. J., & Davis, G. E. (2009). Pericyte recruitment during vasculogenic tube assembly stimulates endothelial basement membrane matrix formation. *Blood, The Journal of the American Society of Hematology, 114*(24), 5091-5101.

Swift, M. R., & Weinstein, B. M. (2009). Arterial–venous specification during development. *Circulation research, 104*(5), 576-588.

Tasoglu, S., Yu, C. H., Liaudanskaya, V., Guven, S., Migliaresi, C., & Demirci, U. (2015). Magnetic levitational assembly for living material fabrication. *Advanced healthcare materials, 4*(10), 1469-1476.

Thomson, J. A., Itskovitz-Eldor, J., Shapiro, S. S., Waknitz, M. A., Swiergiel, J. J., Marshall, V. S., & Jones, J. M. (1998). Embryonic stem cell lines derived from human blastocysts. *Science, 282*(5391), 1145-1147.

Wagenseil, J. E., & Mecham, R. P. (2009). Vascular extracellular matrix and arterial mechanics. *Physiological reviews, 89*(3), 957-989.

Waring, M. J., Arrowsmith, J., Leach, A. R., Leeson, P. D., Mandrell, S., Owen, R. M., . . . Wang, J. (2015). An analysis of the attrition of drug candidates from four major pharmaceutical companies. *Nature reviews Drug discovery, 14*(7), 475-486.

Weisel, J. W. (2004). The mechanical properties of fibrin for basic scientists and clinicians. *Biophysical chemistry, 112*(2-3), 267-276.

Wu, P., & Ringeisen, B. (2010). Development of human umbilical vein endothelial cell (HUVEC) and human umbilical vein smooth muscle cell (HUVSMC) branch/stem structures on hydrogel layers via biological laser printing (BioLP). *Biofabrication, 2*(1), 014111.

Wu, W., DeConinck, A., & Lewis, J. A. (2011). Omnidirectional printing of 3D microvascular networks. *Advanced materials, 23*(24), H178-H183.

Xiong, R., Zhang, Z., Chai, W., Huang, Y., & Chrisey, D. B. (2015). Freeform drop-on-demand laser printing of 3D alginate and cellular constructs. *Biofabrication, 7*(4), 045011.

Xu, F., Finley, T. D., Turkaydin, M., Sung, Y., Gurkan, U. A., Yavuz, A. S., . . . Demirci, U. (2011). The assembly of cell-encapsulating microscale hydrogels using acoustic waves. *Biomaterials, 32*(31), 7847-7855.

Zhang, K., Fu, Q., Yoo, J., Chen, X., Chandra, P., Mo, X., . . . Zhao, W. (2017). 3D bioprinting of urethra with PCL/PLCL blend and dual autologous cells in fibrin hydrogel: An in vitro evaluation of biomimetic mechanical property and cell growth environment. *Acta biomaterialia, 50*, 154-164.

Zhang, Y. S., Yue, K., Aleman, J., Mollazadeh-Moghaddam, K., Bakht, S. M., Yang, J., . . . Shin, S. R. (2017). 3D bioprinting for tissue and organ fabrication. *Annals of biomedical engineering, 45*(1), 148-163.

Zhao, Y., Yao, R., Ouyang, L., Ding, H., Zhang, T., Zhang, K., . . . Sun, W. (2014). Three-dimensional printing of Hela cells for cervical tumor model in vitro. *Biofabrication, 6*(3), 035001.

Zheng, Y., Chen, J., Craven, M., Choi, N. W., Totorica, S., Diaz-Santana, A., . . . Stroock, A. D. (2012). In vitro microvessels for the study of angiogenesis and thrombosis. *Proceedings of the National Academy of Sciences, 109*(24), 9342-9347. doi:10.1073/pnas.1201240109

Zhu, W., Qu, X., Zhu, J., Ma, X., Patel, S., Liu, J., . . . Xu, Y. (2017). Direct 3D bioprinting of prevascularized tissue constructs with complex microarchitecture. *Biomaterials, 124*, 106-115.